UNIVERSITY OF CALIFORNIA
RIVERSIDE

Effect of Sound Barriers on Dispersion from Roadways

SYSTEMATICAL PHYSICAL MODELING OF SOUND WALLS, TREE-
LINES, SUNKEN AND RAISED ROADWAYS

Prepared by

Brandn Gazzolo, P.E.
Sam Pournazeri, Ph.D.
Marko Princevac, Ph.D., Project PI

Experimental Support Provided by

Matti Azard
Trevor Brown
Raul-Delga Delgadillo
Trent Nash
Senyeung Shu

This Report Presents a Supplement to the Digital Catalog

This work is taken from the Master Thesis of Brandn Gazzolo titled "Near Field Modeling of the Effects of Sound Barriers on Flow and Dispersion"

Contents

Nomenclature

AC	Air Change
AQMD	Air Quality Management District
C	Concentration
C_{non}	Normalized Concentration
CARB	California Air Resources Board
CCD	Charged Coupled Device
CFD	Computational Fluid Dynamics
cfm	Cubic Feet per Minute
CEC	California Energy Commision
C_p	Specific Heat
f	Body Force
F_{net}	Net Force
FOALIF	Fiber Optic Assisted Laser Induced Fluorescence
g	Gravity Constant
H	Height
H_{down}	Downwind Sound Barrier Height
h_e	Source Height
H_{SB}	Sound Barrier Height
H_{up}	Upwind Sound Barrier Height
k	Von Karman Constant
L	Length
LANL	Los Alamos National Laboratory
LEFM	Laboratory for Environmental Flow Modeling
LIF	Laser Induced Fluorescence
l_{mix}	Mixing Length
L_x	Horizontal Length Scale
L_y	Lateral Length Scale
m	Mass
MPH	miles per hour
P	Pressure
PIV	Particle Image Velocimetry
PLIF	Planar Laser Induced Fluorescence
Q	Emission Rate
Q_o	Kinematic Heat Flux
QUIC	Quick Urban and Industrial Complex
RANS	Reynolds Averaged Navier-Stokes Equations
RMS	Root Mean Square
SB	Sound Barrier
SG	Specific Gravity
SHF	Sensible Heat Flux
T	Temperature
T'	Temperature Fluctuation
T_a	Air Temperature
T_p	Parcel Temperature
TIT	Traffic Induced Turbulence
U	Wind Speed

u	Horizontal Velocity
u_i	Indexed Velocity
u_*	Friction Velocity
UCR	University of California, Riverside
V	Volume
v	Lateral Velocity
v	Kinematic Viscosity
W	Road Width
w	Vertical Velocity
w'	Vertical Velocity Fluctuation
w_*	Convective Velocity Scale
x	Horizontal Coordinate
y	Lateral Coordinate
z	Vertical Coordinate
z_o	Surface Roughness
β	Thermal Expansion Coefficient
Δ	Difference
ΔT	Temperature Difference
ρ	Density
ρ_a	Air Density
ρ_p	Parcel Density
S_{ij}	Deformation Tensor
σ_y	Lateral Spread
σ_z	Vertical Spread
θ	Angle
θ_{wind}	Wind Angle

1. Introduction

Sound barriers (SB) are very commonly seen on the sides of roadways and their primary purpose is to dampen roadway noise. However, this research focuses on their influence on the dispersion of traffic related pollutants from roadways. Vehicular emissions are one of the major sources of air pollution in urban areas (Kodama et al., 2002) and several epidemiological studies have shown that long term exposure to vehicle related pollutants increases the risk of respiratory diseases, birth defects, premature mortality, cardiovascular disease, and cancer (McConnell et al., 2006; Wilhelm and Ritz, 2003; Jerrett et al., 2005; Peters et al., 2004; Harrison et al., 1999). It has been found that more than 24,000 child care centers in California are within 200 m of highly trafficked roadways with more than 50,000 vehicles per day (Houston et al., 2006). There are residential areas all over Southern California that sit directly next to busy freeways, with SBs being the only separation between the two. Local examples of this can be observed along the SR60, SR91 and I-15 freeways. With increased traffic and thus increased vehicular emissions it is important to see how pollutants from such roads can affect adjacent urban areas.

In the past, research on the impact of SBs including field studies, wind tunnel experiments and numerical modeling has been conducted. A short summary of recent findings follows. It has been shown that a near road concentration decrease of up to 50% compared with an unobstructed roadway can be achieved with different roadway configurations (Finn et al., 2010). This research shows that roadside SBs can influence the dispersion of pollutants by creating complex flow field consisting of updraft and downdraft air motions, which depends on the SB configuration, and by increasing turbulence and mixing. Results from the model by Bowker et al. (2007) showed that the presence of both sound barriers and tall vegetation (height taken from photographs but not specified in their work) can significantly reduce the concentration downwind by producing more turbulence and mixing. Baldauf et al. (2008) showed that roadside

1

barriers generally lead to decreased pollutant concentrations near the road. However, they also showed that for low wind speeds and stable atmospheric conditions, noise barriers can trap pollutants on the upwind side of the barrier and transport some of the pollutants back towards the source, increasing on-road pollutant concentrations (similar finding as Finn et al., 2010). A wind tunnel study (Heist et al., 2009) showed that the smallest reduction in ground-level concentrations occurs for elevated roadways without sound barriers and the maximum decrease occurs for depressed roadways with sound barriers on the sides.

The presented research addresses the effects of SBs by systematic laboratory experiments accompanied with limited Quick Urban and Industrial Complex (QUIC) CFD and URB numerical modeling and followed up with traditional simple Gaussian-type dispersion models. Since field measurements are expensive and are always specific to site geometry and meteorological conditions laboratory experiments are the only useful way to conduct a systematical generalized study. The laboratory experiments from this project are aimed to:

- delineate the effects of various SB configurations

- serve as a preliminary verification tool for the numerical models: Quick Urban and Industrial Complex (QIUC), two dimensional advection-diffusion model and the Gaussian model.

2. Laboratory

All experiments were performed at the Laboratory for Environmental Flow Modeling (LEFM) at the University of California, Riverside (UCR), which consists of a custom made water channel (Figure 2-1). The test section of the water channel is 1.5 m long, 1 m wide and 0.5 m deep and water is circulated by a 15 hp axial pump (Carry Manufacturing, Inc.) which can produce a maximum mean velocity of 0.5 m s^{-1} in the test section. The pump speed is proportional

to the mean velocity of the test section, and is controlled by a variable frequency drive which has a resolution of 1/100 Hz. Flow conditioning in the test section is achieved by using honeycombs and if necessary perforated screens can be used to achieve a desired velocity profile. The flow in the water channel is steady and fully turbulent.
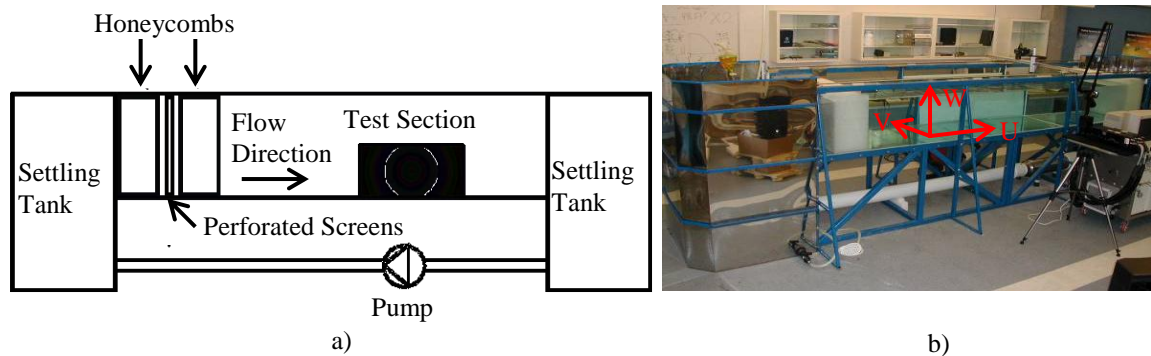

Figure 2-1. (a) Water Channel Schematic; b) UCR Water Channel Facility Located in the Laboratory for Environmental Flow Modeling (LEFM), Bourns Hall B262

At the LEFM, different types of experiments involving Particle Image Velocimetry (PIV), Planar Laser Induced Fluorescence (PLIF), Fiber Optic Assisted Laser Induced Fluorescence (FOALIF) and dye release visualizations can be performed. PIV experiments are used to find detailed velocity fields, PLIF measurements are used to find detailed concentration fields in a selected plane and FOALIF experiments are used for precise concentration measurements at selected points. Dye release visualizations are useful in showing the dispersion pattern and plume rise in and around complex geometries. More information on the water channel and the various types of experiments can be found in Princevac et al. 2010. A brief introduction for each experimental technique is given next.

2.1. Particle Image Velocimetry

Detailed velocity field is measured by Particle Image Velocimerty (PIV). The PIV system at the LEFM consists of a 400 mJ Nd-YAG laser (Big Sky Laser Technologies Inc.), Laser pulse synchronizer (TSI Inc.) and a PowerView Plus 2M and 11M camera. The laser produces a 532 nm wavelength laser beam with a frequency range of 1 to 14 Hz and the beam is expanded into a sheet using sheet forming optics (cylindrical lenses). Pliolite Ultra 100 particles (Eliokem) are used for seeding the water channel. The fluid's velocity can be measured by using two separate recorded exposures. A pair of laser pulses is produced and the illuminated flow region is recorded. The recorded frames are then split into a number of interrogation areas. Through image processing, by looking for a correlation maxima, it is then possible to calculate a displacement vector for each interrogation area. This displacement is converted to a velocity using the time step between consecutive images (in most experiments this was set to Δt=1500 μs). Insight 3G (TSI Inc.) software is used for data collection and image processing. PIV measurement technique is well established and widely used for fluid flow investigations (Adrian, 1988, 1991, 1997; Prasad et al., 1992) and will not be discussed further.

The measured incoming velocity profile for a pump speed of 17.5 Hz is shown in Figure 2-2. Most of the experiments were done at a pump speed setting of 17.5 Hz (mean velocity of 0.042 m s-1 at 0.1 m above the channel bottom) and selected experiments were done at a pump speed setting of 5 Hz (mean velocity of 0.015 m s-1 at 0.1 m above the channel bottom) to look at the effects of varying the free stream velocity.
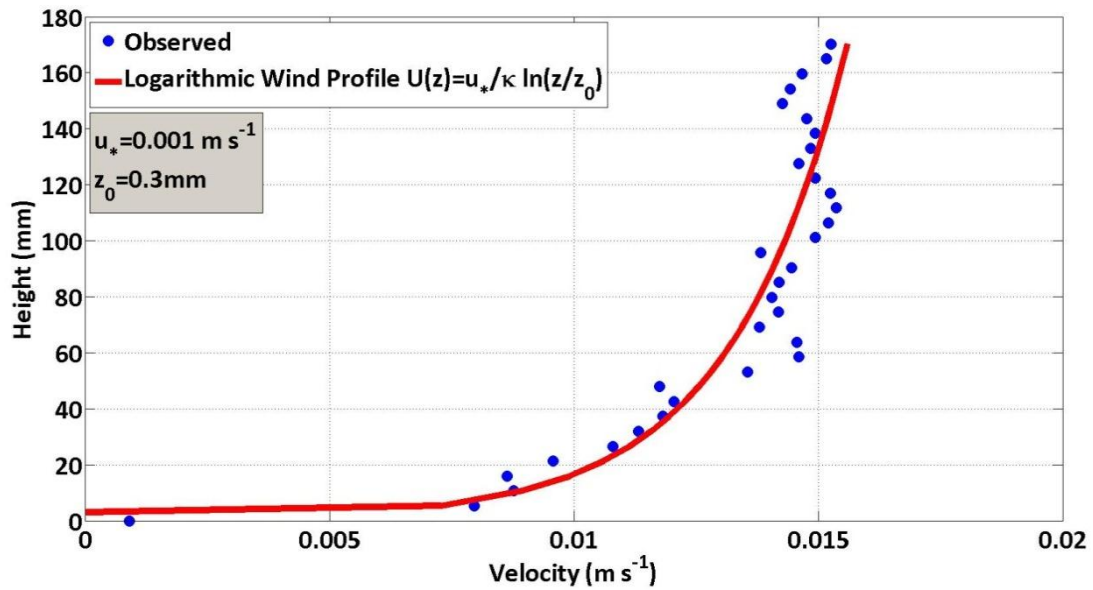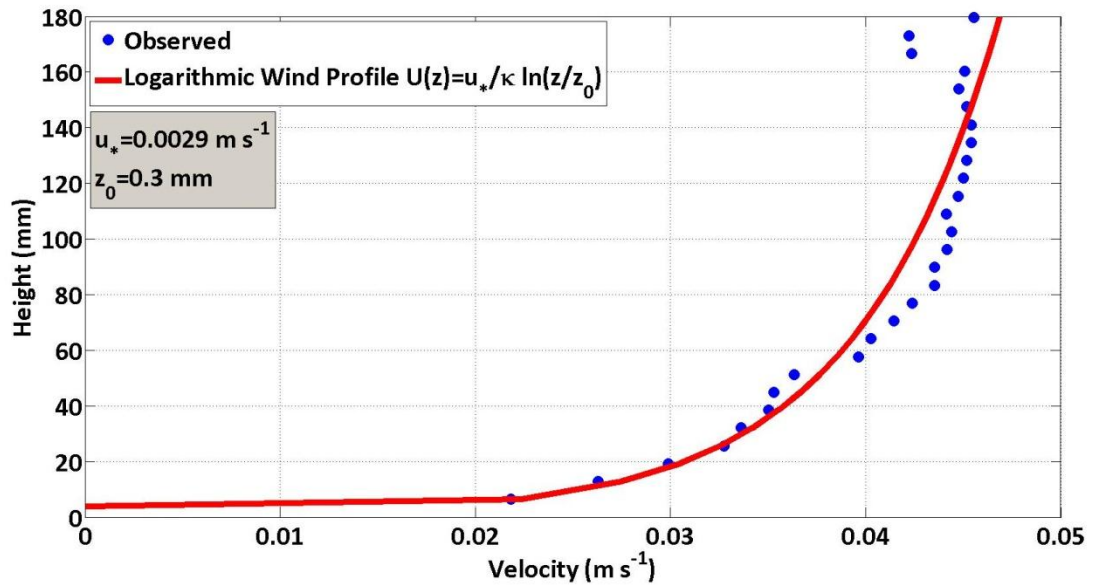
Figure 2-1. Incoming Velocity Profile for Pump Setting 17.5 Hz (top); Pump Setting 5 Hz (bottom)

2.2. Visualization Techniques

As a systematic laboratory effort, dye release visualizations were done in order to look at the dispersion pattern and time averaged plume behavior resulting from different roadway configurations. Uranine dye is used for the visualizations because it has a high fluorescence in the

visible spectrum. Visualizations are achieved by releasing the dye from a line source and taking a long exposure (over 30 s) image. The result is an image of the time averaged plume, which was used to study the dispersion pattern and plume rise for different roadway configurations. A mixture of uranine dye and water (neutral buoyancy) is pumped through a line source. Water and alcohol (SG=0.8) can be mixed together to obtain a buoyant release. The presented research is done with a neutrally buoyant release; however, the effects of buoyancy will be briefly discussed. The line source is modeled using a porous rubber tubing which is common to irrigation applications and can be found at local hardware stores.

2.3. Fiber Optic Assisted Laser Induced Fluorescence (FOALIF)

Concentration measurements utilizing PLIF were not done since the results would be limited to a small window of two dimensional concentration measurements, whereas ground level concentration measurements in the near and far field are desired. Also, the recirculation of the water channel leads to background concentrations that can skew the PLIF results. Instead, FOALIF was utilized for precise point concentration measurements using a fluorescent tracer dye (Rhodamine B, $C_{28}H_{31}ClN_2O_3$). Rhodamine B is water soluble, up to 50 g L^{-1}, and has an absorption spectrum of 460 nm – 590 nm along with an emission spectrum of 550 nm – 680 nm, with the maximum being 590 nm. The linear concentration intensity of Rhodamine B has been reported in several studies, all of which reported different results. Princevac et al. (2010) showed that Rhodamine B exhibits a linear concentration intensity behavior up to 10 mg L^{-1}.

The FOALIF system consists of a 400 mJ Nd-YAG laser (Big Sky Laser Technologies Inc.), which produces a 532 nm wavelength laser beam with the frequency of up to 15 Hz, laser pulse synchronizer (TSI Inc.), high resolution (1600 x 1192) POWERVIEW 2M CCD camera (TSI Inc.), and a 575 – 585 nm light filter. The basic operation of FOALIF is as follows: the laser

expands into a sheet and enters the fiber optic bundle, next the laser light is carried via the emitting fibers to the sensors, which are placed at desired locations in the water channel. The emitting fibers at the sensors will illuminate any dye that is in vicinity and the dye will fluoresce. That fluorescent light, as well as residual light from the laser, is captured by the receiving fibers. The light captured by the receiving fibers is sent through a filter so that only the desired fluorescent light is captured and recorded by the CCD camera. The intensity of this captured light is proportional to the concentration. Guilbault (1973) showed the induced fluorescence intensity, I_f, can be related to the fluorescent dye concentration by:

$$I_f = 2.3 \, \Phi \, I_0 \, \varepsilon \, b \, c \tag{2-1}$$

where Φ is the quantum efficiency, the ratio between the energy that is emitted to that of absorbed, I_0 is the light intensity, ε is the molar absorptivity, b is the absorption path length and c is the concentration of the fluorescent dye. Further information on the setup, basic theory and operation of FOALIF can be found in Princevac et al. (2010).

The FOALIF schematic is shown in Figure 2-3 and the experimental setup is shown in Figure 2-4. Rhodamine B is released through a porous line source (to simulate vehicular emissions) located in the center of the roadway. Fifteen fiber optic sensors plus one background sensor were placed at ground level in the water channel. A background sensor allows for longer concentration averaging times by providing real time corrections for the increasing background concentrations. The background dye is well mixed since it has to go through the axial pump and a big settling tank prior to be recirculated back to the test section. Each sensor has an emitting fiber (delivery of the laser beam) and a receiving fiber (delivery of fluorescent light to the CCD Camera). Kulchin et al. (2007) has shown that optimal performance of the sensors is when the two fibers are at a 26° angle to each other. A mixture of Rhodamine and water (60 mg L^{-1}) was pumped through the line source at a rate of 3.87 mL s^{-1}. The water channel is scaled by 100

relative to the field. Lego type blocks were used to construct the SBs in the channel and they spanned the whole width of the channel as to simulate that of infinite SBs (Figure 2-4). The road width was chosen as 30 cm (30 m scaled to the field) and a finite line source of 20 cm (20 m scaled to the field) was placed in the center of the roadway. One rationale for not using the full channel width for the source length was that the main focus in visualizations was the center line and we were concerned that dye rising next to the glass (channel walls) would impede the visualization quality (as it happened in the experiments for traffic induced turbulence, see section 5.7. All FOALIF experiments were done with an incoming logarithmic velocity profile with a free stream velocity of 4.2 cm s^{-1} (4.2 m s^{-1} scaled to the field). This results in Reynolds number of ~3,700 based on the barrier height, but the flow was anyway turbulent due to the boundary layer development prior to the test section and the pump action. Scaling details are explained in Pournazeri et al. 2012.
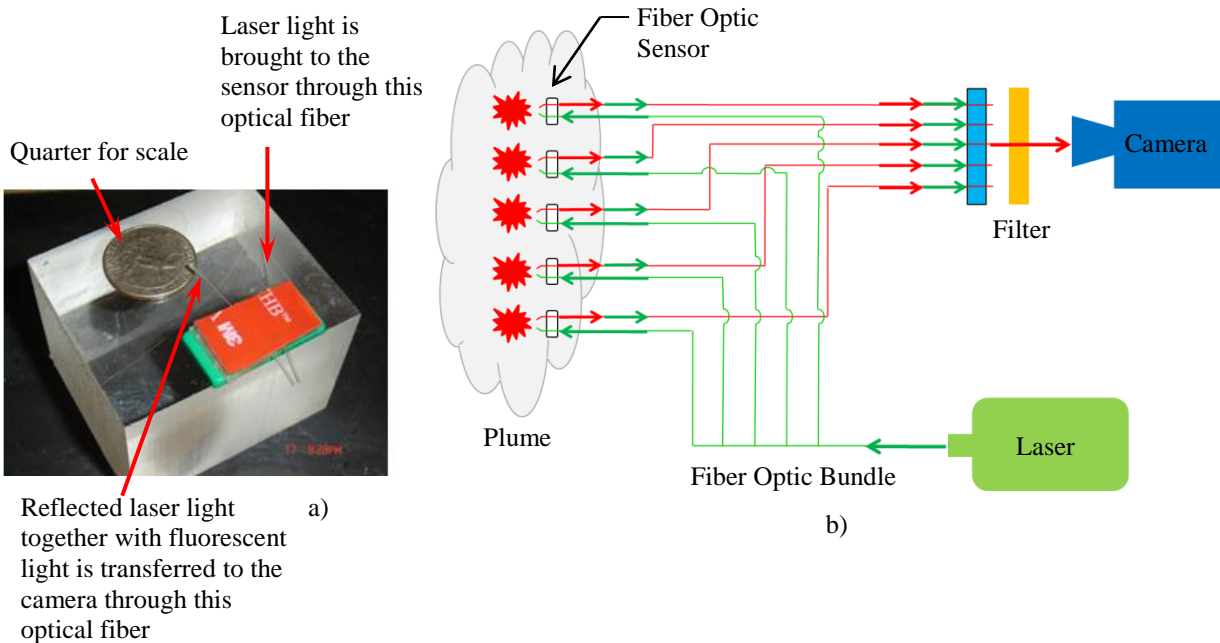
Figure 2-2. Fiber Optic Assisted Laser Induced Fluorescence (FOALIF): a) Photograph of Fiber Optic Sensor; b) FOALIF Schematic
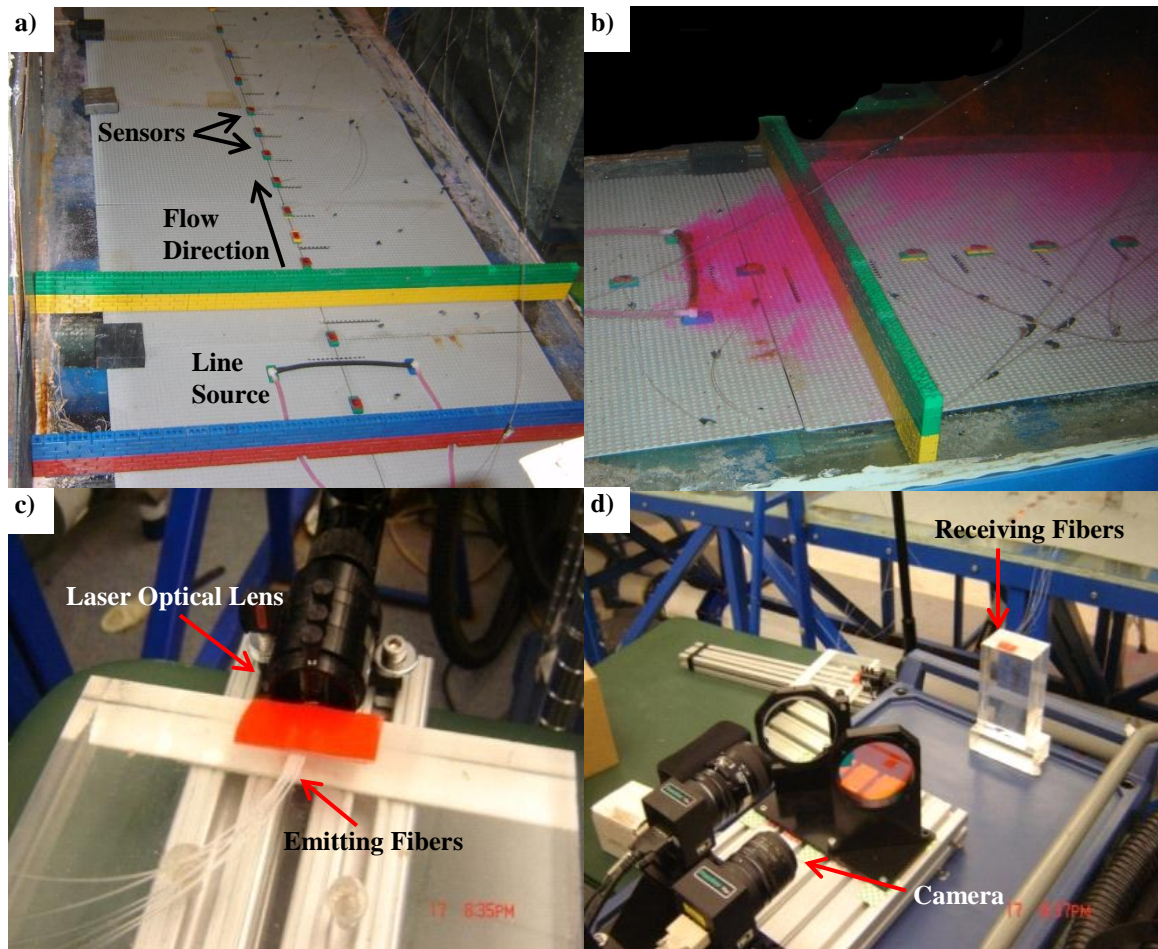
Figure 2-3. a) FOALIF sensors installed in the Water Channel; b) Exampleof Rhodamine release; c) Laser setup; d) Camera setup

3. Modeling

Since developing a sophisticated numerical model can be very time consuming and expensive, and there are already numerous codes available that have been in development for many years, there was no need to develop a new numerical model. It was more practical to use the existing fast response 3D model, Quick Urban and Industrial Complex (QUIC) for simulations of the flow and concentration fields and the simple Gaussian-type models for concentration only. QUIC was developed for the Department of Homeland Security (Pardyjak and Brown, 2003) as a diagnostic tool for studying and predicting the dispersion of toxic releases

in urban areas. QUIC is composed of a parametric 3D wind model, QUIC-URB, a Computational Fluid Dynamics (CFD) model, QUIC-CFD and a Lagrangian Particle Dispersion model, QUIC-PLUME. In addition to using QUIC, for only concentration field modeling, a two dimensional advection diffusion model originally developed by van Ulden (1978) and modified by Venkatram (2004) and the Gaussian Model were tested.

3.1. QUIC-URB

QUIC-URB is a fast semi-empirical 3D wind model and is based on the Rockle's (1990) thesis (Pardyjak and Brown, 2001). An initial flow field is prescribed based on the incident flow and various time averaged flow effects associated with building geometries are superimposed (Figure 3-1), and then the model is iterated until the continuity equation is satisfied (Pardyjak and Brown, 2001) (Figure 3-2). Around the buildings in the model, empirical parameterizations are invoked to produce a velocity field that maintains important features of the time averaged flows (Pardyjak and Brown, 2003), such as the wake zone and cavity (Figure 3-3).
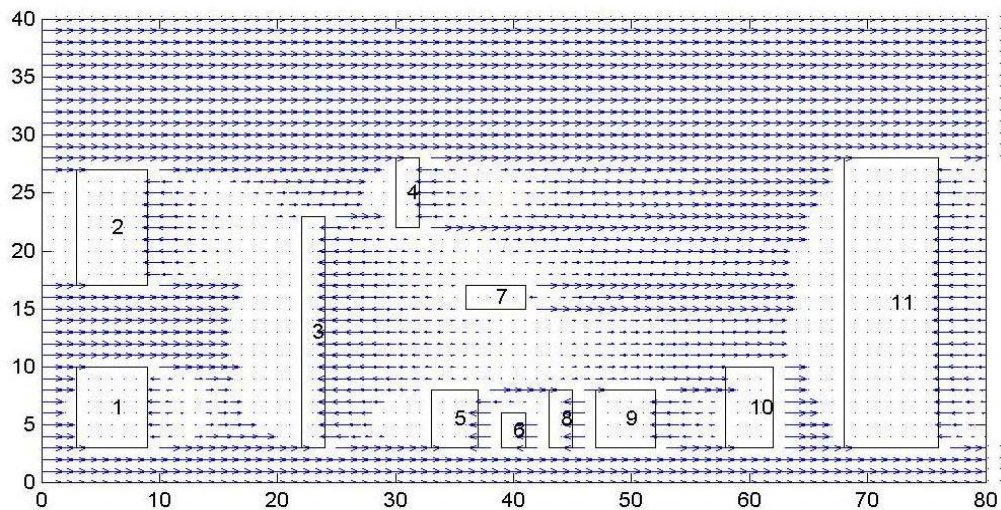
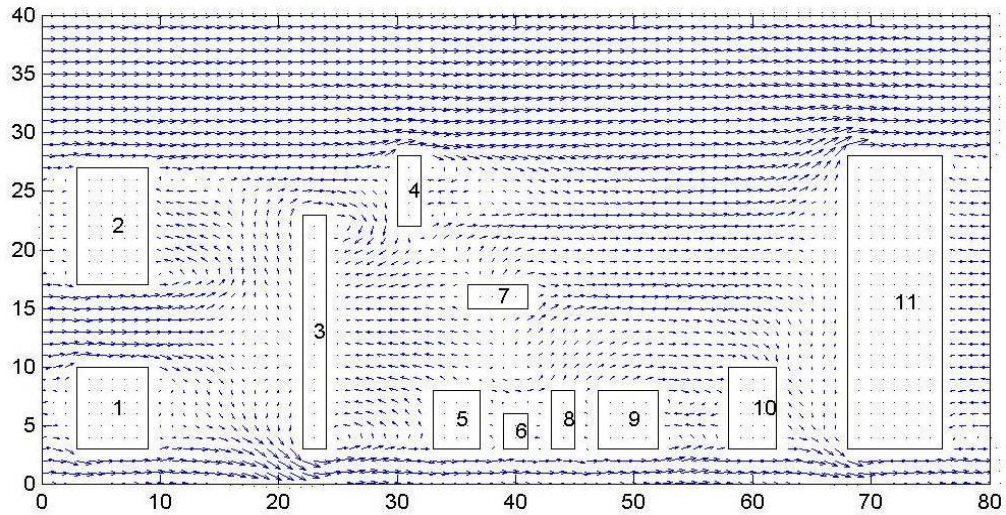**Figure 3-1.** QUIC-URB Initial Flow Field

10

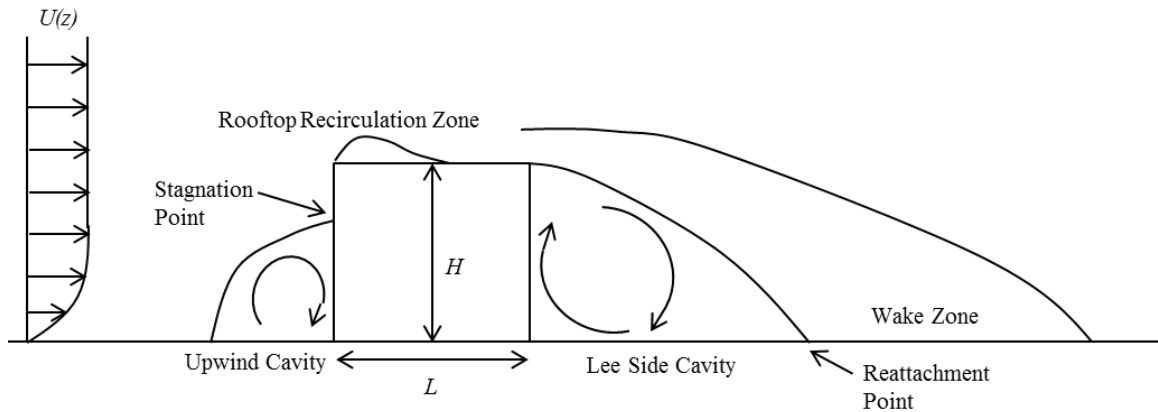**Figure 3-2.** QUIC-URB Continuity Satisfied Final Flow Field

Figure 3-3. Building Parameterization zones

3.2. QUIC-CFD

QUIC-CFD is much slower than QUIC-URB but it should yield more realistic wind field solutions (Nelson and Brown, 2009). It will be shown later that for the case of sound barriers, the results from QUIC-URB produced better concentration results than that of QUIC-CFD. This is likely due to the simplified turbulence model used to keep the model fast. QUIC-CFD solves a simplified version of the Reynolds Averaged Navier-Stokes (RANS) equations:

$$\frac{\partial \overline{u_i}}{\partial t} + \frac{\partial \overline{u_i u_j}}{\partial x_j} = -\frac{1}{\rho}\frac{\partial \overline{P}}{\partial x_i} + f_i + v\frac{\partial^2 \overline{u_i}}{\partial x_j^2} - \frac{\partial \overline{u_i' u_j'}}{\partial x_j} \qquad (3\text{-}1)$$

where u (m s-1) is velocity, P (N m-2) is pressure, f (N kg-1) represents body forces per unit mass (ex. gravity), ρ (kg m-3) is density, and ν (m2 s-1) is the kinematic viscosity. The over bar represents averaged quantities and i is the free index and j is the repeated index. In order to speed up the CFD model, QUIC-CFD assumes incompressible flow, neglects body forces and uses a zeroth order (algebraic) turbulent closure, (Gowardhan et al., 2010) which simplifies (3-1) to

$$\frac{\partial \overline{u_i}}{\partial t} + \frac{\partial \overline{u_i u_j}}{\partial x_j} = -\frac{1}{\rho}\frac{\partial \overline{P}}{\partial x_i} + v_t\frac{\partial^2 \overline{u_i}}{\partial x_j^2} \qquad (3\text{-}2)$$

The turbulent closure is a simple eddy viscosity approach based on Prandtl's mixing length theory (Gowardhan et al., 2010). The turbulent viscosity is calculated as follows:

$$v_t = l_{mix}^2 \sqrt{\overline{S_{ij} S_{ij}}} \qquad (3\text{-}3)$$

$$l_{mix} = k y_{min} \qquad (3\text{-}4)$$

where κ is the Von Karman constant, y_{min} (m) is the shortest distance from a wall or the ground and S_{ij} (s^{-1}) is the deformation tensor (Gowardhan et al., 2010). A comparison of the flow field produced by QUIC-URB and QUIC-CFD can be seen in Figure 3-4 for a mock building configuration. Some predictable flow patterns applied around the buildings in QUIC-URB can be seen. In the QUIC-URB results there is a counter rotating vortex in the wake of each building. This is a typical flow field produced by an isolated (not influenced by other obstacles) building. The QUIC-CFD results show how the combined influence of each building produces an entirely different flow pattern.
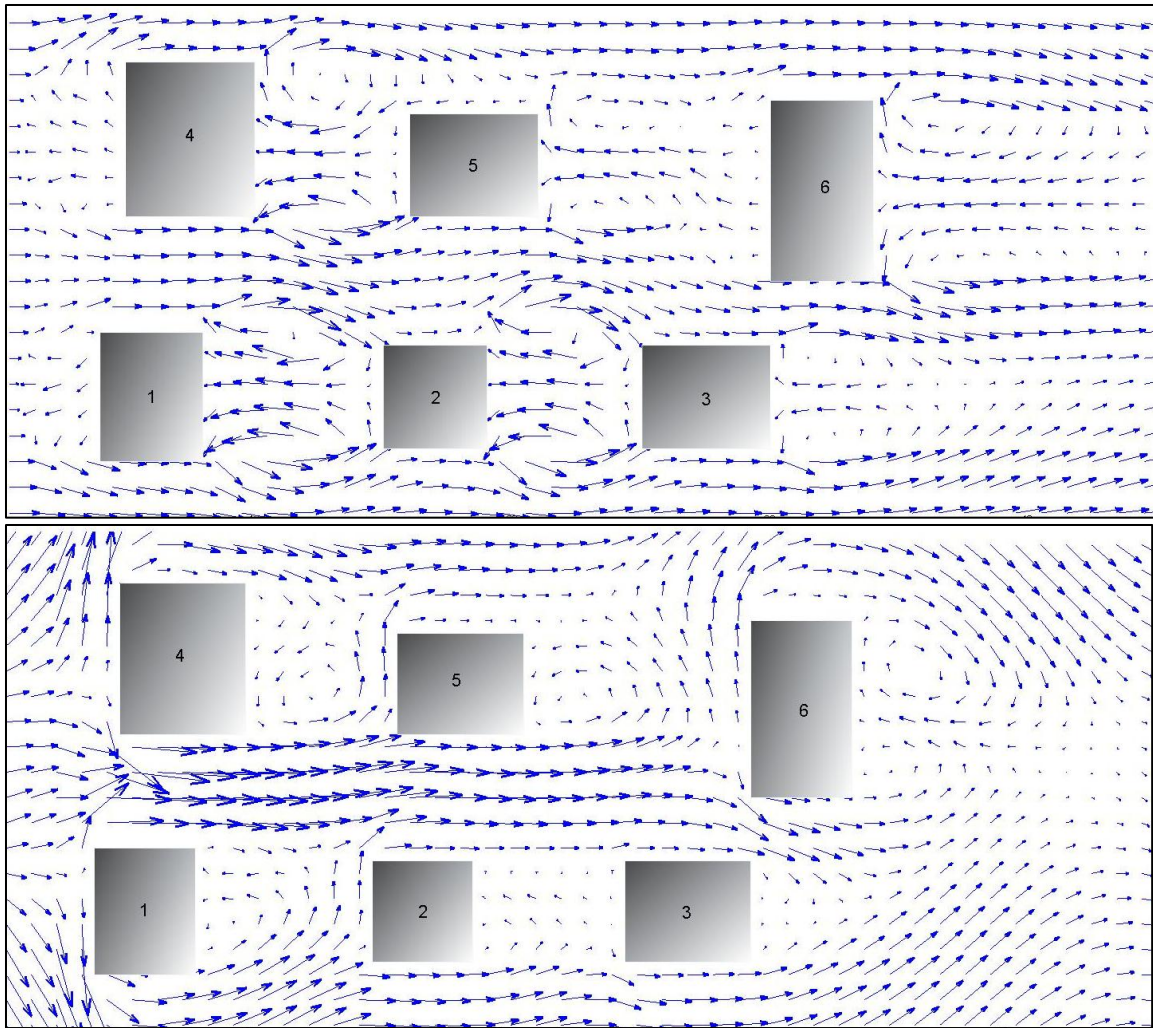
Figure 3-4. QUIC-URB (top) versus QUIC-CFD (bottom)

3.3. QUIC-PLUME

QUIC-PLUME is a Lagrangian random walk dispersion model for computing concentration and deposition fields around buildings (Nelson and Brown, 2009). QUIC-PLUME uses the mean wind fields produced by either QUIC-URB or QUIC-CFD and turbulent winds computed internally using Langevin Random walk equations (Williams et al., 2004). Due to the inhomogeneity of flow around buildings QUIC-PLUME uses a coordinate rotation approach and more terms than the traditional three term random walk equations (Williams et al., 2004). This

model describes dispersion by releasing particles and moving them with an instantaneous wind, which is composed of a mean wind and a turbulent wind (Williams et al., 2004). An example of particles being released and an example of a ground level concentration field produced in QUIC is shown in Figure 3-5.
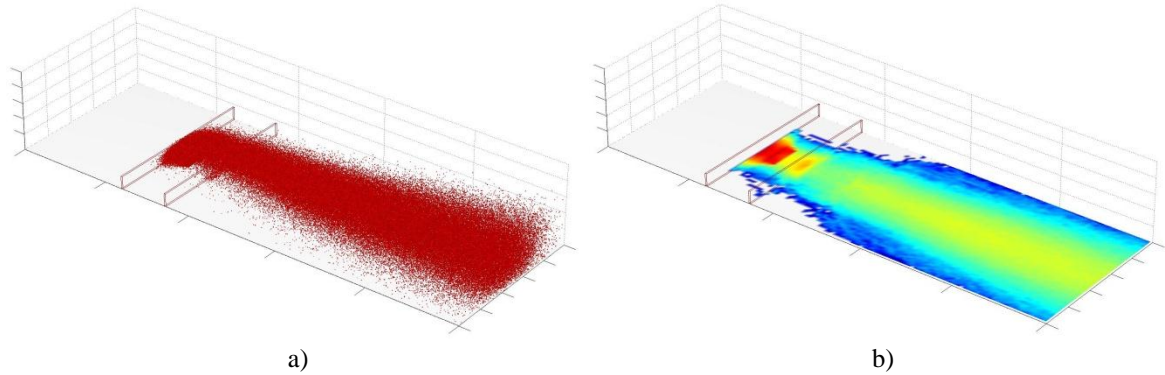
Figure 3-5. QUIC-PLUME: a) Particle Release; b) Ground Level Concentration Field

3.4. Gaussian Dispersion Model for a Line Source

As part of the systematical research, an effort of concentration prediction was done utilizing the well know Gaussian dispersion model (USEPA regulatory model AERMOD, which is originally developed for simple terrain, is Gaussian):

$$C(x,y,z) = \frac{Q}{2\pi\sigma_y\sigma_z U} exp\left(-\frac{y^2}{2\sigma_y^2}\right) exp\left(-\frac{z^2}{2\sigma_z^2}\right) \qquad (3\text{-}5)$$

where C (kg m^{-3}) is the concentration, Q (kg s^{-1}) is the emission rate, U (m s^{-1}) is the wind speed, σ_y (m) is the lateral spread and σ_z (m) is the vertical spread. In order to make sure that there is no flux through the ground ($z = 0$) an imaginary source is placed in the negative z direction, and this will cancel any flux that may have gone through the ground.

$$C(x,y,z) = \frac{Q}{2\pi\sigma_y\sigma_z U} exp\left(-\frac{y^2}{2\sigma_y^2}\right)\left[exp\left(-\frac{(z-h_e)^2}{2\sigma_z^2}\right) + exp\left(-\frac{(z+h_e)^2}{2\sigma_z^2}\right)\right] \qquad (3\text{-}6)$$

where h_e (m) is the source height. This model has been shown to be effective in predicting the downwind concentrations for elevated releases in the absence of buildings or other obstacles. One has to always keep in mind that Gaussian based models (eq. 3.5 or 3.6) by their very nature are not made to reproduce the mean flow field disturbances caused by various obstacles and can only try to account for such disturbances by different tweaks to the plume spread formulations, initial spread or even source location changes. This research is focused on the modeling of vehicular emissions, which is to be modeled using line sources and so the Gaussian model can be modified to simulate line sources by integrating over a large number of point sources. One approach to adapting this model to roadways with SBs is to place the source on top of a SB, thus eliminating the presence/effects of obstacles and assuming that the velocity above the SB is constant. When placing the source on top of a SB, initial spread (σ_0)is adjusted to account for the plume spread that has occurred between the release on the roadway and top of the SB (Figure 3-6).
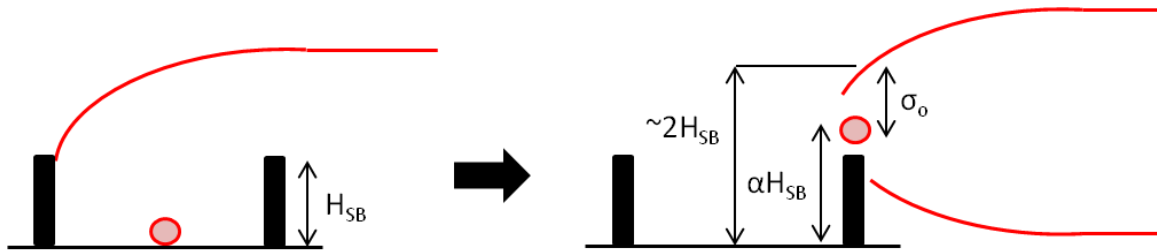
Figure 3-6. Gaussian Model for SBs. To try to compute the effects of the recirculation and listing of the plume between the barriers the source is placed on the top of SB and initial spread is adjusted.

In order to find the initial spread (σ_o) a top hat model is compared to that of the Gaussian model (Figure 3-7). For the top hat model the properties are constant over the plume cross section and for the Gaussian model the properties follow a Gaussian distribution over the plume cross section. The centerline ground level concentrations should be the same so setting equation (3-7) equal to equation (3-8) gives a result for the initial vertical spread (3-9). Equation (3-10) is then

solved numerically to find the non-dimensional ground level concentration for each SB configuration. α is varied depending on the SB configuration and this value is determined based on the plume centerline, which is found from the visualizations. To investigate the dispersion pattern only, not affected by emission rate Q, normalized concentration C/Q, referred as dilution is presented (s/m^3, μs/m^3).
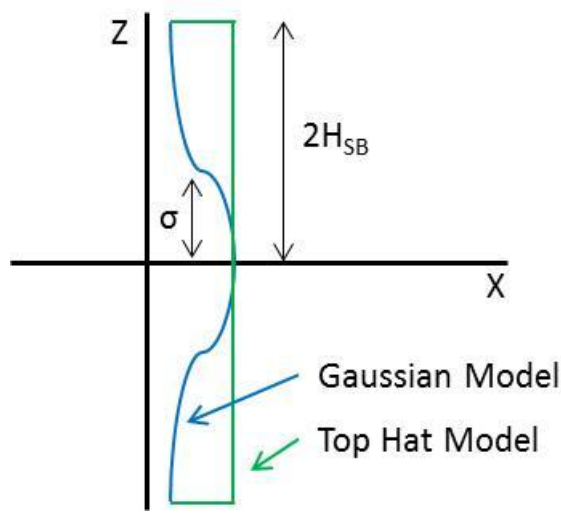

Figure 3-7. Model Comparison

$$\frac{C(x,0,0)}{Q} = \frac{1}{2\pi\sigma^2 U} \tag{3-7}$$

$$\frac{C(x,0,0)}{Q} = \frac{1}{(2H_{SB})^2 U} \tag{3-8}$$

$$\sigma = \sigma_o = \sqrt{\frac{2}{\pi}} H_{SB} \tag{3-9}$$

$$\frac{C(x,y,0)}{Q} = \frac{1}{\pi\sigma_y\sigma_z U} exp\left(-\frac{y^2}{2\sigma_y^2}\right) exp\left(-\frac{(\alpha H_{SB})^2}{2\sigma_z^2}\right) \tag{3-10}$$

Equation (3-10) was derived from equation (3-6) by taking $z = 0$, since ground level concentrations are desired, and placing the source on top of a SB ($h_e = \alpha H_{SB}$). The lateral (3-11)

16

and vertical (3-12) plume spreads are given by Briggs (1973) and x_{oy} and x_{oz} are based on the

water channel cross section of 1 m and 0.5 m respectively.

$$\sigma_y = 0.16x_r \left(1 + \frac{x_r}{x_{oy}} \right)^{-\frac{1}{2}} \qquad (3\text{-}11)$$

$$\sigma_z = 0.14x_r \left(1 + \frac{x_r}{x_{oz}} \right)^{-\frac{1}{2}} \qquad (3\text{-}12)$$

3.5. van Ulden 1978 with Modifications by Venkatram 2004 Model

In 1978 van Ulden introduced a model suitable for surface releases as a solution of the

advection diffusion equation. van Ulden (1978) derived the governing equations by using a wind

speed of $u(z) = u_1 z^n$, where u1 and n are constants, to account for the velocity changes with

height. This model was modified by Venkatram (2004). As mentioned in the preceding section, a

line source can be modeled as set of point sources and the contribution of each point source is

computed as follows (Venkatram, 2004):

$$\frac{C(x,y,z)}{Q} = \frac{A}{\sqrt{2\pi}\sigma_y \overline{U}\overline{z}} exp\left[-\left(\frac{Bz}{\overline{z}} \right)^s \right] exp\left[-\frac{y^2}{2\sigma_y^2} \right] \qquad (3\text{-}13)$$

$$B = \frac{\Gamma\left(\frac{2}{s} \right)}{\Gamma\left(\frac{1}{s} \right)} \qquad (3\text{-}14)$$

$$A = \frac{sB}{\Gamma\left(\frac{1}{s} \right)} \qquad (3\text{-}15)$$

where C (kg m^{-3}) is the concentration, Q (kg s^{-1}) is the emission rate, $\overline{U}$ (m s^{-1}) is the mean plume

velocity, $\overline{z}$ (m) is the mean plume height, σ_y (m) is the lateral plume spread and s depends on the

stability. The value of s was taken to be 1.5, which is an average value that was shown by van

Ulden (1978) and Venkatram (2004) to compare well with field experiments. The mean plume

velocity is a function of a horizontal velocity profile that is represented by a power law. A logarithmic velocity profile (Figure 2-2) was used in the water channel and QUIC, however, for this case, the PIV data was fitted to a power law profile and this resulted in $U(z) = 0.0422z^{0.2803}$. One of the main disadvantages of Gaussian dispersion models, and two dimensional advection diffusion models, is that it is not straightforward to implement any three dimensional changes in the mean flow (e.g. channeling) that may result from obstacles such as sound barriers and buildings.

The results of each of the described techniques will be presented.   PIV flow measurements (Section 4) are first, since these velocity measurements are essential for interpretations of all results from other techniques. Next, in Section 5, the qualitative plume behavior obtained through visualizations is presented. These qualitative results were used to select relevant configurations for quantitative concentration measurements which are presented together with numerical modeling results in Section 6.

4.   Particle Image Velocimetry (PIV) Results

PIV measurements were conducted as described in Section 2.1. PIV is invaluable for determining the mean flow pattern induced by different roadway configurations, which can help explain pollutant dispersion and the results of visualizations. The effects of SBs were studied for each of the roadway configurations shown in Figure 4-1. In Figure 4-1 $U(z)$ refers to the incoming wind profile and the red line represents the line source. The effects of vegetation, terrain (raised and sunken roadways), buoyancy, ground heating, traffic induced turbulence (TIT) and mechanical ventilation (addition of fans) were studied only for the configurations of No SB and SBs of equal height ($H_{up} = H_{down}$).
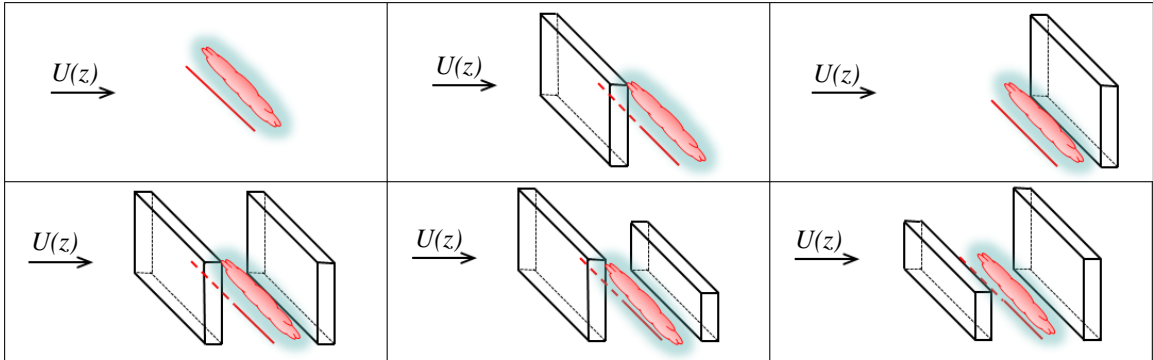
Figure 4-1. Water Channel SB Configurations

4.1. Results of Flat Roadway Configurations

Figure 4-2 shows the PIV results for the flat roadway configurations. It is noted that there is only one velocity scale shown, and this applies to all the plots in the figure and this is typical of all PIV Figures in this chapter. Shown in the upper right hand corner of each plot in Figure 4-2 is a schematic of the roadway configuration tested along with a blue window which outlines the section in which PIV was done, this is typical for all PIV Figures in this chapter. The PIV results show that the presence of SBs produces a recirculating flow on the roadway, which increases the mixing of pollutants. This can also be seen in the visualizations (Section 5.1). The recirculating flow is heavily dependent on the SB configuration. For the roadway configuration of upwind only SB (Figure 4-2b) there is a recirculating flow on the roadway extending up to 2 SB heights downwind of the road. This recirculation causes pollutants to be brought back toward the barrier resulting in higher on road concentrations. For the case of downwind only SB (Figure 4-2c), there is a small recirculation on the upwind side of the barrier, which can trap pollutants on the edge of the road. For the case of $H_{up} = H_{down}$ (Figure 4-3a), this recirculating flow is limited to the roadway width. For the case of $H_{up} = 2H_{down}$ (Figure 4-3b) and $H_{down} = 2H_{up}$ (Figure 4-3c) there is recirculating flow that develops on the roadway which is dominated by the taller SB and this recirculation is smaller than the case of $H_{up} = H_{down}$.

19
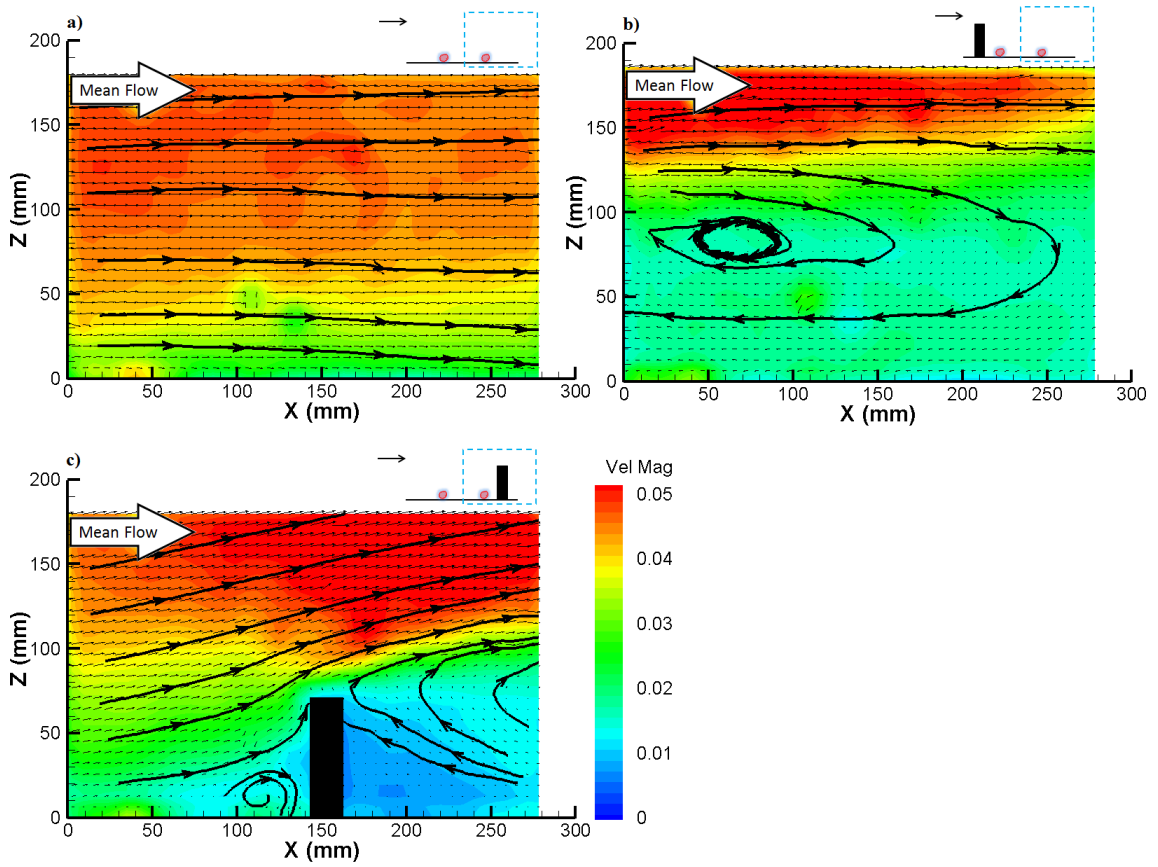
Figure 4-2. PIV Flat Roadway: a) No SB; b) Upwind Only SB; c) Downwind Only SB. Thick lines represent the streamlines. Light blue rectangle on the schematics in upper right corners represents the region of presented PIV measurements.
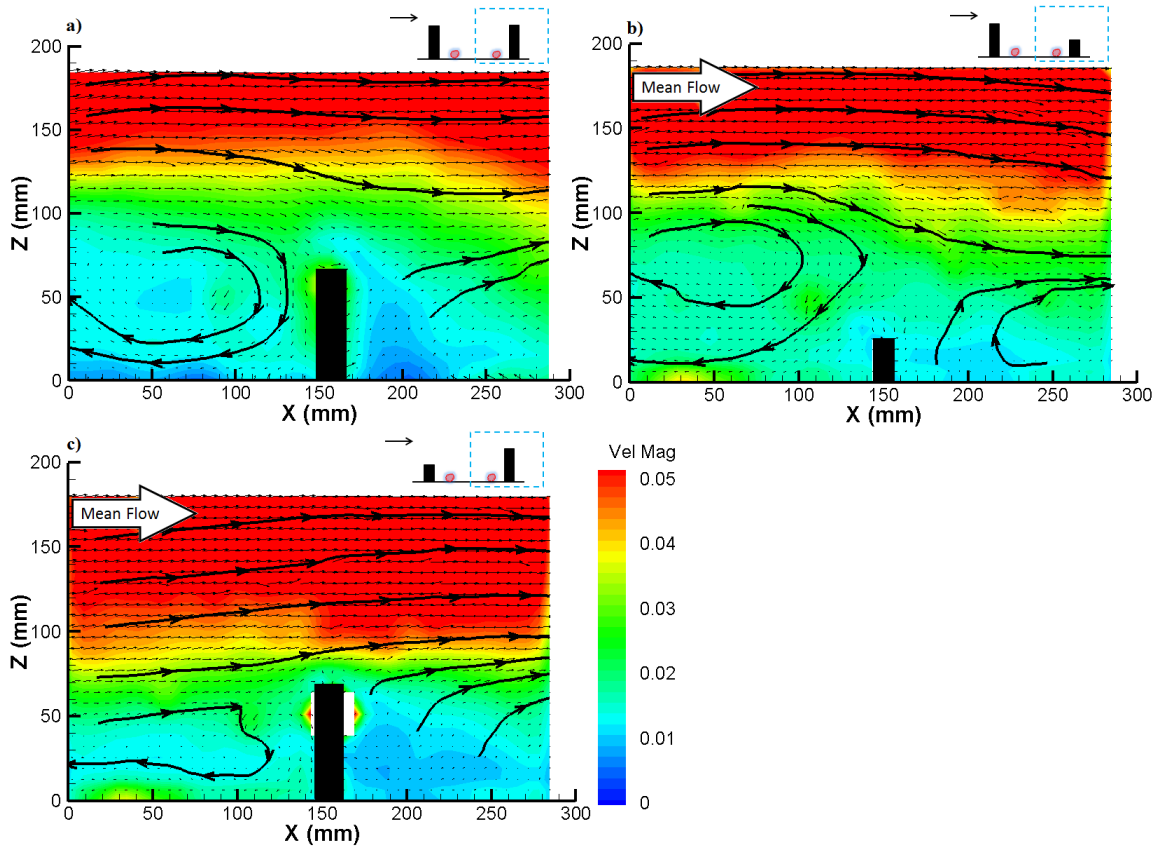
Figure 4-3. PIV Flat Roadway with upwind and downwind SB: a) $H_{up} = H_{down}$; b) $H_{up} = 2H_{down}$; c) $H_{down} = 2H_{up}$

4.2. Results of Vegetation

Due to its porous nature, the addition of vegetation does not have as significant impact on the flow as the SBs do. The three models in tested configurations have leaf area index between 0.67 and 0.85. Deposition on the trees is not considered which is not an issue since tree surfaces become saturated fast. It is seen that the vegetation does decrease the velocity compared to the flat roadway case of No SB. Low velocities are observed on the lee side of the vegetation resulting in a small wake region (Figure 4-4b, c). Increased turbulence in the wake results in increased mixing and increased vertical spread of the plume compared to the flat roadway case of No SB (see section 5, Figure 5-12).
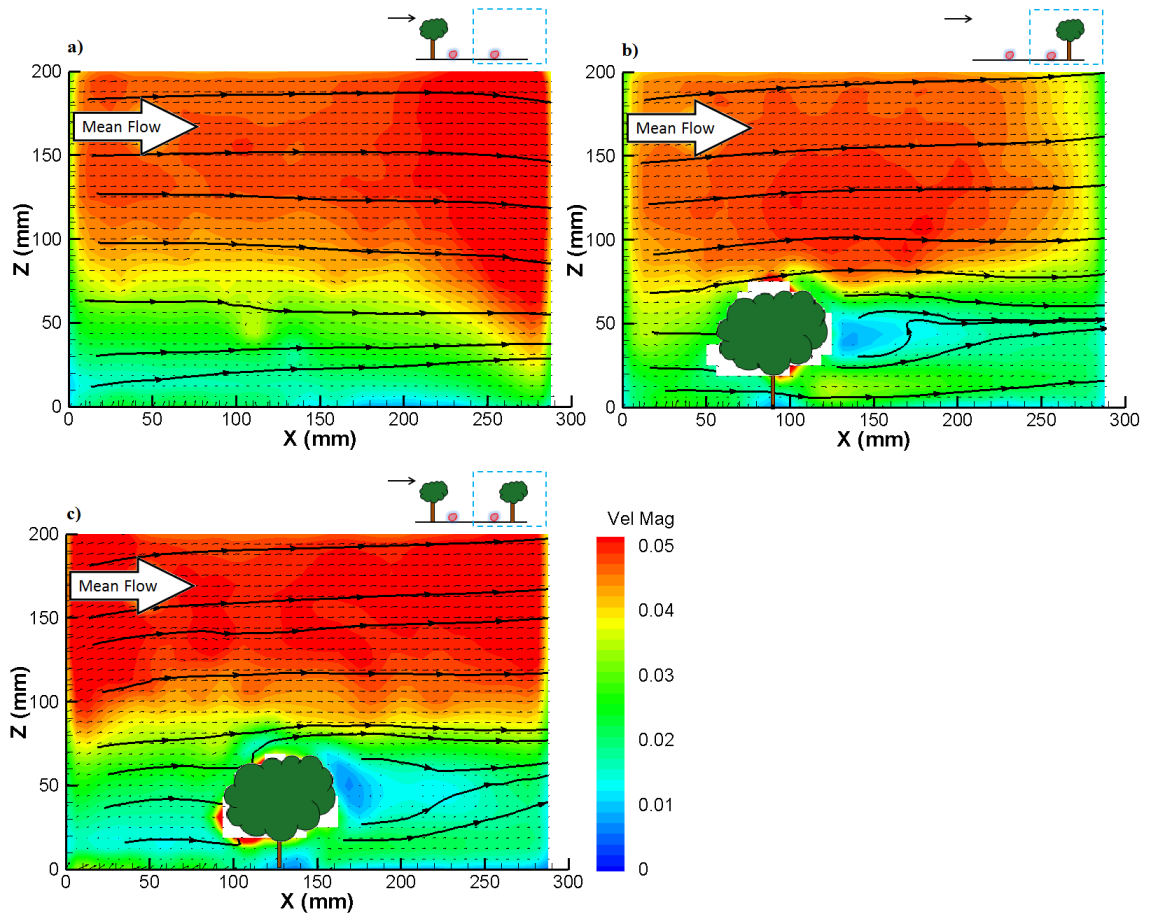
Figure 4-4. PIV Vegetation: a) Upwind Only Trees; b) Downwind Only Trees; c) Trees on Both Sides of the Road

4.3. Results of Raised Roadways

For the case of No SB there are strong downdrafts observed downwind of the roadway due to the depression in the terrain (Figure 4-5a). These downdrafts can cause the plume to descend towards the ground and the high velocities can reduce the vertical spread resulting in higher ground level concentrations. The presence of SBs causes recirculation on the roadway as well as recirculation on the downwind sloping terrain which mixes the pollutants (Figure 4-5b). Due to the elevation of the plume and the recirculation caused by the SBs, the ground level concentrations should be less than that of the same SB configuration for a flat roadway. Raised

roadway with SBs effectively makes the source higher which leads to lower ground level concentrations. Similar is and with overpasses: emission source is high and the wake of the overpass would be small to bring the plume down (overpass configuration was not tested). Likely problem with the overpass configuration is trapping of emissions released from other sources beneath the overpass.
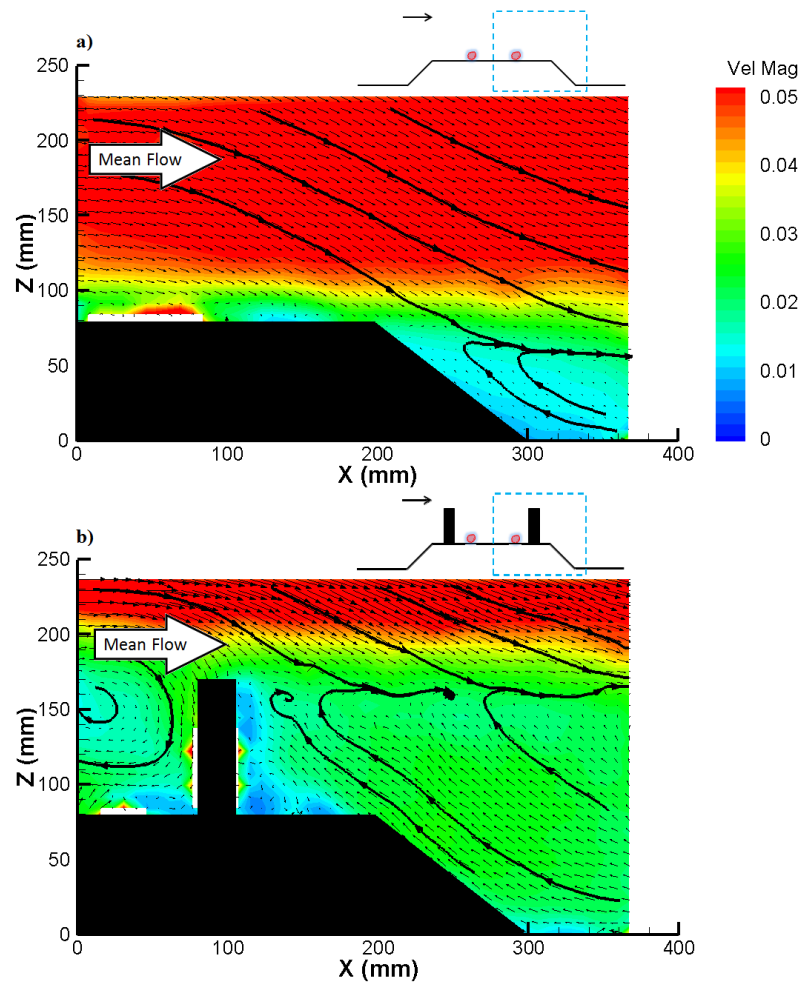
Figure 4-5. PIV Raised Roadway: a) No SB; b) $H_{up} = H_{down}$

4.4. Results of Sunken Roadways

For the case of No SB the flow follows the terrain and lower velocities on the roadway are observed (Figure 4-6a), this would result in no significant change in the concentrations compared to the flat roadway. The presence of SBs produces recirculation on the roadway (Figure 4-6b) and, due to the depressed terrain, low on road velocities are observed compared to the flat roadway. This large recirculation and lower velocities results in greater on road vertical spread of the plume but higher on road concentrations compared to No SB.
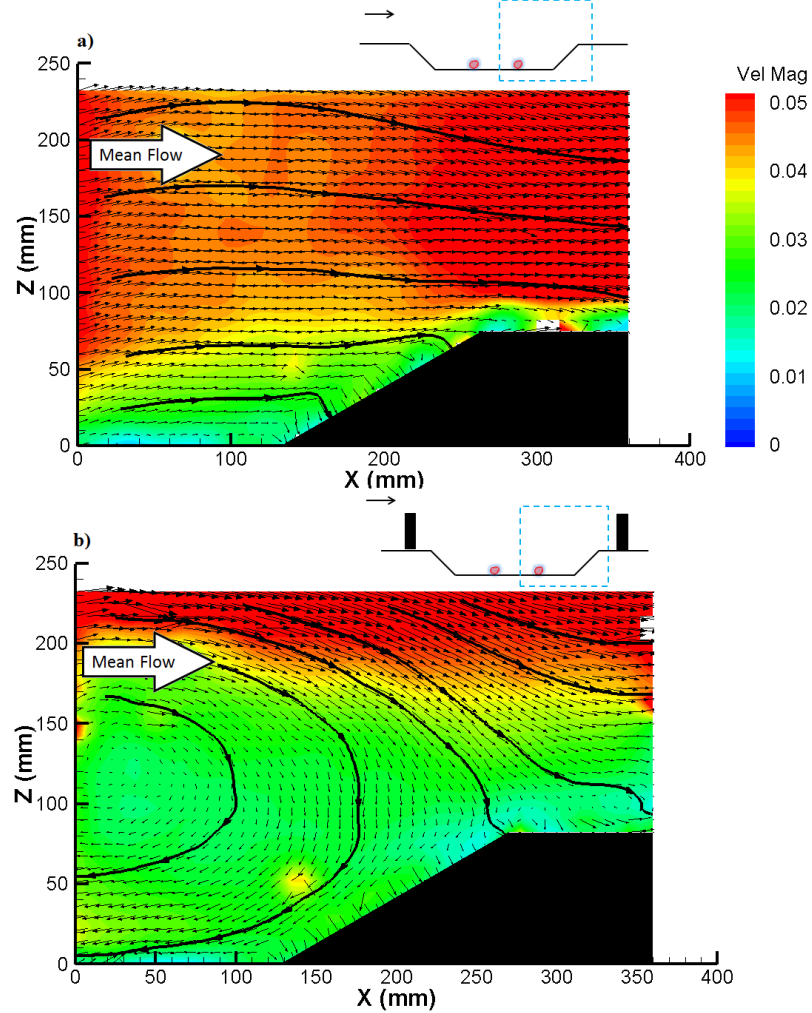
Figure 4-6. PIV Sunken Roadway: a) No SB; b) $H_{up} = H_{down}$

4.5. Results of Varying Wind Direction

The effects of varying the wind angle on the flow field between the barriers are shown in Figures 4-7 and 4-8. The SB models (50 cm long) were placed in the middle of the channel with enough space from the ends of SB to the channel walls (approximately 25 cm on each side) to allow for along the road channeling to occur. All horizontal velocity fields presented in this section were measured at the half height of the sound barriers. The effect of wind angle was studied by varying the roadway angle relative to the incoming flow, since the flow in the water channel is unidirectional. For wind perpendicular to the SBs there is a pair of counter rotating eddies that develops in the roadway as well as on the lee side of the downwind barrier. Increasing the wind angle increases the channeling effect and decreases the strong on road horizontal recirculation. As shown, with a wind angle of 60° from normal, there is extreme channeling in which the flow in the bulk of the roadway is nearly aligned with the incoming wind. Large wind angles, that change the flow from recirculating to channeling, result in high on road concentrations as little or no pollutants will be removed from the road.

Additional experiments were done in which the SBs were rotated at two degree increments (Figures 4-9 through 4-13), which simulates an incoming wind at an angle of 2° to 10° from normal. At 2° there is almost no effect, there are still two counter rotating eddies on the road. At 4° there is an increased effect in which the center of the left eddy is shifted towards the left end of the SB. At 6° to 10° there is the presence of some channeling as the flow is brought towards the upwind side of the downwind SB and there is flow reversal at the left side of the downwind SB. The full channeling does not occur as it is evident from the presence of the on road eddy, which is now shifted from the center of the roadway to the right side of the upwind

SB. As the wind angle increases the on road eddies will disappears and the full, along the road, channeling will exist.

These types of findings are relevant for off ramps. At the off ramps the channeled pollutants on the roadway will find its way out. Off ramps are not in the scope of present project but are important topic for future work.
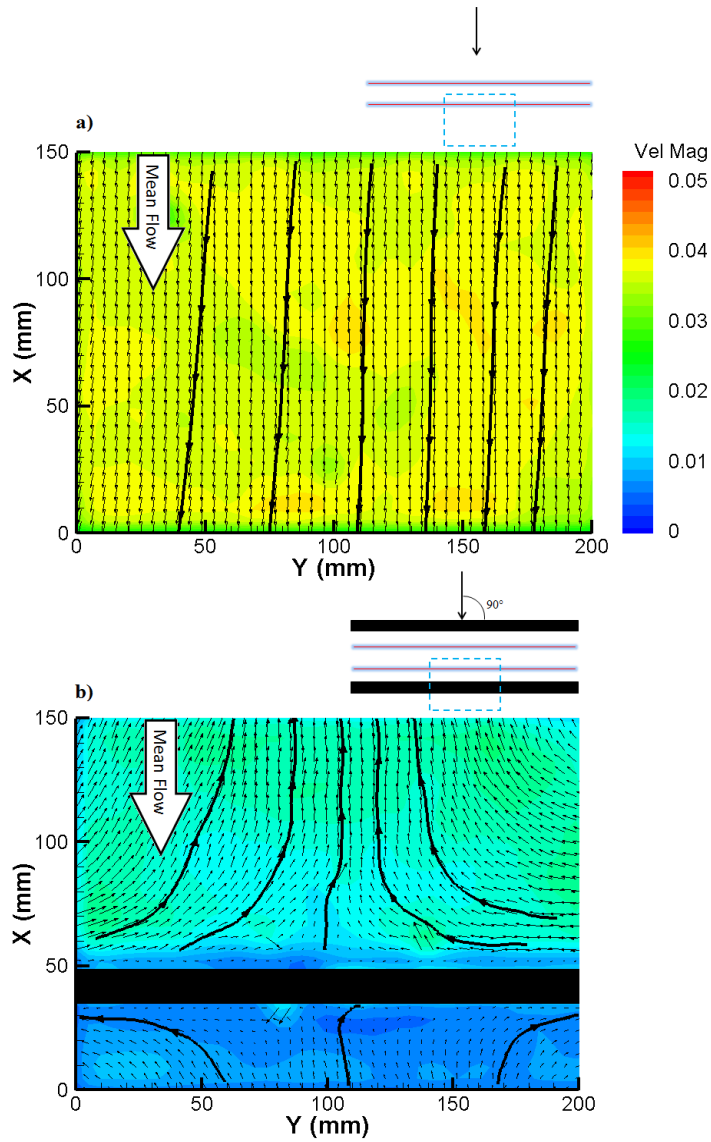

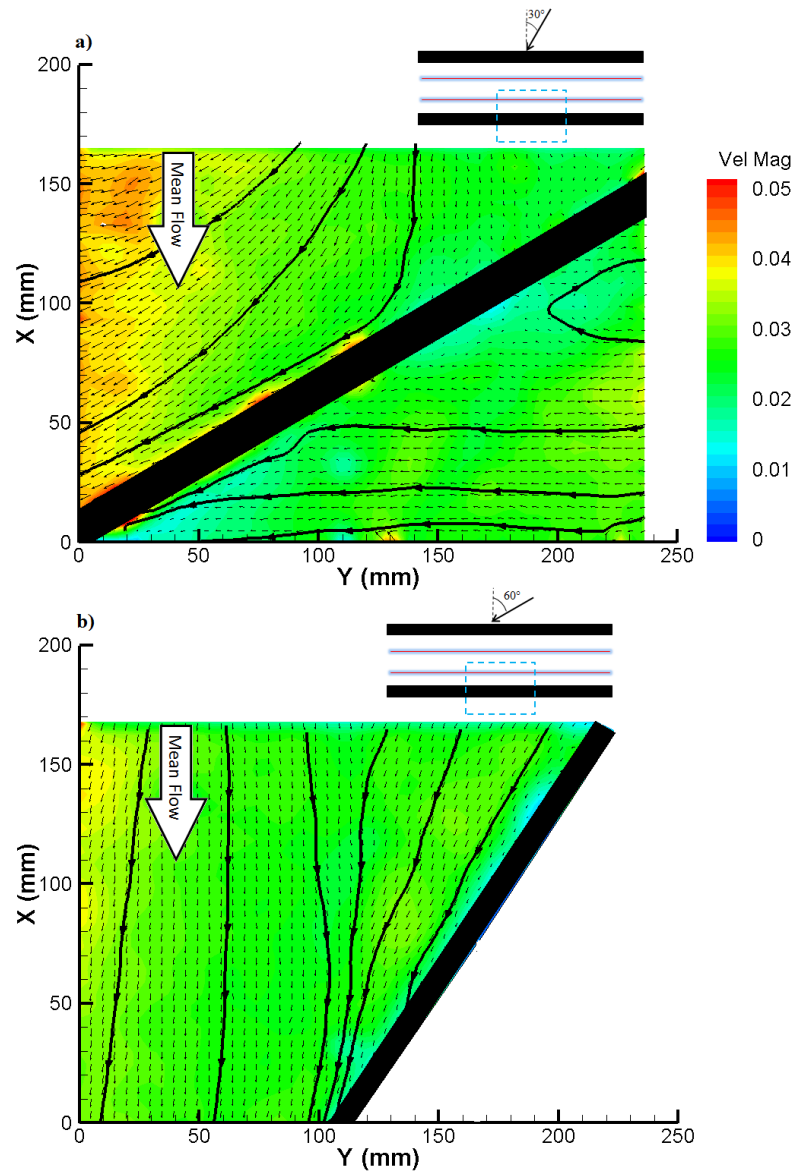**Figure 4-7.** PIV Wind Direction: a) No SB, $\theta_{wind} = 90°$; b) $H_{up} = H_{down}$, $\theta_{wind} = 90°$

Figure 4-8. PIV Wind Direction, $H_{up} = H_{down}$: a) $\theta_{wind} = 30°$; b) $\theta_{wind} = 60°$
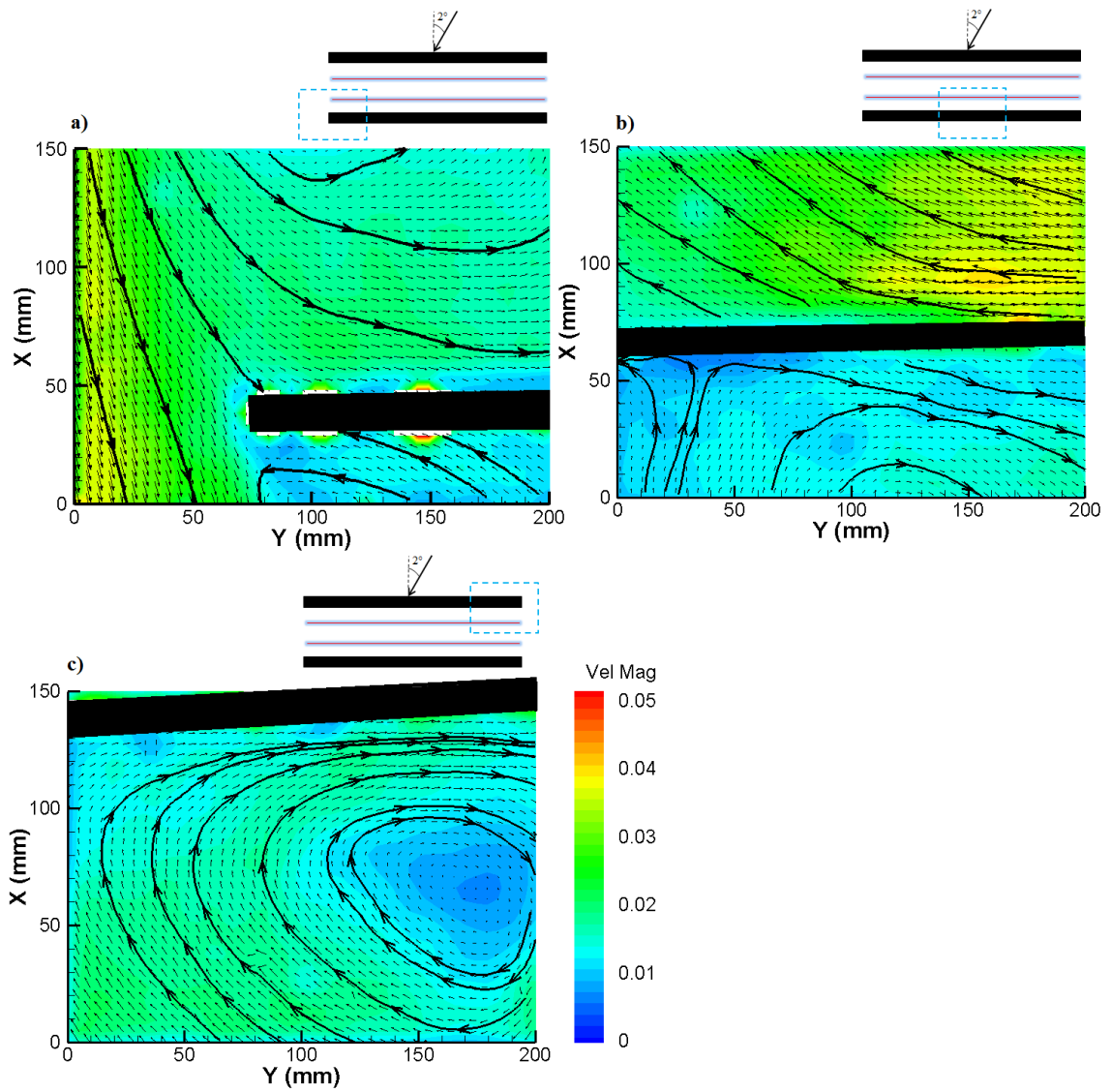
Figure 4-9. PIV Wind Direction, $H_{up} = H_{down}$: a) Left Side, $\theta_{wind} = 2°$; b) Center, $\theta_{wind} = 2°$; c) Right Side, $\theta_{wind} = 2°$
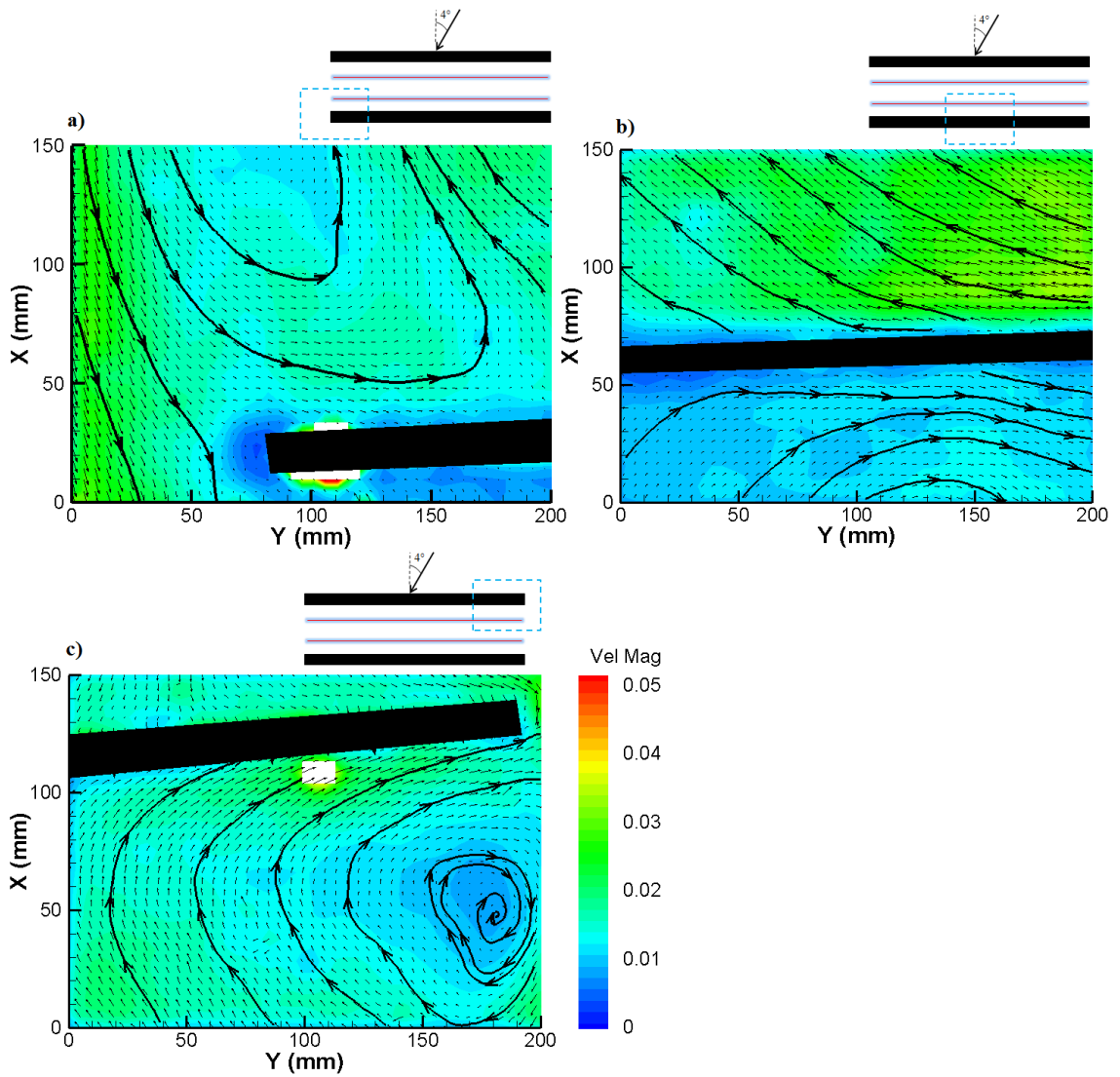
Figure 4-10. PIV Wind Direction, $H_{up} = H_{down}$: a) Left Side, $\theta_{wind} = 4°$; b) Center, $\theta_{wind} = 4°$; c) Right Side, $\theta_{wind} = 4°$
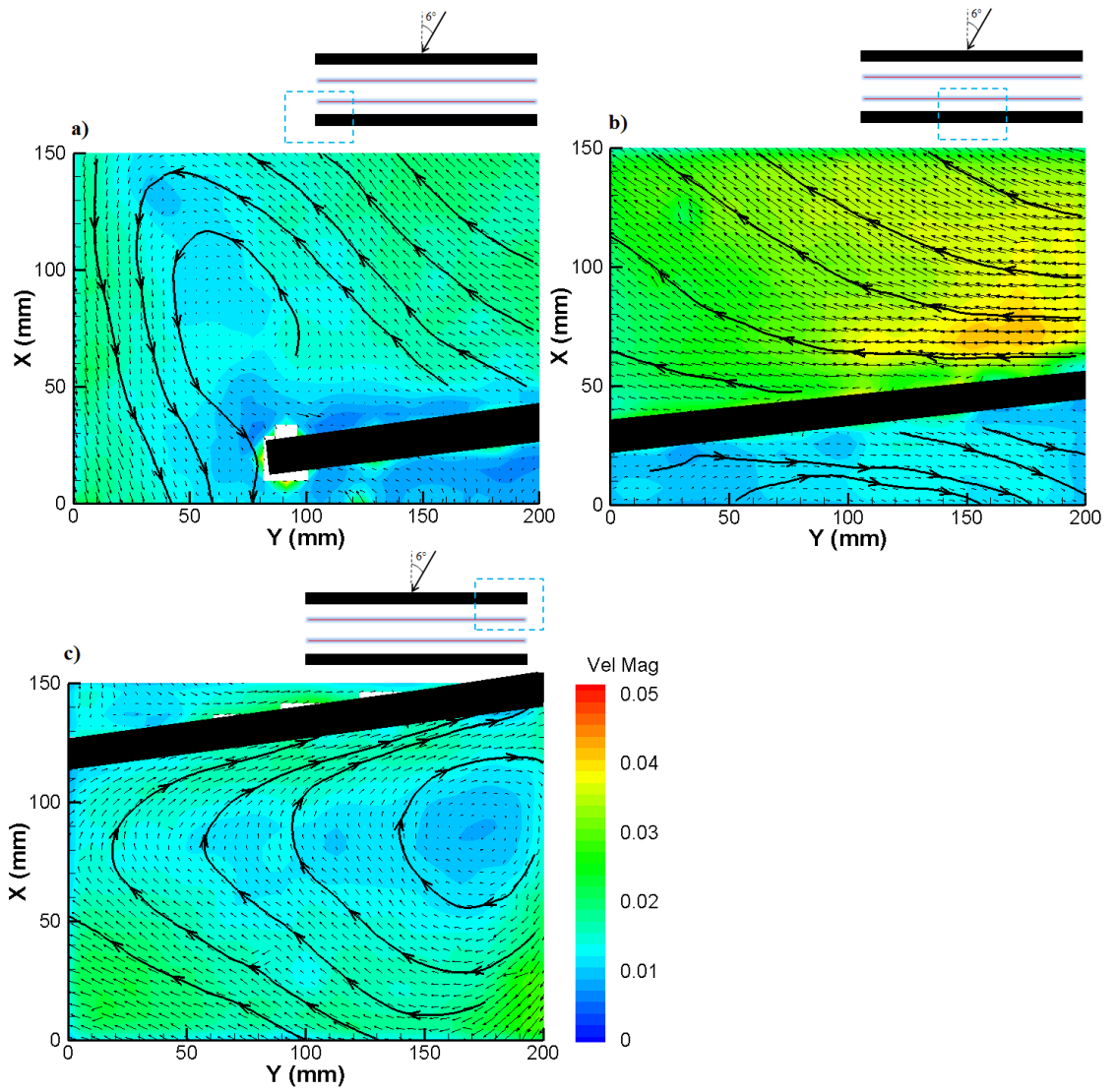
Figure 4-11. PIV Wind Direction, $H_{up} = H_{down}$: a) Left Side, $\theta_{wind} = 6°$; b) Center, $\theta_{wind} = 6°$; c) Right Side, $\theta_{wind} = 6°$
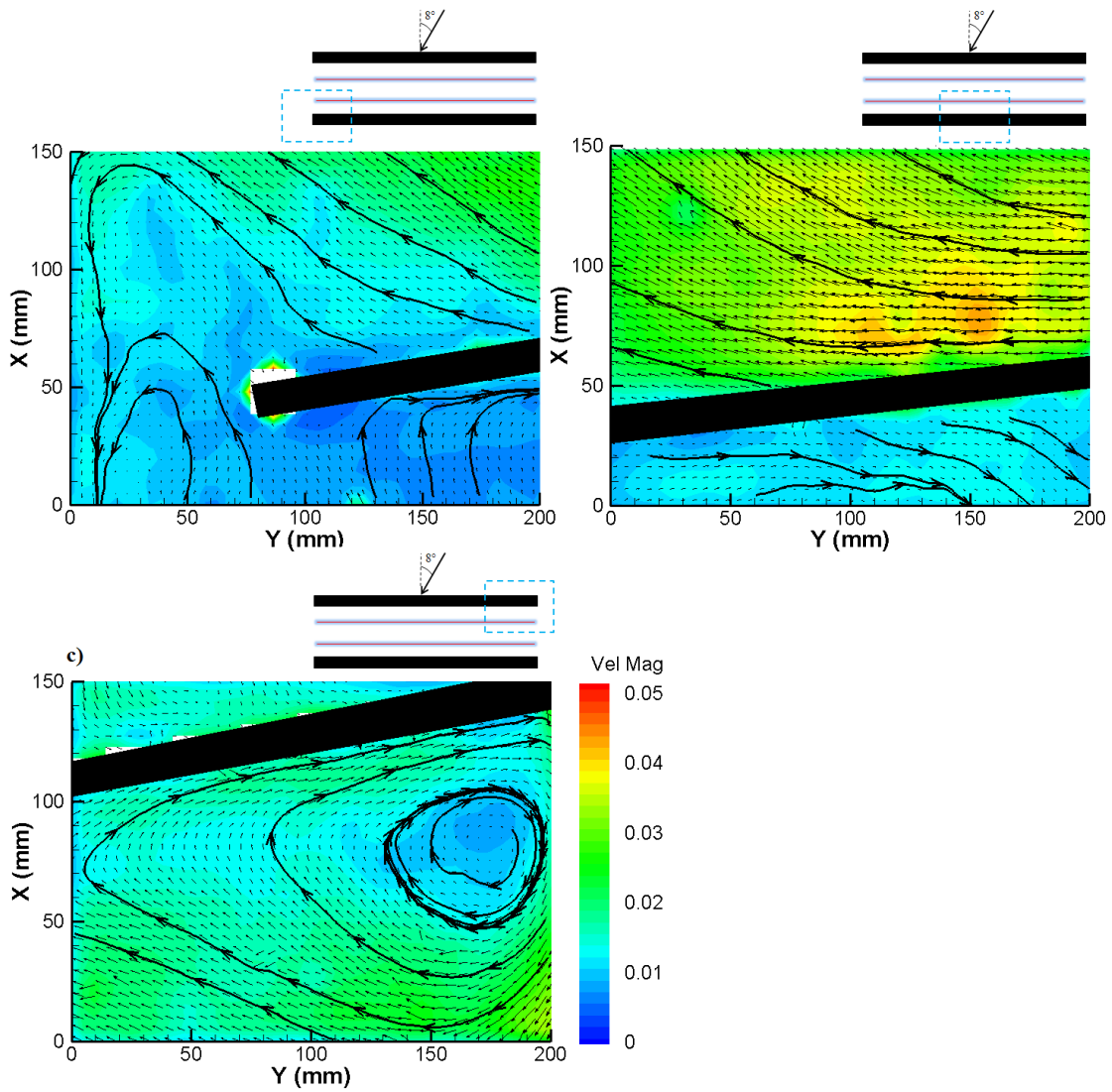
Figure 4-12. PIV Wind Direction, $H_{up} = H_{down}$: a) Left Side, $\theta_{wind} = 8°$; b) Center, $\theta_{wind} = 8°$; c) Right Side, $\theta_{wind} = 8°$
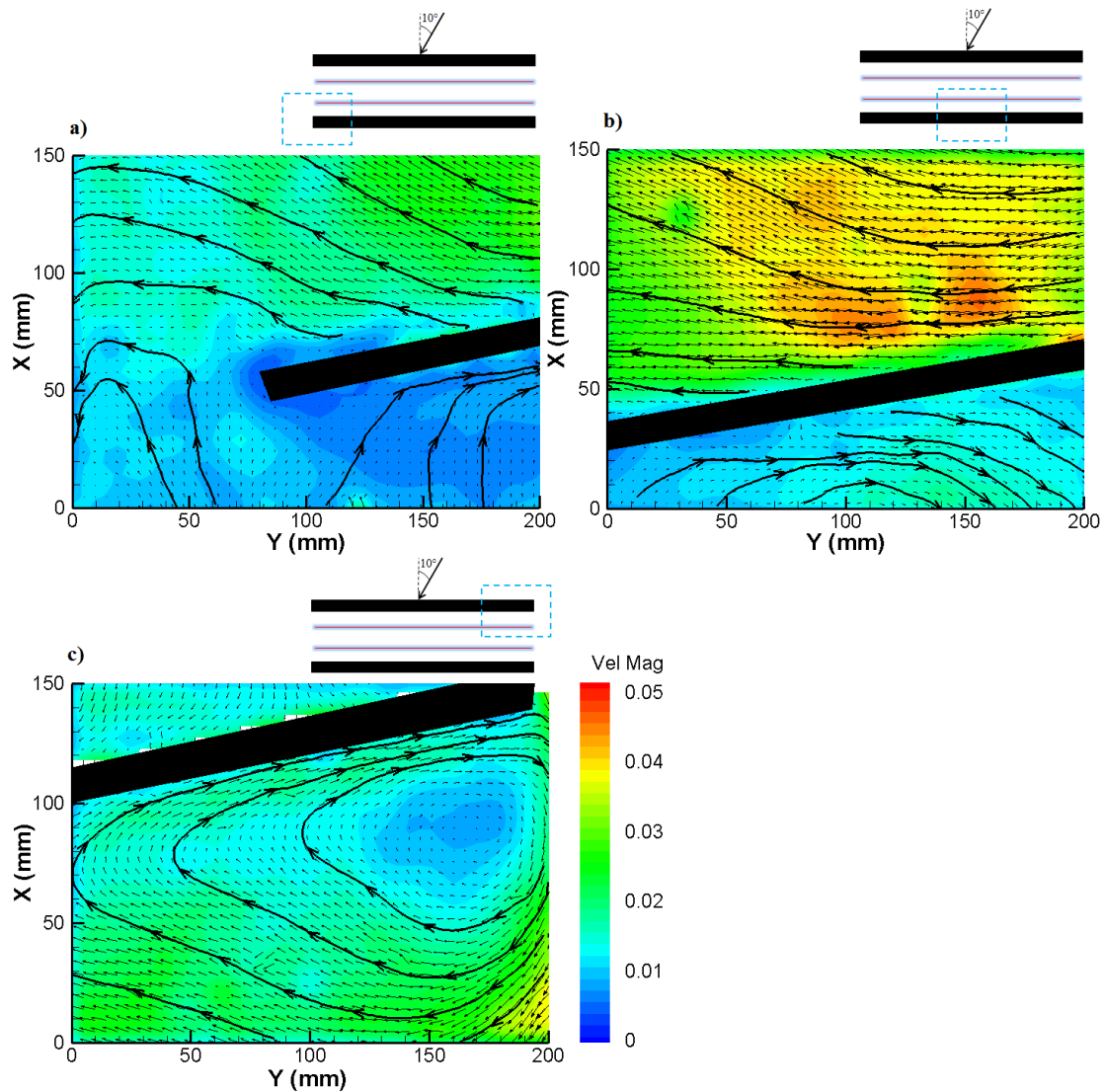
Figure 4-13. PIV Wind Direction, $H_{up} = H_{down}$: a) Left Side, $\theta_{wind} = 10°$; b) Center, $\theta_{wind} = 10°$; c) Right Side, $\theta_{wind} = 10°$

4.6. Results of Traffic Induced Turbulence

The effects of Traffic Induced Turbulence (TIT) were studied using a custom made traffic simulator (Figure 4-14). Due to size limitations of the water channel it was not possible to have traffic flow in one direction only. Instead, a custom designed slider crank oscillating mechanism was used. As shown in Figure 4-14 there are two tracks with cars, which are out of phase, and the number of cars and the spacing between each car can be changed and this changes

the traffic density. Due to the strong mechanical mixing in the wake of vehicles, any plume rise due to heated exhaust is expected to be small (Rao et al., 2002). Traffic rates were selected based on the 2010 Traffic Volumes from the California Department of Transportation, which contains data for all California state highway locations. Throughout the state the peak traffic volume ranges from 10 to 30,000 vehicles per hour depending on area. The flow rate of 1.4 vehicles-s^{-1} (approximately 121,000 Annual Average Daily Traffic (AADT) traveling in one directions) was found to be an average traffic flow rate in the Inland Empire and Los Angeles areas. Doubling this traffic flow rate (2.8 vehicles-s^{-1}) was also studied and these two frequencies are used to test the effects of traffic instead of vehicle velocity. This data was also used to look at traffic densities as the data shows the number of miles per traffic volume. A rough estimate of the number of vehicles per freeway mile in the Inland Empire and Los Angeles areas is between 100 vehicles-mi^{-1} to 200 vehicles-mi^{-1}. To look at the effects of traffic density the cars where spaced two car lengths apart for low traffic density and one car length apart for high traffic density, this translates to 0.079 vehicle-cm^{-1} (127 vehicles-mi^{-1} scaled to the field) and 0.16 vehcles-cm^{-1} (257 vehicles-mi^{-1} scaled to the field) respectively. This type of car spacing can be observed during daily driving on freeways.

The effects of traffic were studied for both low and high traffic frequencies (1.4 Hz and 2.8 Hz) as well as low and high traffic densities (0.079 vehicle-cm^{-1} and 0.16 vehicle-cm^{-1}). Here one has to keep in mind that the flow of traffic was simulated by oscillatory motion of obstacles. As such, the obstacles accelerate in one direction, decelerate and start moving in different direction which makes the averaged model velocity zero. However, we can interpret the frequency of oscillations as the number of cars that pass through a highway cross-section. Assuming vehicle length of 5 m and distance between the vehicles to be also 5 meters, the frequency of 1.4 Hz would translate to turbulence caused by average vehicle velocity of 31 MPH.

As shown in the PIV results, the addition of vehicles influences the flow field along the *X-Z* Plane more so due to the presences of the vehicles then the effects of motion, this is especially true for the higher wind speeds. In low wind speed conditions, increasing the traffic frequency decreases the downdraft due to the vehicles and increases the velocity near the vehicles, this is shown to be true with and without the presences of SBs. For the case of No SB with high wind speed, increasing the traffic frequency results in decreased velocity on the lee side of the vehicles. This is due to the increased perturbations from the vehicles counter acting with the higher wind speed, thus reducing the overall velocity magnitude on the lee side of the vehicles.
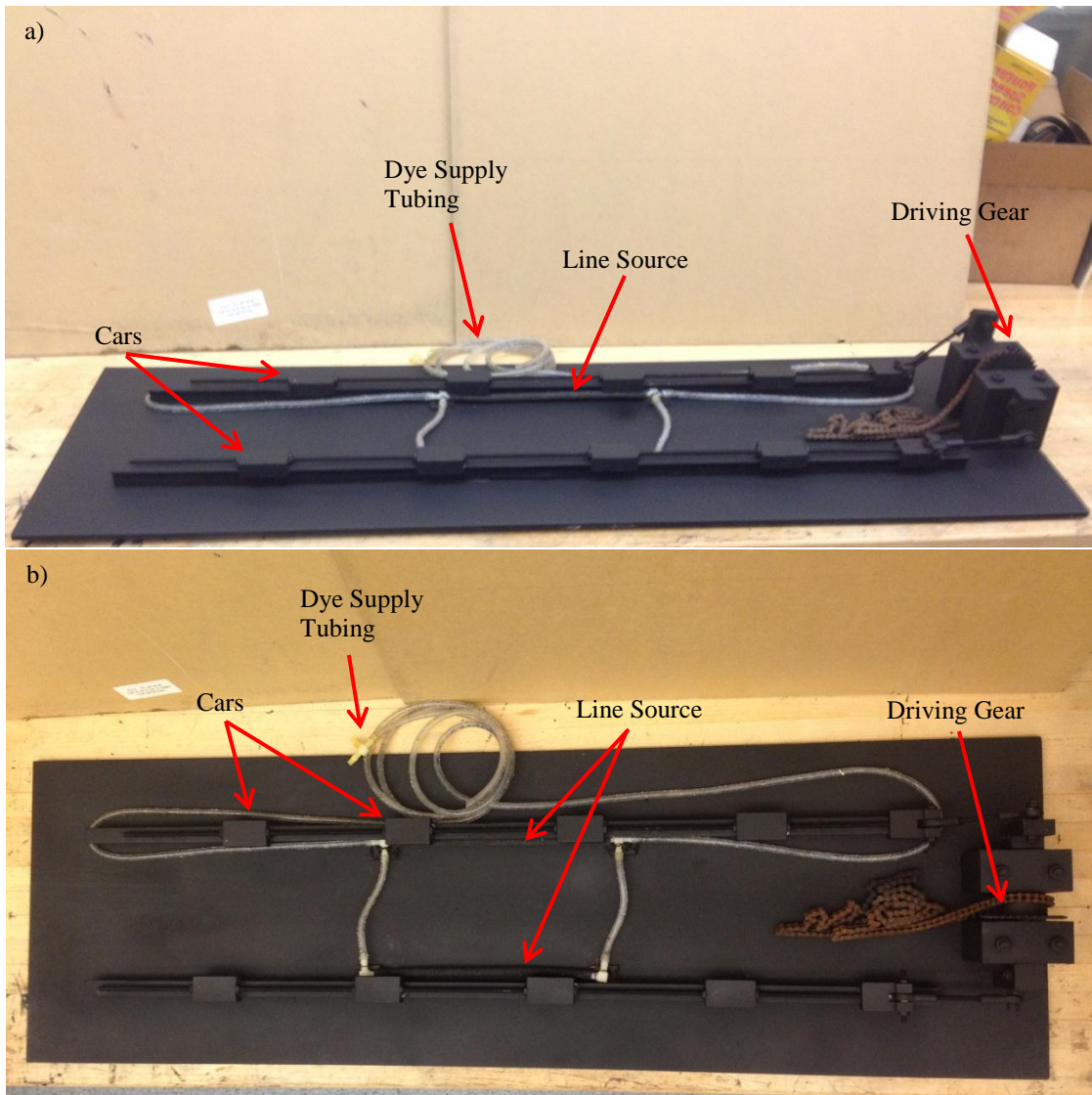
Figure 4-14. Traffic Simulator: a) Side View; b) Top View
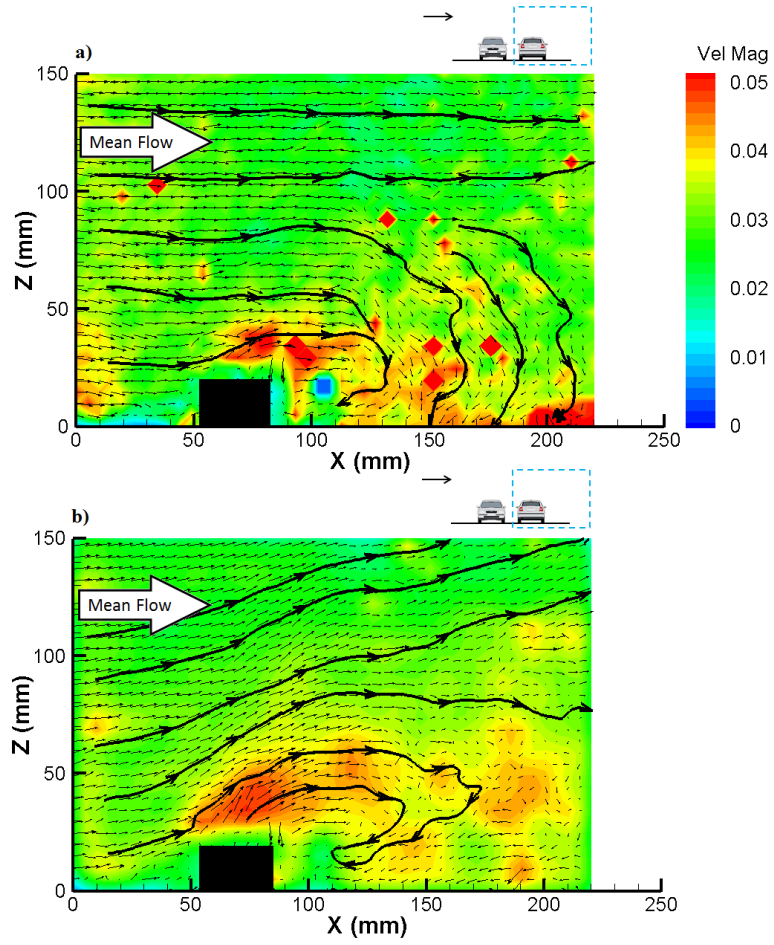
Figure 4-15. PIV measurements of Traffic Induced Turbulence (TIT) for High Traffic Density and Low Ambient Wind Speed: a) No SB and Low TIT Frequency; b) No SB and High TIT Frequency
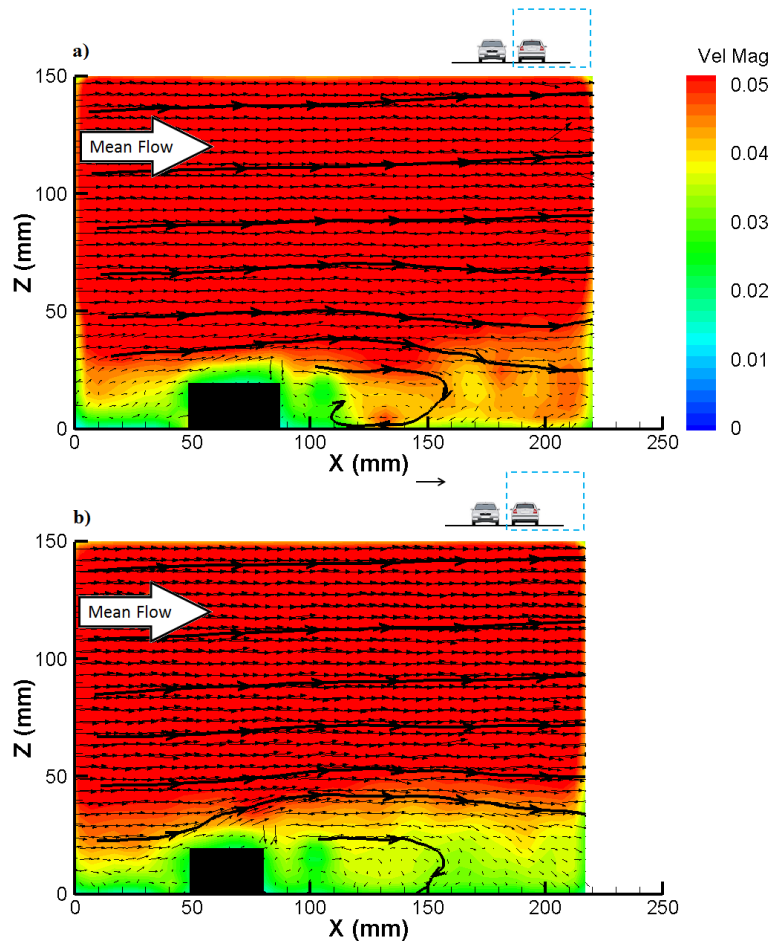
Figure 4-16. PIV measurements of Traffic Induced Turbulence for High Traffic Density and High Ambient Wind Speed: a) No SB and Low TIT Frequency; b) No SB and High TIT Frequency
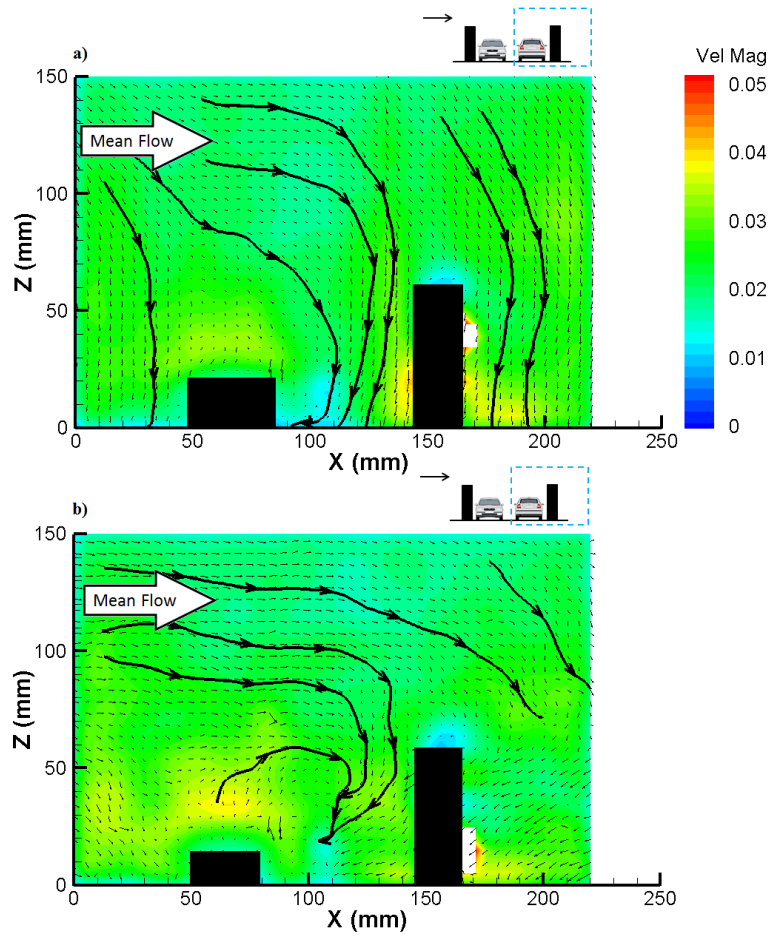
Figure 4-17. PIV measurements of Traffic Induced Turbulence (TIT) for High Traffic Density and Low Ambient Wind Speed: a) $H_{up} = H_{down}$, and Low TIT Frequency; b) $H_{up} = H_{down}$ and High TIT Frequency
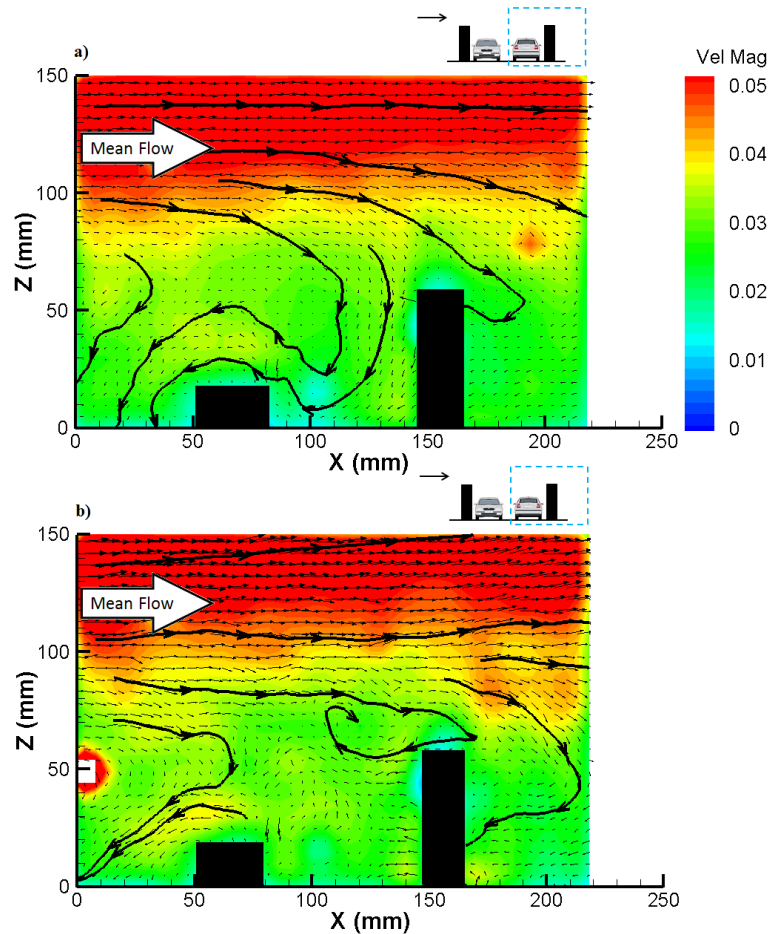
Figure 4-18. PIV measurements of Traffic Induced Turbulence (TIT) for High Traffic Density and High Ambient Wind Speed: a) $H_{up} = H_{down}$ and Low TIT Frequency; b) $H_{up} = H_{down}$ and High TIT Frequency

4.7. Results of Mechanical Ventilation (Fans)

During low wind speed conditions it may be best to look at mechanical (active) means of removing pollutants from the roadway. For that reason fans were deployed in the water channel to look at the effects of ventilating pollutants from the roadway. A custom made apparatus composed of three fans was fabricated (Figures 4-19, 20). Each fan measures 40mm and they are powered by a grinder through a gear train. For this application, the most important aspects are the outlet velocity and the flow rate, which is dictated by the fan size and speed, and this has a significant impact on the power requirements. Referring to pump and fan affinity laws, the power

requirement is proportional to the flow rate cubed. Thus a small change in the flow rate (or given a fixed fan size, a change in velocity) can result in a large increase in the power needed. Through internet research or available solar panels, it appears that the maximum available size (suitable for SB applications) of a solar panel is approximately 70"×40"×2", and the power output is roughly 250 W (1/4 hp). The type of fan recommended would be an axial type of fan. Through internet research of well-known fan companies it was found that axial fans can provide approximately 3,000 cfm (1.4 $m^3 s^{-1}$) at 1/4 hp. These fans vary in size from 18 in (46 cm) to 30 in (76 cm) and can achieve the desired outlet velocity of approximately 5 m s^{-1}. This application would most likely require a custom design due to the environment, and the power and velocity requirements.
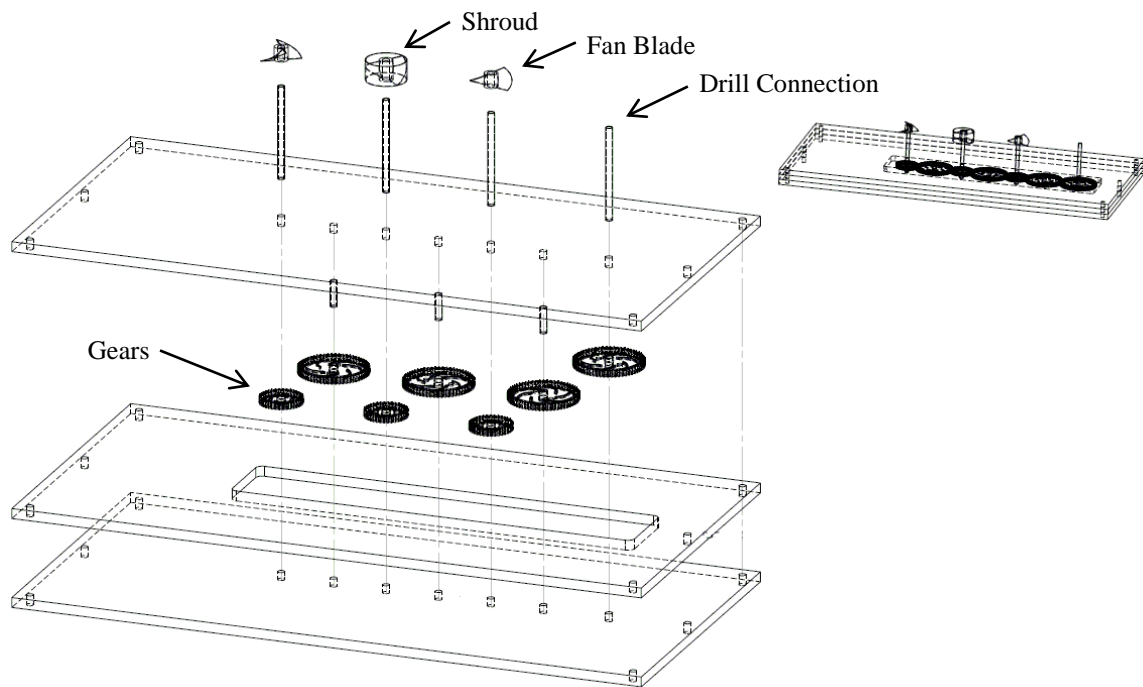
Figure 4-19. Schematic of the Fan Simulator Model
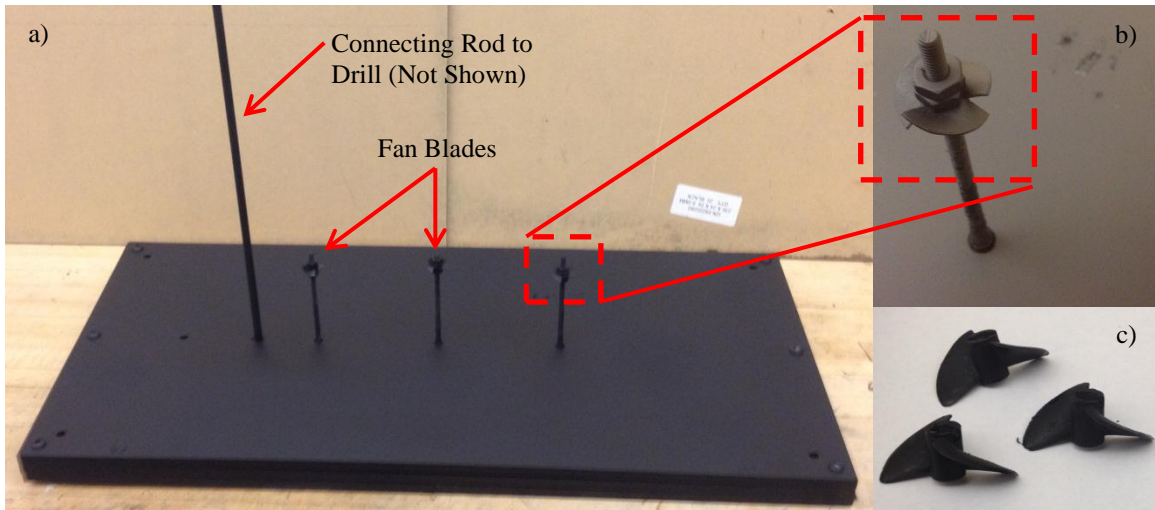
Figure 4-20. Fan Simulator: a) Working Model; b) Custom Fan Blade; c) Propellers

In a realistic field application, fans would most likely be installed along short stretches of highways in which SBs separate roadways from critical areas, such as schools and homes. One way to approach this problem is to look at a segment of roadway as a box with dimensions $H \times W \times L$, with the height (H) of this box being 4 m (26 ft). The SB height used in most of this research was 8 m and the ventilation height was chosen as half the SB height because vehicle height is less than the SB height and also because vehicular emissions are output close to the ground. Since the height is specified, the volume now becomes a function of the roadway area, where W is the width and L is the length. The major driver of the number and size of fans is dictated by the ventilation volume, but if the requirement existed, the number air changes per hour (AC-hr^{-1}) could be the driver. Since there is currently no requirement for the number of air changes per hour for roadways, assumptions can be made. Assuming a single fan can exhaust 3,000 cfm at 1/4 hp, the number of AC-hr^{-1} was varied and it was found that 0.004 fans-m^{-3} are needed for 20 AC-hr^{-1} and 0.002 fans-m^{-3} are needed for 10 AC-hr^{-1}. For example, in order to flush a segment of roadway that is 4m×30m×30m, 14 fans would be needed for a requirement of 20 AC-hr^{-1} and 7 fans would be needed for a requirement of 10 AC-hr^{-1}. Larger fans can pull

more volume and the number of fans needed would decrease, but in order to maintain 1/4 hp, the outlet velocity would suffer.

The fans were tested at the following three settings/speeds: 1) Low setting with a mean outlet velocity of 2 m s^{-1} 2) Medium setting with a mean outlet velocity of 5 m s^{-1} and 3) High setting with a mean outlet velocity of 9 m s^{-1}. From the PIV results (Figures 4-21, 22 and 23) it is seen that that fans have the most impact under low wind speed conditions. The fans loft the plume vertically which increases the overall plume rise and reduces the ground level concentrations by getting the plume above the downdraft on the lee side of the downwind barrier. There is very little impact under high wind speed conditions except for the fan setting of high, though a slight loft of the plume can be observed in the visualizations.
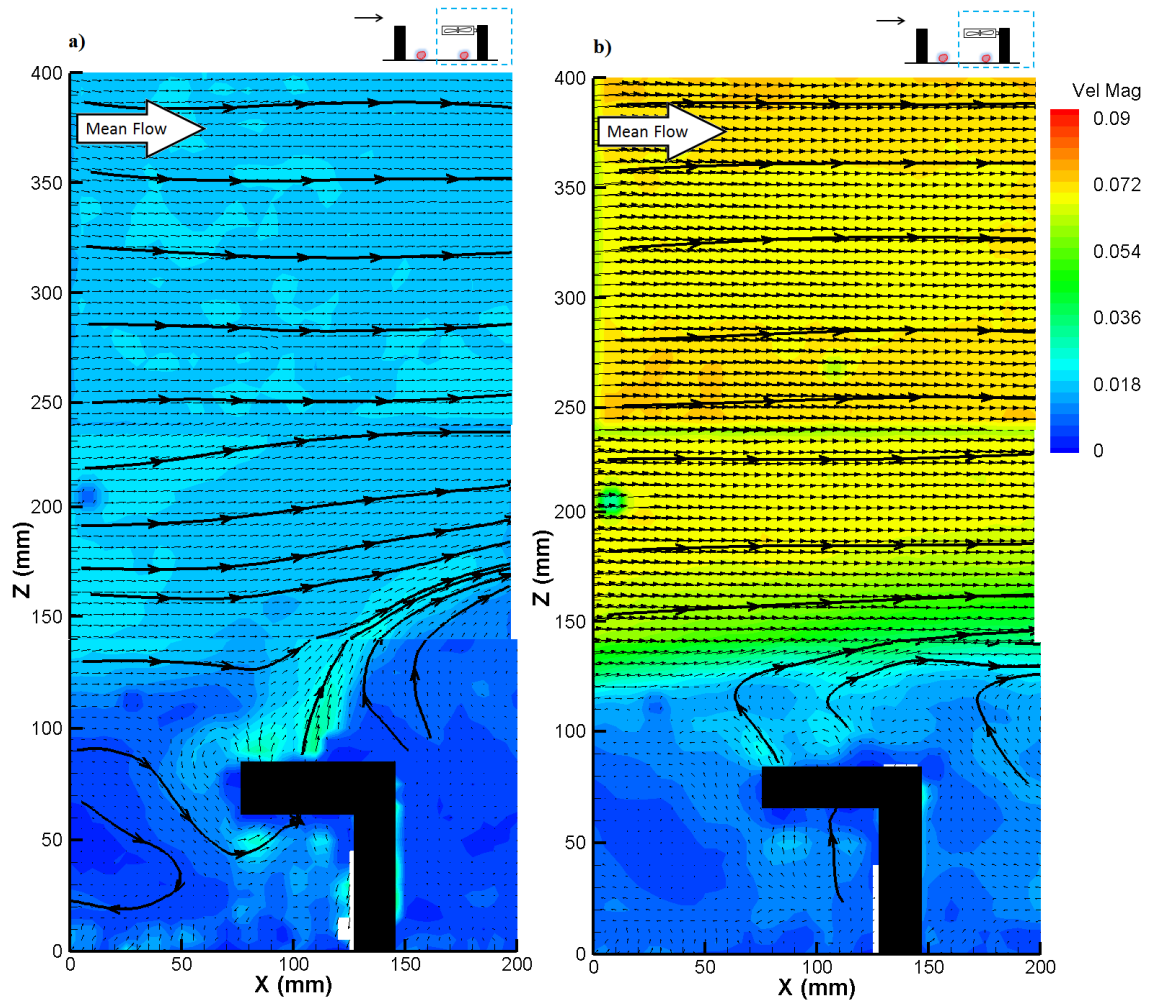
Figure 4-21. PIV measurements of Fans, $H_{up} = H_{down}$: a) Low Wind Speed and Low Fan Setting; b) High Wind Speed and Low Fan Setting

43
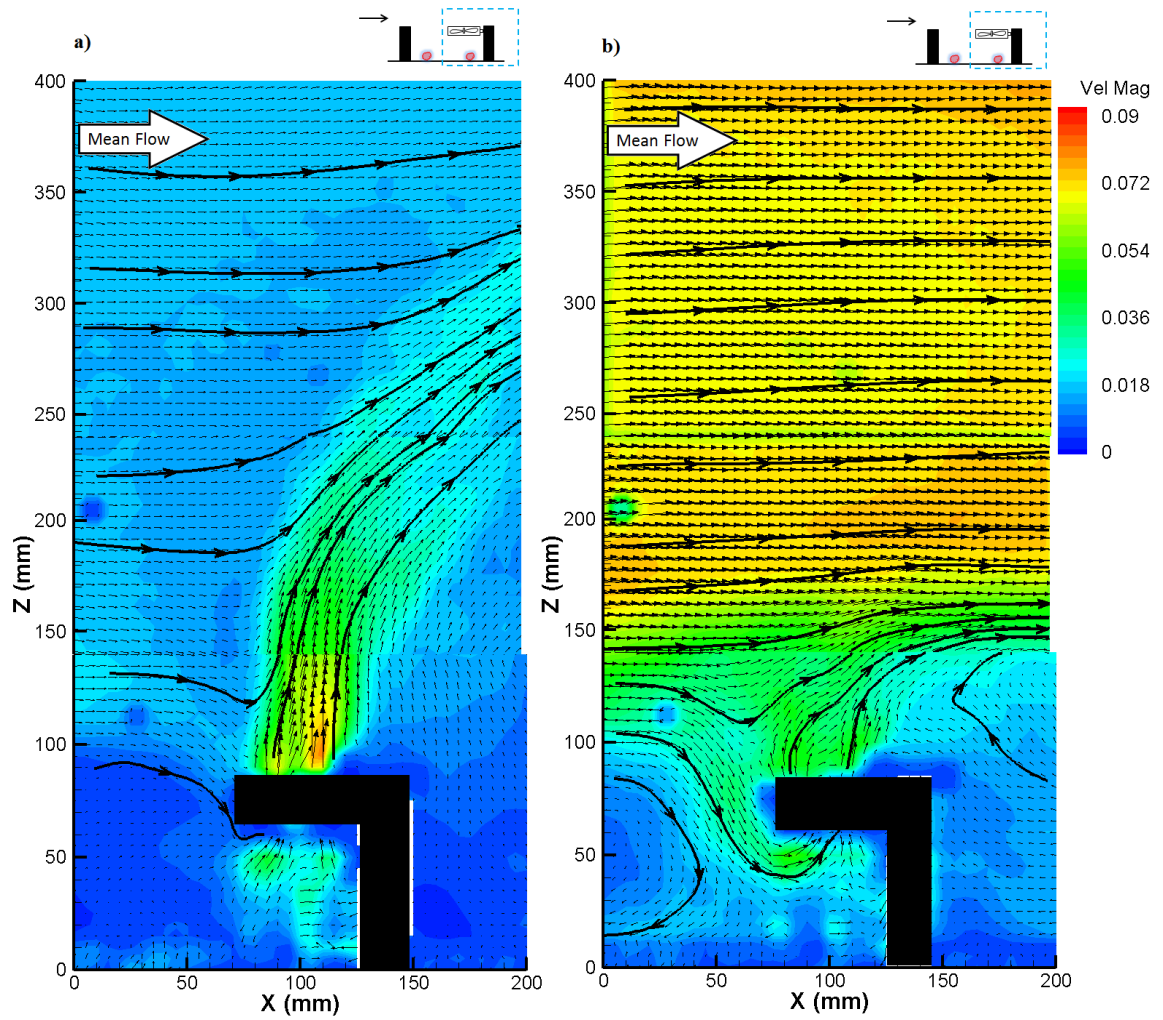
Figure 4-22. PIV measurements of Fans, $H_{up} = H_{down}$: a) Low Wind Speed and Medium Fan Setting; b) High Wind Speed and Medium Fan Setting
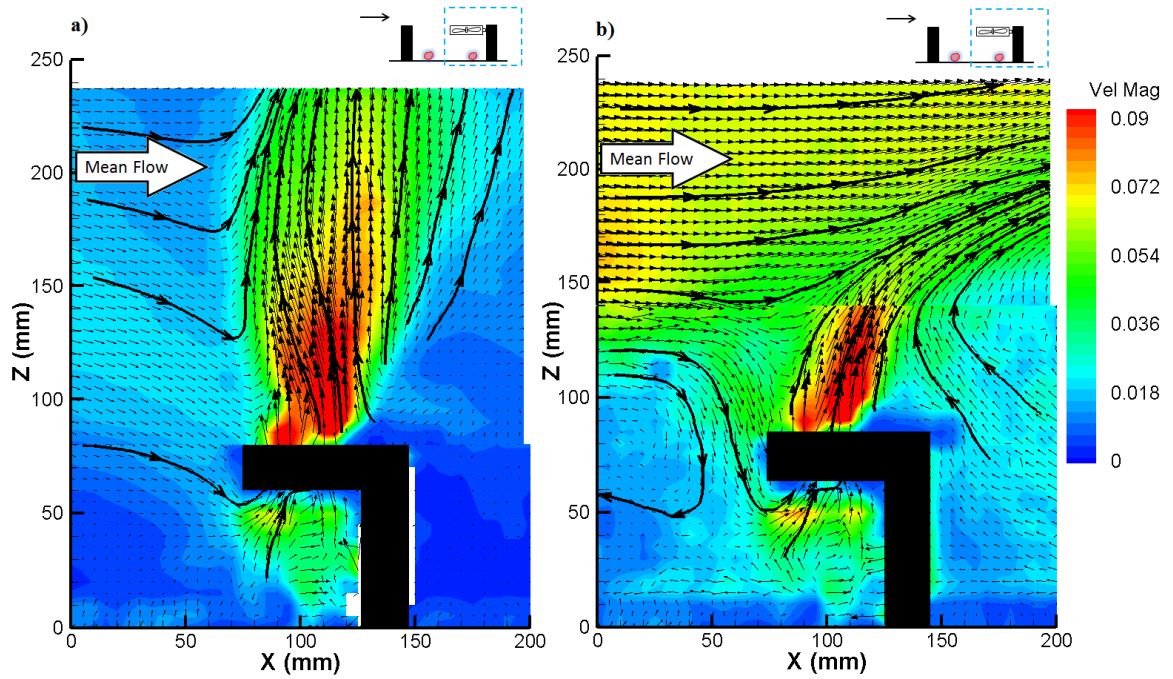
Figure 4-23. PIV Fans, $H_{up} = H_{down}$: a) Low Wind Speed and High Fan Setting; b) High Wind Speed and High Fan Setting

Through the PIV results for the fans, the average outlet velocity and vertical displacement was found. This is shown in Figure 4-24, and this gives an idea of the vertical loft and speed of the plume at various fan and wind speeds.
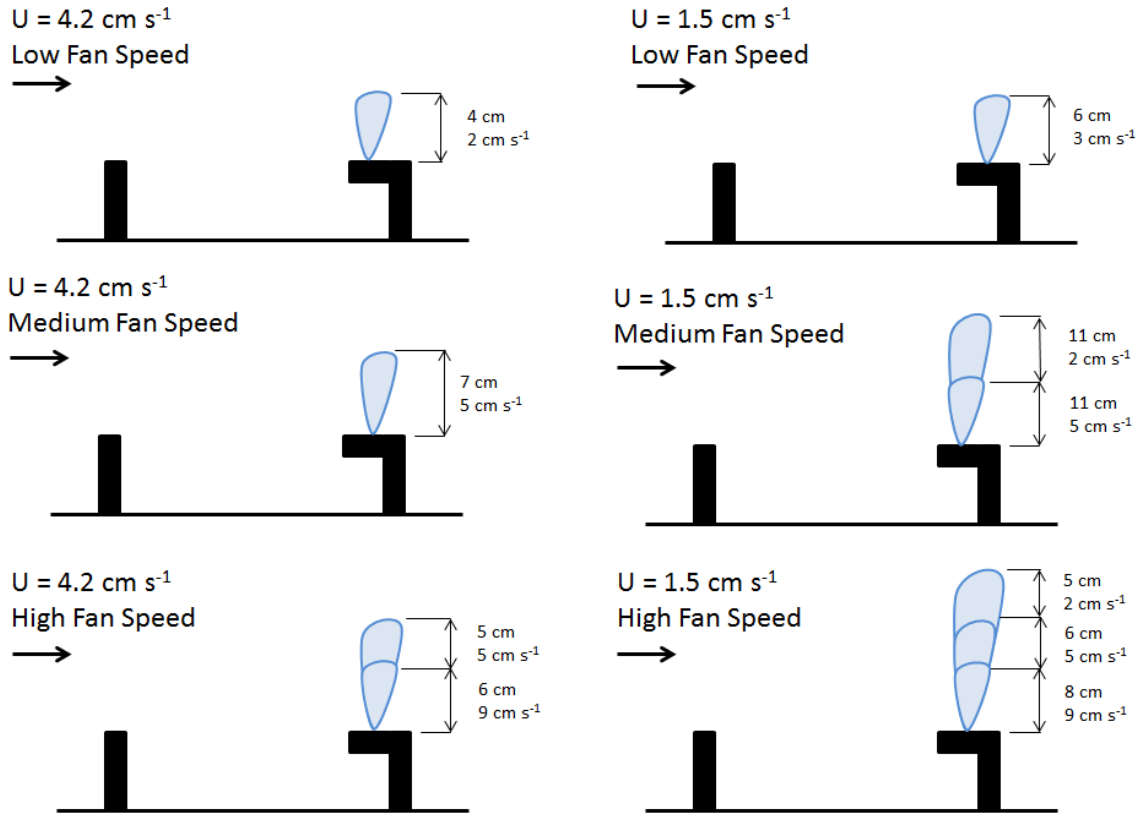
Figure 4-24. Fan Outlet Velocity and Displacement per Varying Fan and Wind speeds

4.8. Turbulence and Shear Stress

The turbulence induced by the presence of SBs is analyzed by looking at the Turbulent Kinetic Energy (TKE) and the Turbulent Intensities. The Shear Stress is analyzed by investigating the distribution of the Reynolds Stresses. This was done for the main roadway configurations and selected configurations of traffic. TKE, Turbulent Intensity and Reynolds Stress is calculated as follows:

$$TKE = \frac{1}{2}(u_{RMS}^2 + w_{RMS}^2) = \frac{1}{2}(\overline{u'u'} + \overline{w'w'}) \qquad (4\text{-}1)$$

$$I_{turb} = \frac{\sqrt{TKE}}{\overline{V}} = \frac{\sqrt{\frac{1}{2}(u_{RMS}^2 + w_{RMS}^2)}}{\sqrt{u^2 + w^2}} = \frac{\sqrt{\frac{1}{2}(\overline{u'u'} + \overline{w'w'})}}{\sqrt{u^2 + w^2}} \qquad (4\text{-}2)$$

$$R_{ij} = \overline{u_i' u_j'} = \overline{u'w'} \tag{4-3}$$

where *TKE* (m^2 s^{-2}) is the Turbulent Kinetic Energy, u_{RMS} (m s^{-1}) is the standard deviation of the horizontal velocity fluctuations and w_{RMS} (m s^{-1}) is the standard deviation of the vertical velocity fluctuations, u' (m s^{-1}) is the horizontal velocity fluctuation, w' (m s^{-1}) is the vertical velocity fluctuation, $\overline{V}$ (m s^{-1}) is the mean velocity, u (m s^{-1}) is the horizontal velocity, w (m s^{-1}) is the vertical velocity, R_{ij} (m^2 s^{-2}) is the Reynolds Stress tensor where i and j are the two dimensional space indexes (for this case).

As shown, the case of no SB (Figure 4-25) is trivial in which there is relatively little TKE, turbulent intensity and turbulent transport (low Reynolds stresses). The flow is uniform, but still turbulent. It is noted that the 'white holes' in Figure 4-25 and also seen in Figures 4-26 through 4-30 are due to uncertainties in the plots, which may be due to fluctuations spikes, however, the plots still represent the turbulence. For the case of upwind only SB (Figure 4-26) there is high turbulence above the SB that extends further downwind and below this there is high turbulence intensity which is a result of the on road recirculation due to the shear generated by the SB. For the case of downwind only SB (Figure 4-27) there is high shear that is generated by the top of the SB and this results in high TKE. It was shown by the PIV results that there are low velocities and a recirculation cavity on the lee side of the barrier, this results in very low turbulence and low transport which can lead to low concentrations. There is somewhat of a boundary layer created on the lee side of the barrier in which there are much higher velocities and turbulence around it. For the case of $H_{up} = H_{down}$ (Figure 4-28) there is high shear and turbulence above the SBs. Due to the high shear there is transport of on road pollutants that are advected by the upwind SB. There is however, a drop in turbulence and shear near the downwind barrier which is a result of the interaction of the two SBs. For the cases of $H_{up} = 2H_{down}$ and $H_{down} = 2H_{up}$

47

(Figures 4-29 and 4-30) there is stronger turbulence on the lee side of the taller SB. The case of $H_{up} = 2H_{down}$ shows the strongest shear and turbulence (coming off the upwind SB and extending further downwind past the downwind SB) of all the SB configurations but still comparable to the case of upwind only SB. All turbulent quantities are averaged over 30 seconds.
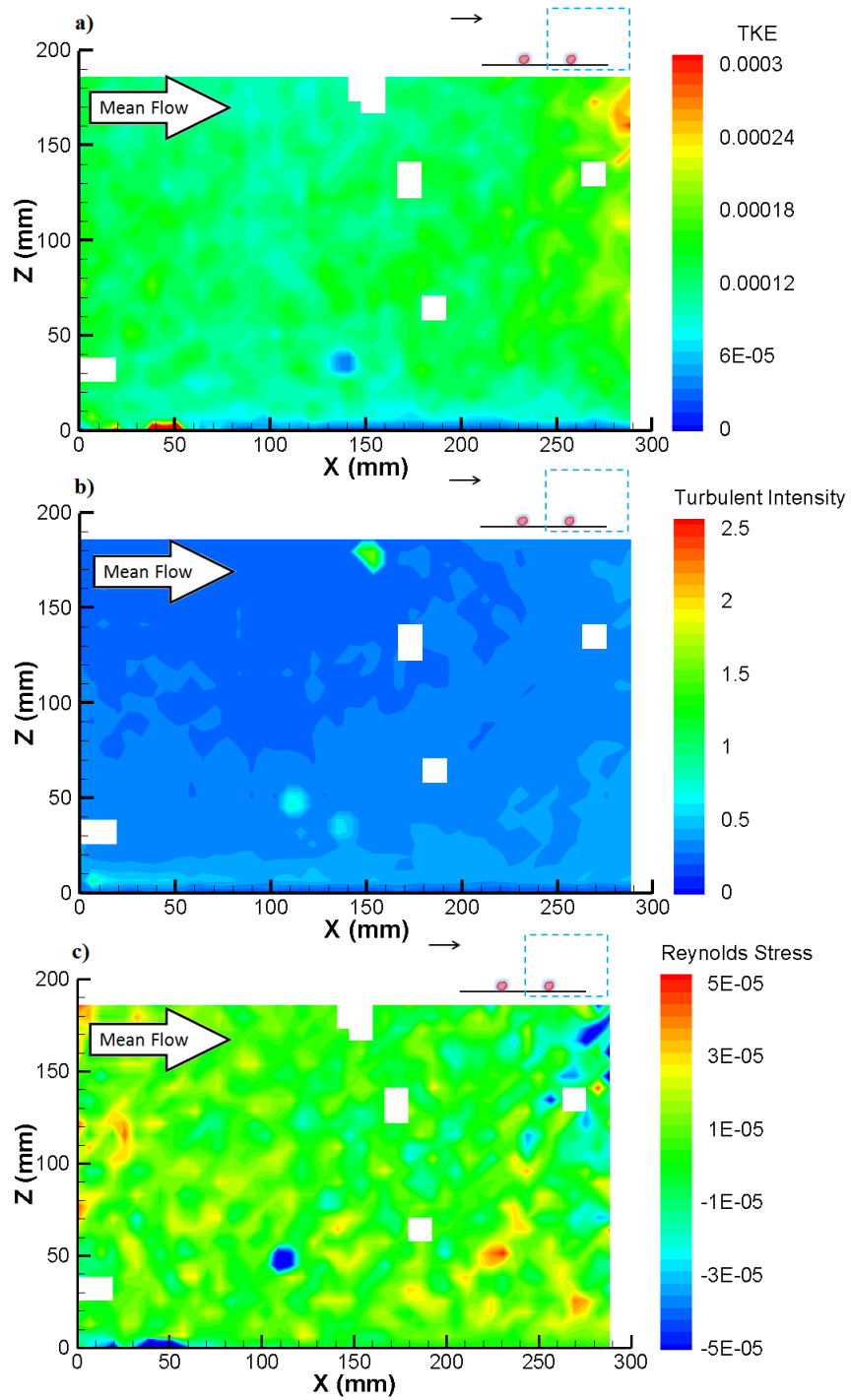
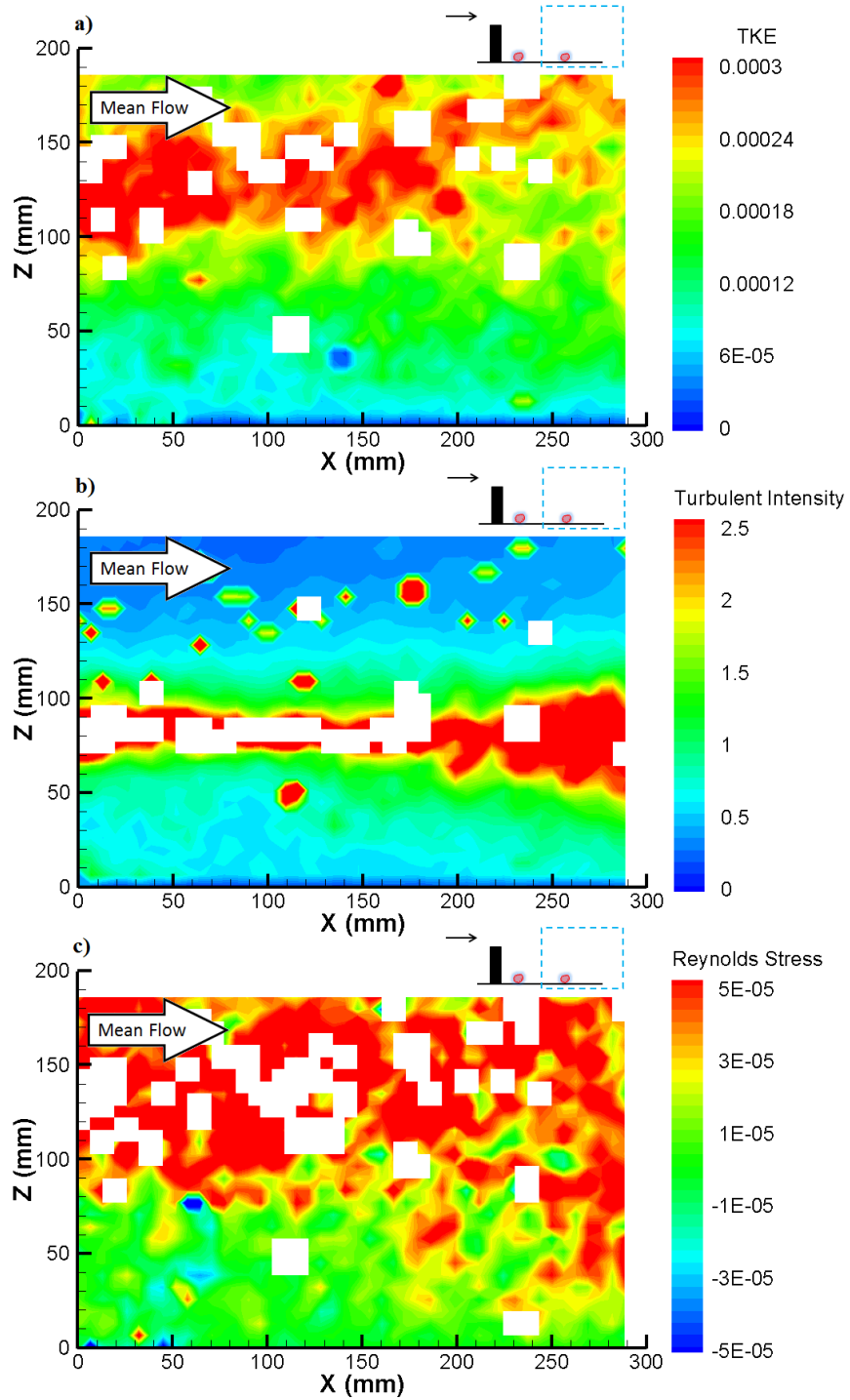**Figure 4-25.** No SB: a) TKE; b) Turbulent Intensity; c) Reynolds Stress

Figure 4-26. Upwind Only SB: a) TKE; b) Turbulent Intensity; c) Reynolds Stress
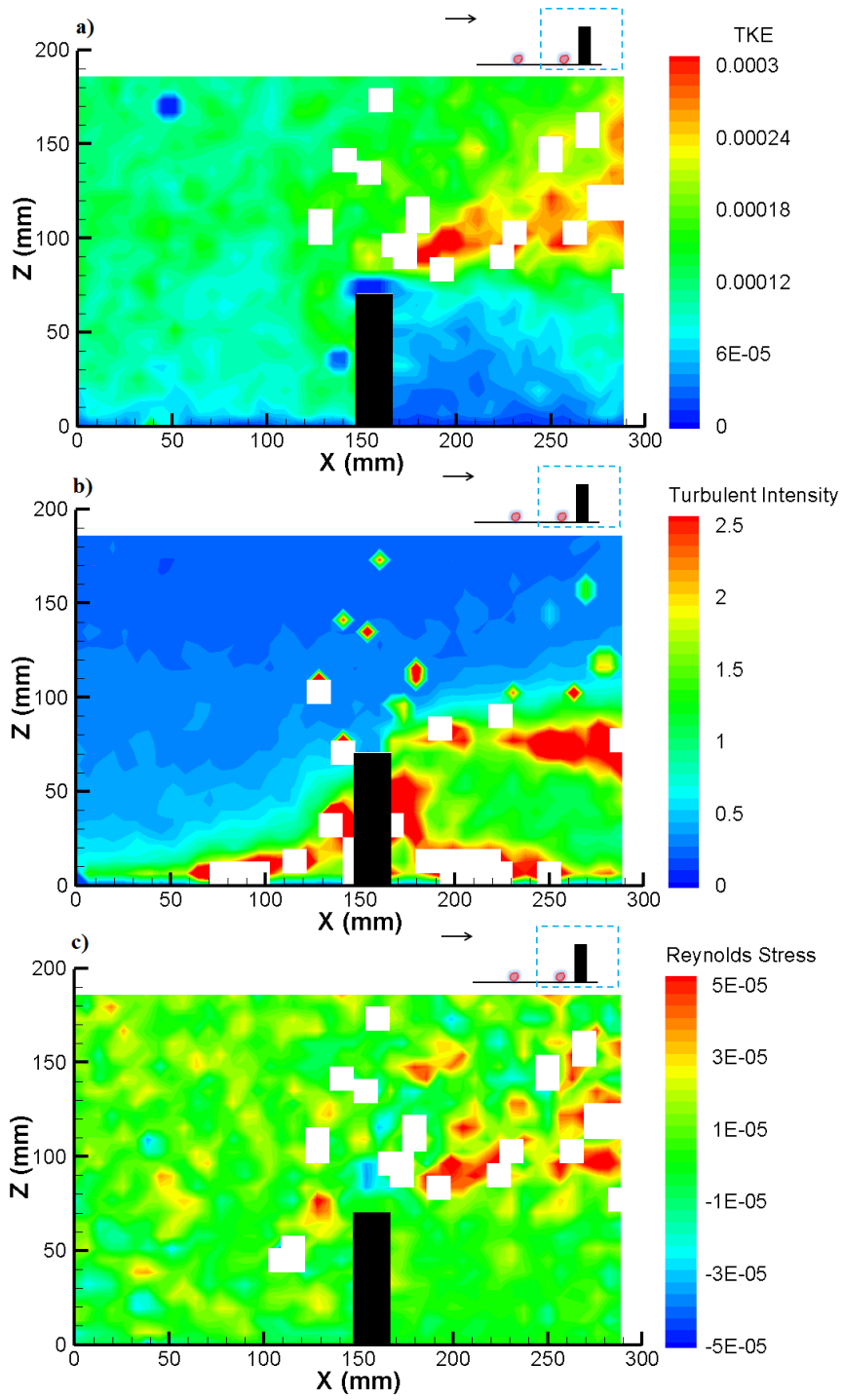
Figure 4-27. Downwind Only SB: a) TKE; b) Turbulent Intensity; c) Reynolds Stress
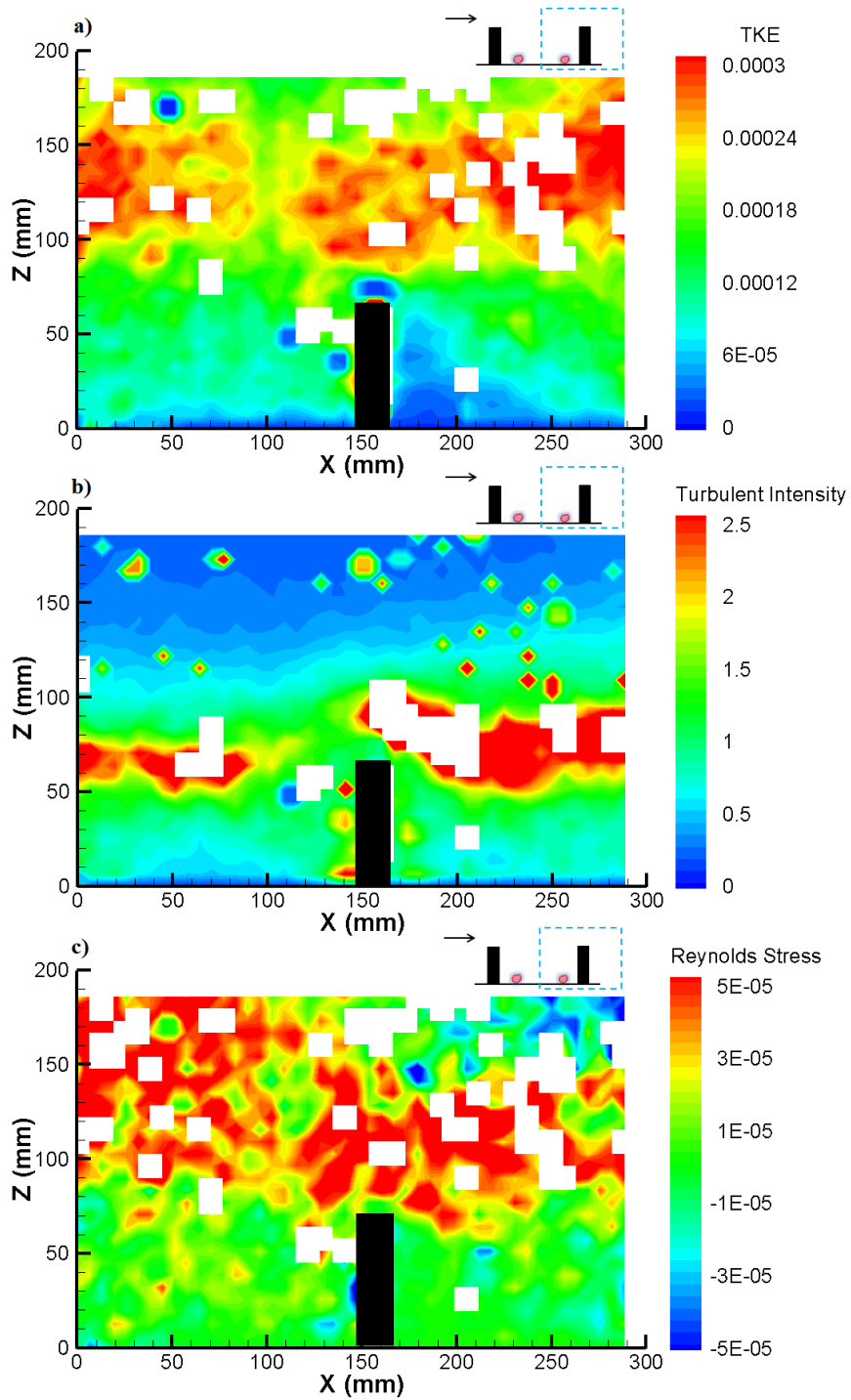
Figure 4-28. $H_{up} = H_{down}$: a) TKE; b) Turbulent Intensity; c) Reynolds Stress
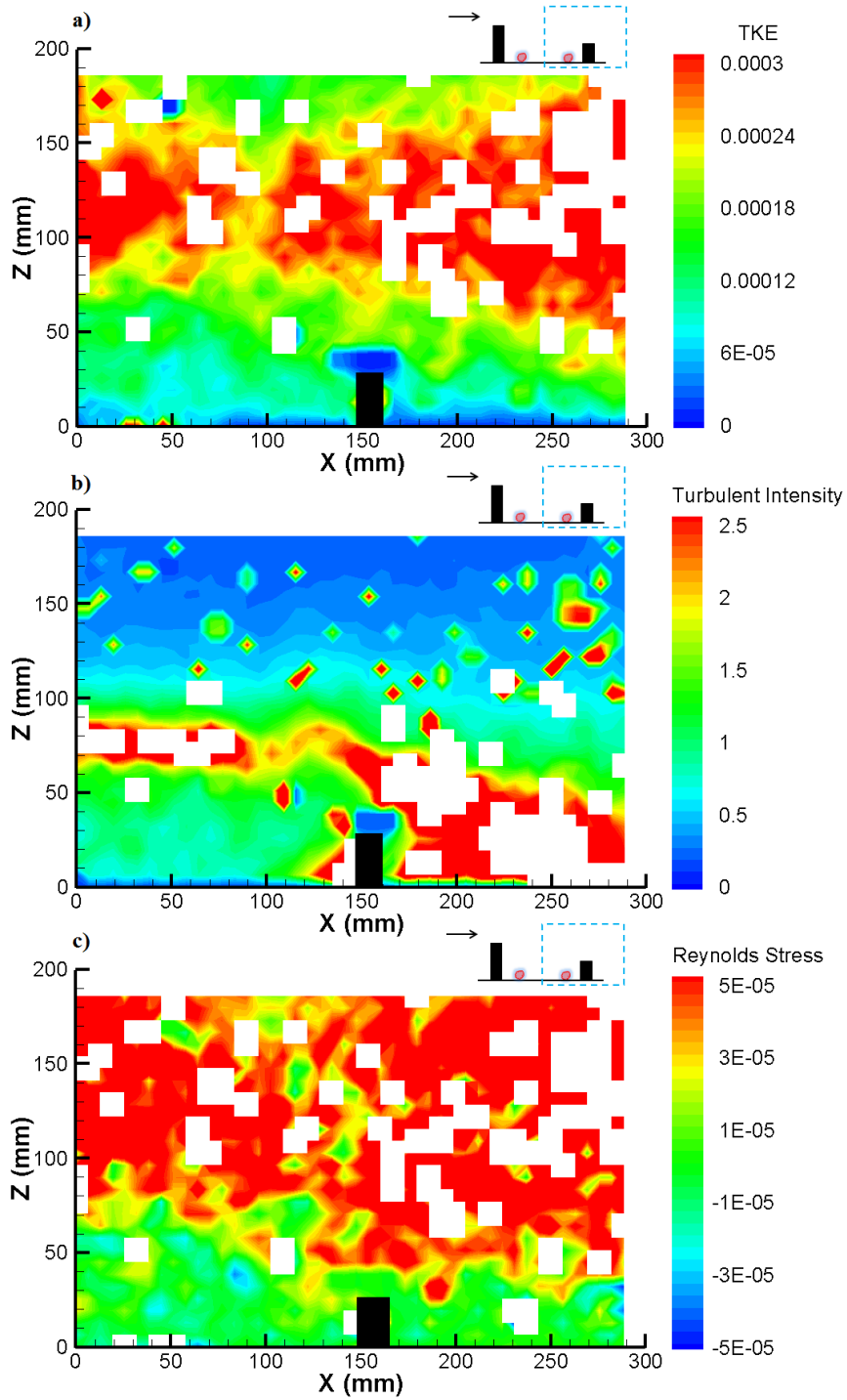
Figure 4-29. $H_{up} = 2H_{down}$: a) TKE; b) Turbulent Intensity; c) Reynolds Stress
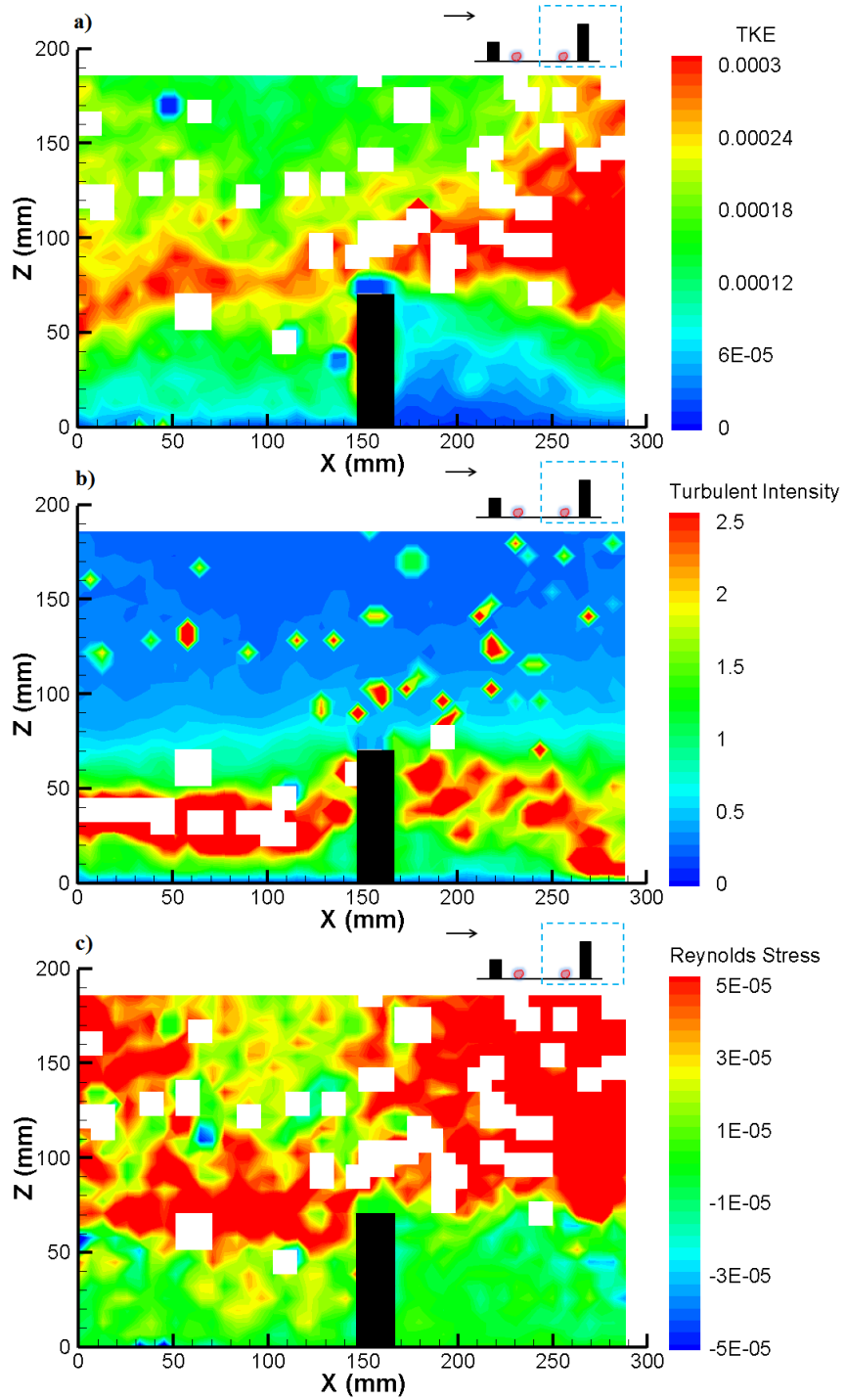
Figure 4-30. $H_{down} = 2H_{up}$: a) TKE; b) Turbulent Intensity; c) Reynolds Stress

The results of PIV show that variations in roadway configurations, SB configurations and wind angles can change the flow pattern and turbulence which influences the near field concentration distributions. Extensive experimenting or sophisticated numerical (CFD) models can be used to study roadway dispersion under various configurations, whereas analytical solutions, such as a Gaussian dispersion model or a two dimensional advection diffusion models by its very nature cannot account for these effects. One may keep on adjusting Gaussian model parameters, which include horizontal and vertical plume spread formulations and initial plume spread, to fit the available measurements on case by case basis (i.e. "build a simple model" for each configuration and wind condition).

5.   Qualitative Results – Visualizations

The roadway configurations tested are the same as those described in Section 4 and to reiterate, they are base case of no SB, upwind only SB, downwind only SB, equal height SBs (H_{up} = H_{down}), upwind SB double the height of the downwind SB ($H_{up} = 2H_{down}$), and downwind SB double the height of the upwind SB ($H_{down} = 2H_{up}$). The effects of varying the wind angle by 30° and 60° from normal were studied for the configuration of $H_{up} = H_{down}$ and these experiments show the effects of channeling. The effects of vegetation, terrain (raised and sunken roadways), traffic and fans were studied for the select cases of No SB and $H_{up} = H_{down}$. Lastly a special case of angled SBs was studied.   Presented visualizations are time exposures over 30 seconds. Additional movies are included as a part of the Digital Catalog.

5.1. Visualization Results of Flat Roadway Configurations

Figure 5-1 shows the visualization for the base case of no SB, and the dispersion pattern is fairly linear. With an upwind only SB present (Figure 5-2) a recirculation cavity develops on the road and pollutants are brought back towards the lee side of the barrier where they get

advected up. This makes the top of the SB act somewhat like an elevated source. With a downwind only SB (Figure 5-3) there is a recirculation cavity on the lee side of the barrier. There is increased plume rise compared to the upwind only SB but less vertical dispersion. For the case of $H_{up} = H_{down}$ (Figure 5-4) the visualizations show a combination of dispersion patterns produced by the two previous cases. On the road the pollutants are brought back toward the upwind barrier and are advected up and there is also a recirculation cavity on the lee side of the downwind barrier. The time averaged plume for the case of $H_{up} = H_{down}$ is somewhat similar to that of upwind only SB and for these roadway configurations the dispersion pattern appears to follow ¼ power pattern (i.e. plume height is proportional to the distance to the power of 0.25). Figures 5-2 through 5-4 also show the results with the SB height halved. The same dispersion patterns can be observed and the plume rise for each case is a little more than half of the previous case. As shown in Figure 5-5, doubling the height of the upwind barrier compares closely to the results of upwind only SB and $H_{up} = H_{down}$. Doubling the height of the downwind SB (Figure 5-6) shows similar pattern to that of downwind only SB, however, the downwind vertical spread compares to that of the upwind only SB and $H_{up} = H_{down}$.
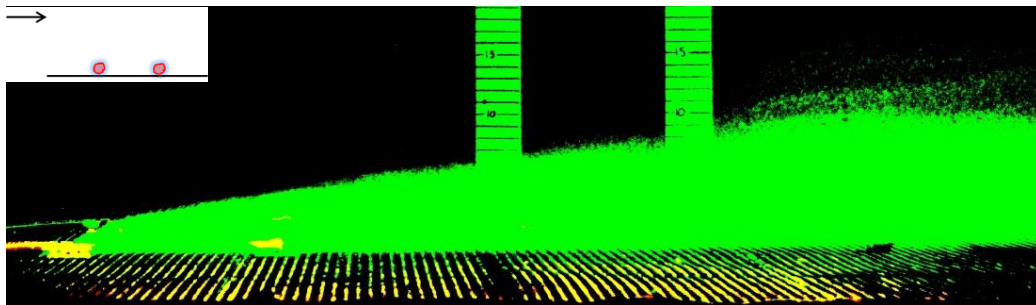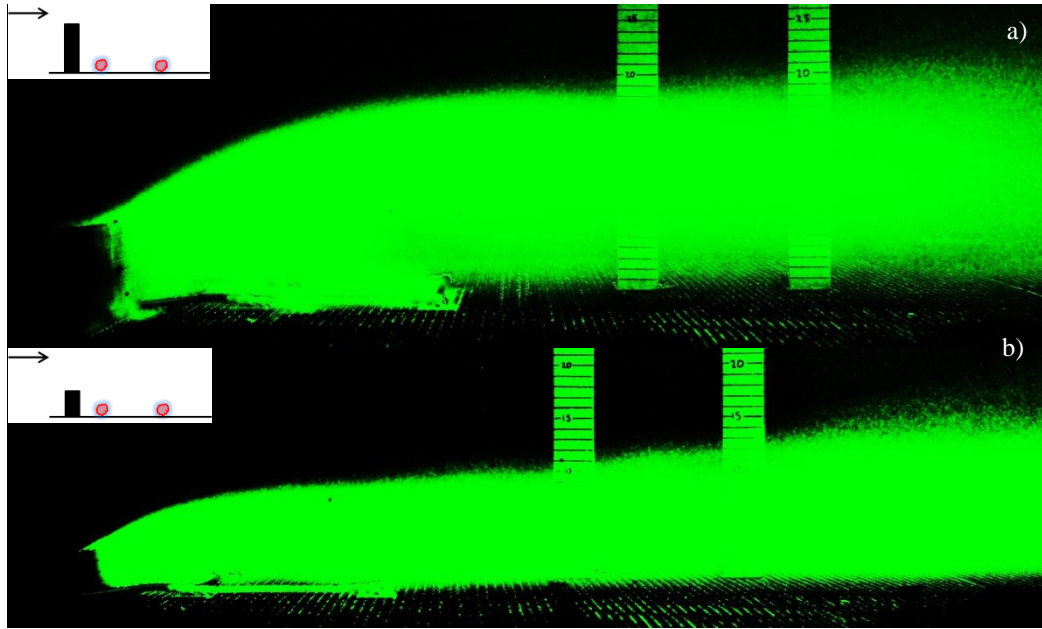

Figure 5-1. Flat Roadway Visualizations: No SB

Figure 5-2. Flat Roadway Visualizations: a) Upwind Only SB; b) Upwind Only SB Half Height
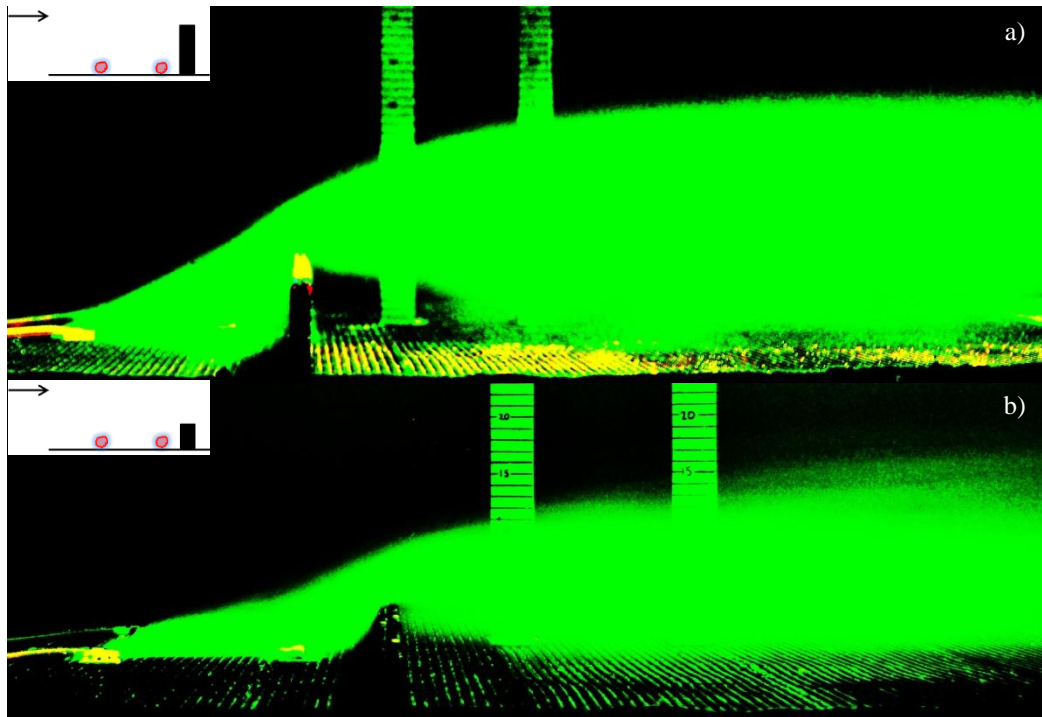

Figure 5-3. Flat Roadway Visualizations: a) Downwind Only SB; b) Downwind Only SB Half Height
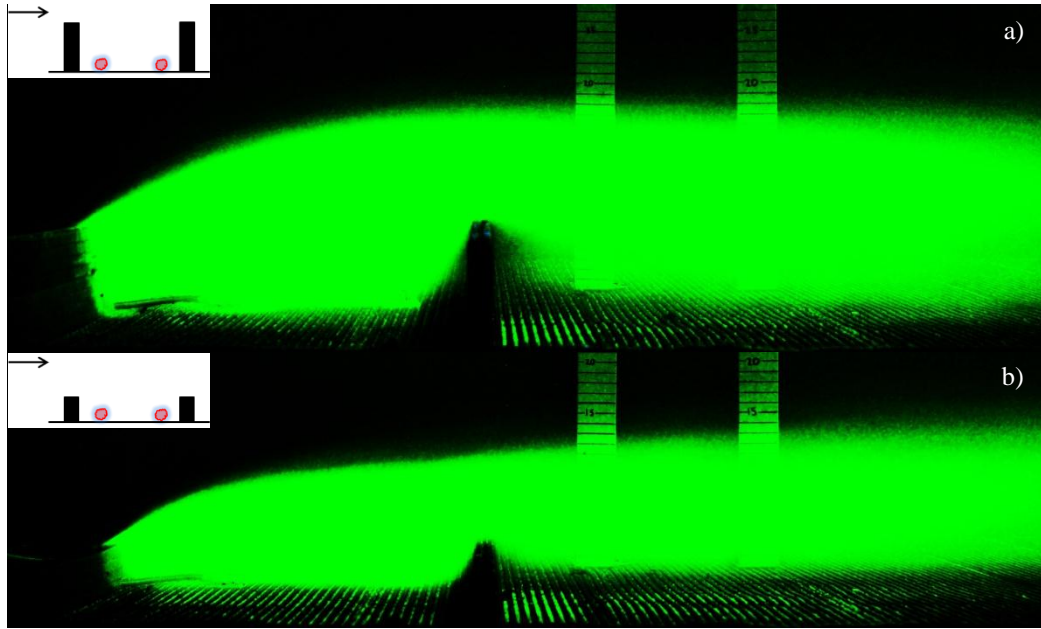
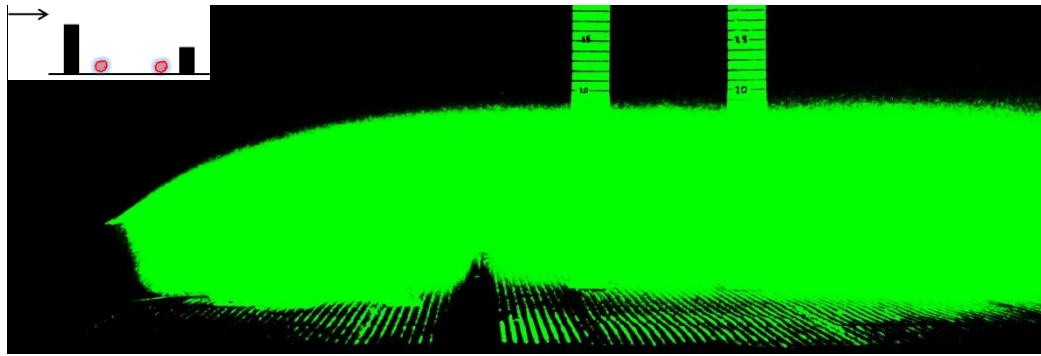**Figure 5-4.** Flat Roadway Visualizations: a) $H_{up} = H_{down}$; b) $H_{up} = H_{down}$ Half Height

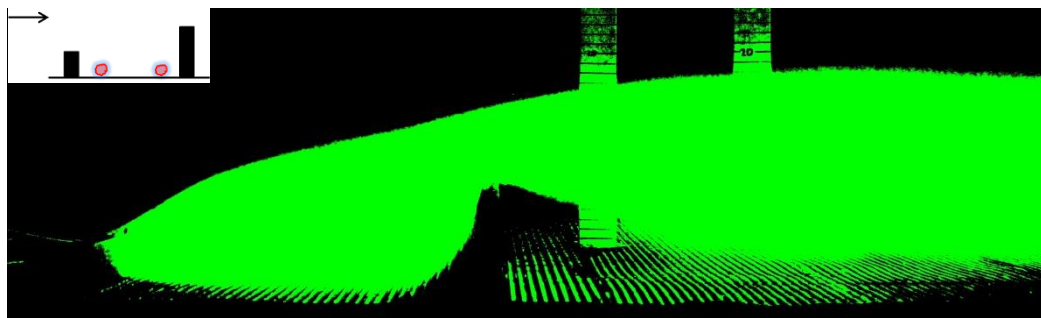**Figure 5-5.** Flat Roadway Visualizations: $H_{up} = 2H_{down}$

Figure 5-6. Flat Roadway Visualizations: $H_{down} = 2H_{up}$

5.2. Visualization Results for Varying Wind Direction

Varying the wind angle (θ_{wind}) by 60° and 30° (relative to the SB) was done for the roadway configuration of $H_{up} = H_{down}$. A top view of the laboratory setup is given in Figure 5-7. A change in the wind direction causes the flow pattern to go from recirculating flow (in the vertical plane) to channeling flow (along the highway). For a wind angle of 60° there is the development of channeling of pollutants along the roadway and recirculating flow appears. For a wind angle of 30° there appears to be almost full channeling of pollutants along the roadway and the effects of recirculating flow are almost nonexistent. A decreasing wind angle, relative to the SB (i.e. increasing wind angle to the normal to SB), causes an increase in channeling flow which increases pollutant concentrations inside of the roadway. As the wind angle decreases, the vertical plume spread becomes less affected by the SBs and is dominated by the channeling flow. Some visualizations are presented in Figure 5.8.
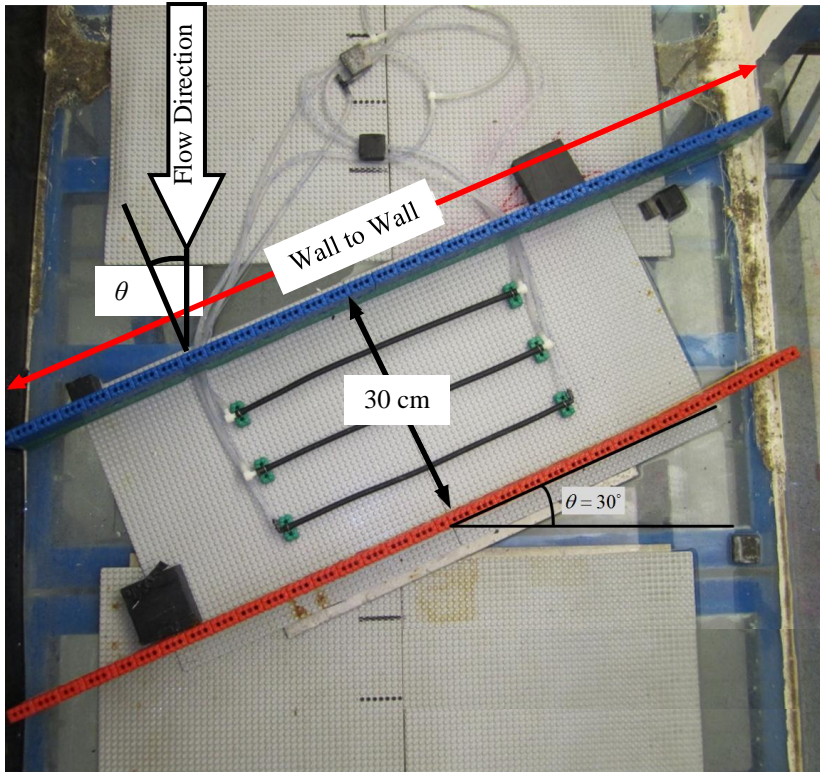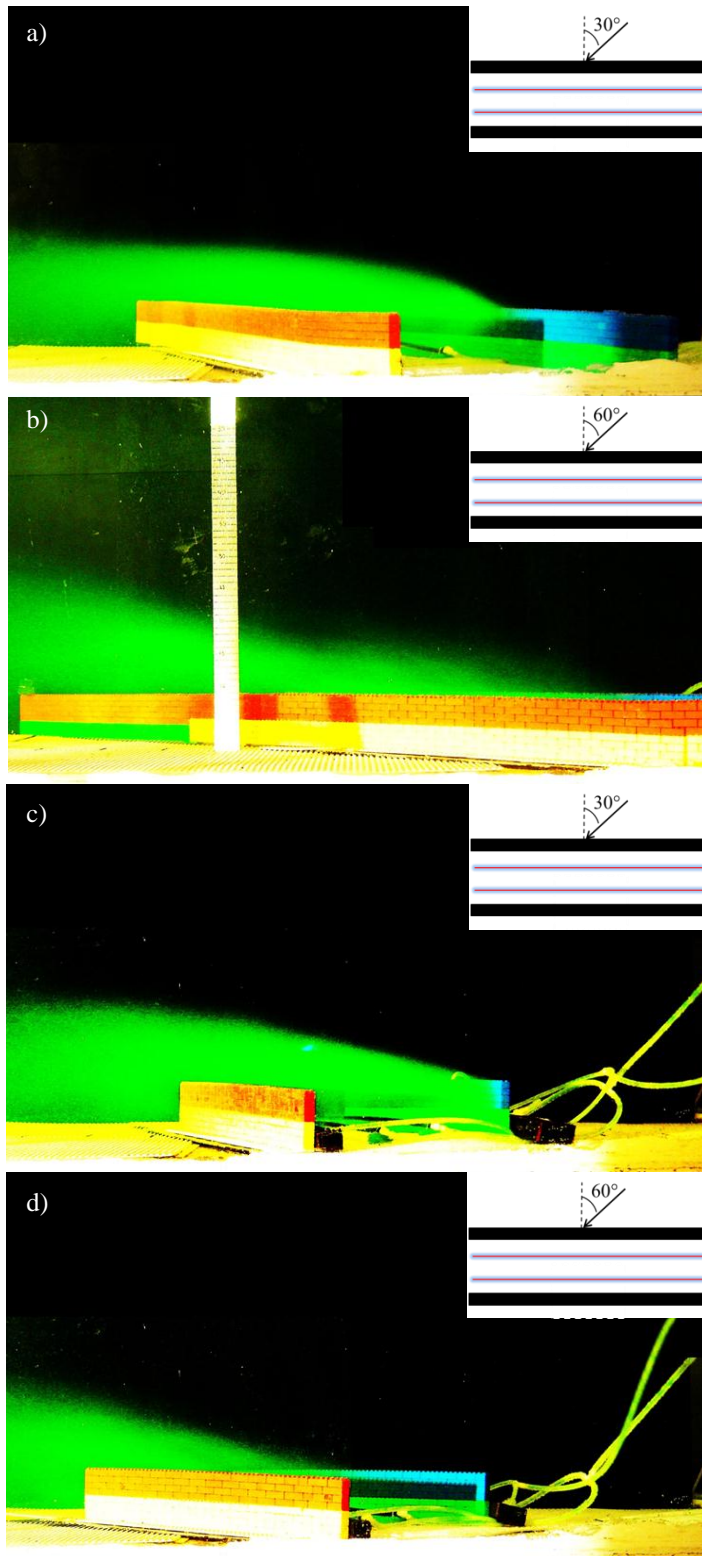
Figure 5-7. Wind Direction Setup

Figure 4. Wind Angle Visualizations: SB from wall to wall of the water channel a) θ=30˚ and b) θ=60˚; and SB only in middle of the water channel c) θ=30˚ and d) θ=60˚

5.3. Visualization Results of Buoyant Release

The effects of buoyancy were studied for the cases of No SB and $H_{up} = H_{down}$ by varying the specific gravity (SG) of dye. A buoyant release is achieved through a mixture of water (SG = 1) and alcohol (SG = 0.8) and the releases studied were those with a SG of 0.8 and 0.9. A heavy release is achieved through a mixture of water and salt (SG = 1.2) and the heavy release studied was that with a SG of 1.02. For the heavy release (SG = 1.02) the pollutants get trapped on the roadway resulting in high on road concentrations and low downwind concentrations. Increasing the buoyancy (SG = 0.9) increases the plume rise and vertical spread of the plume compared to the cases of neutral release. Plume rise and vertical spread are even higher for the case of SG = 0.8. The effects of buoyancy are higher for the roadway configuration of No SB and this is due to the recirculating flow between the barriers, which increases turbulence and entrains ambient air, thus diluting the plume and reducing the plume rise due to buoyancy.
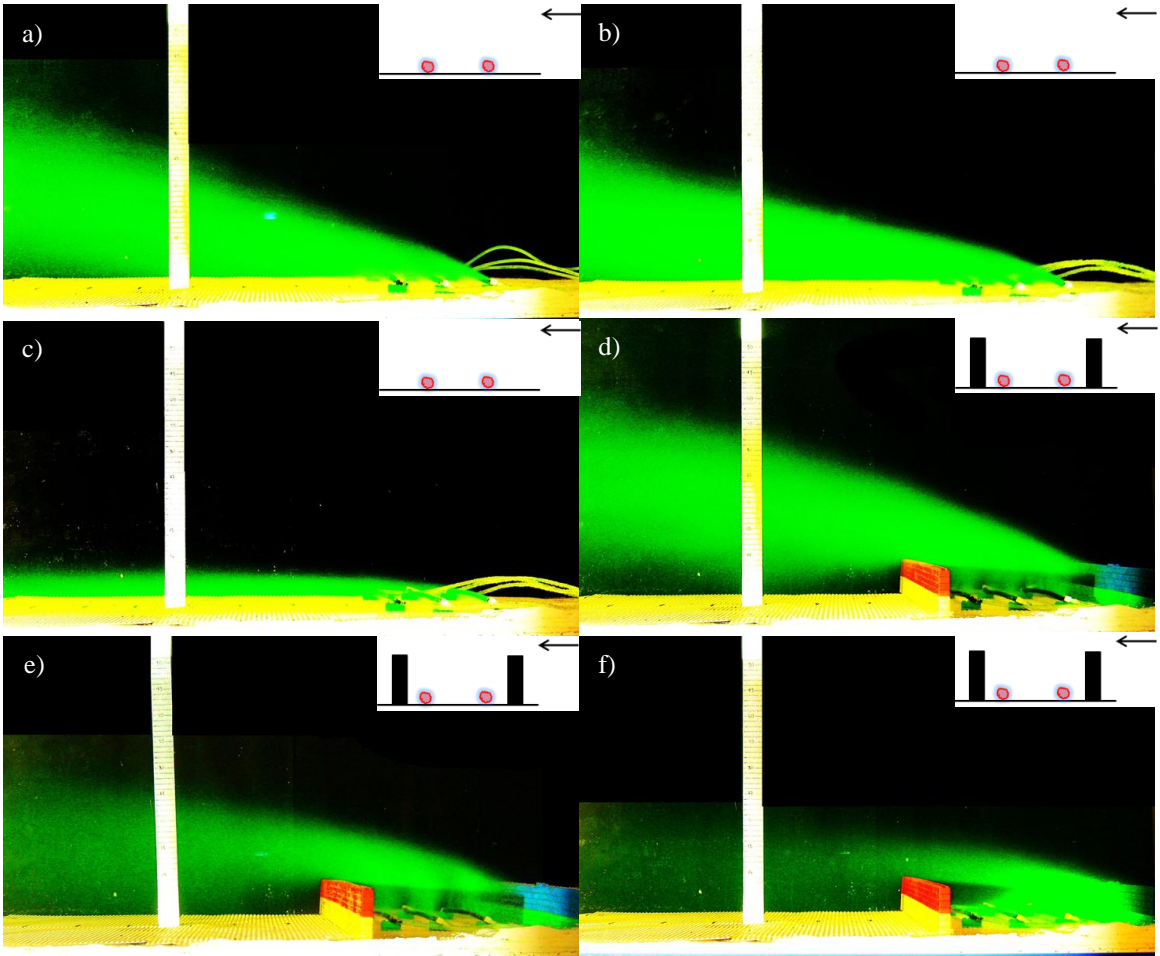
Figure 5-9. Buoyancy Visualizations: a) No SB SG = 0.8; b) No SB SG = 0.9; c) No SB SG = 1.02; d) H_{up} = H_{down} SG = 0.8; e) H_{up} = H_{down} SG = 0.9; f) H_{up} = H_{down} SG = 1.02;

5.4. Visualization Results of Raised Roadways

The effects of raised roadways were studied and these are shown in Figure 5-10. It can be seen that a raised roadway simply elevates the plume, and results in the same dispersion pattern as that of flat roadways. This elevated release however, results in greater vertical dispersion, relative to the ground, which decreases ground level concentrations.
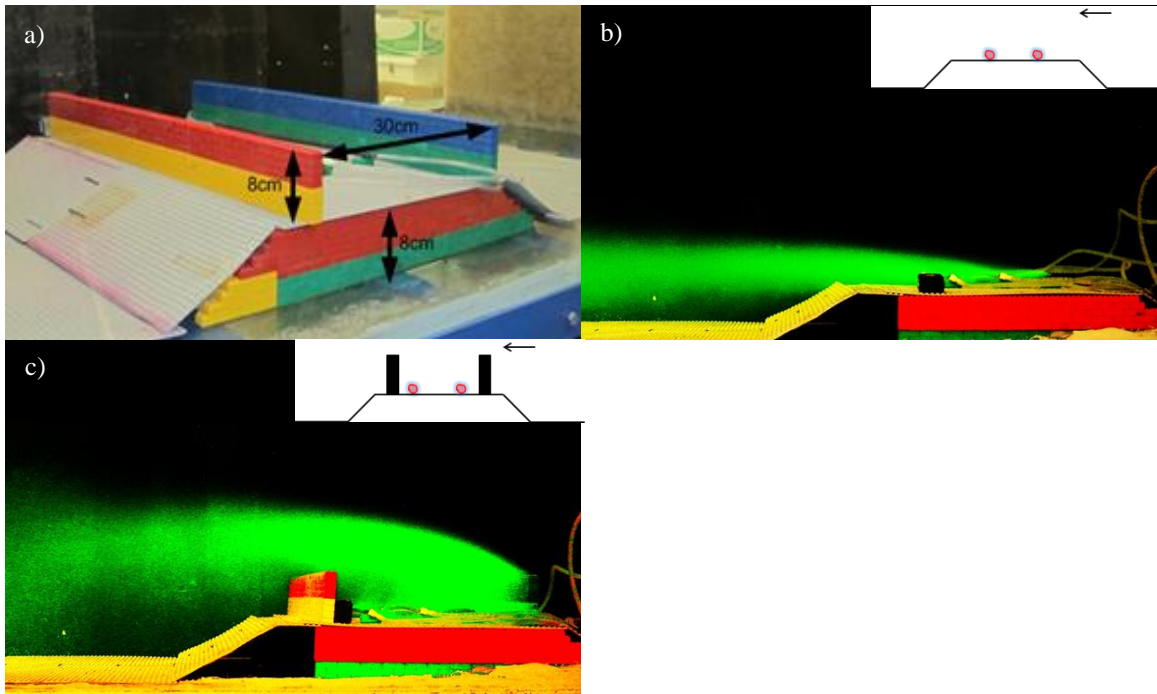
Figure 5-10. Raised Roadway Visualizations: a) Setup; b) No SB; c) $H_{up} = H_{down}$

5.5. Visualization Results of Sunken Roadways

The effects of sunken roadways were studied and these are shown in Figure 5-11. Without the presence of SBs the plume follows the terrain resulting in vertical plume spread that is higher but comparable to that of the flat roadway case. With the presence of SBs there is an increase in the plume rise and vertical spread due to the increased turbulence and large recirculation that develops between the barriers. Referring to Figure 4-6 there is a large on road recirculation induced by the SBs, and the large updrafts near the upwind SB advects the pollutants up where they are entrained in the mean wind leaving lower concentrations near the downwind SB.
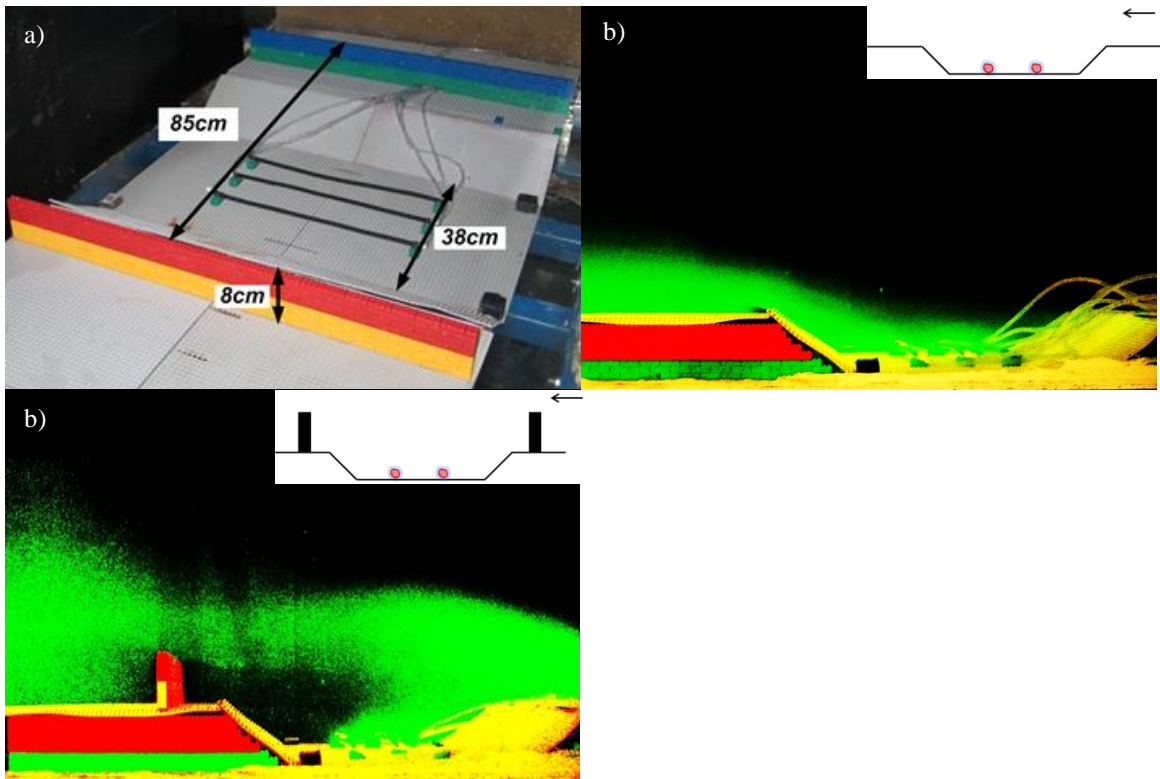
Figure 5-11. Sunken Roadway Visualizations: a) Setup; b) No SB; c) $H_{up} = H_{down}$

5.6. Visualization Results in the Presence of Vegetation

The effects of vegetation were studied using 80 mm model trees (the models were purchased from samtrees.com). The leaf area index is between 0.67 and 0.85. The trees were placed in rows to simulate SBs and the results show that the trees do increase turbulence and vertical spread compared to the case of No SB. However, compared to the case of $H_{up} = H_{down}$ the trees have much less of an impact. This shows the important role SBs can have on the dispersion of vehicular emissions from roadways.
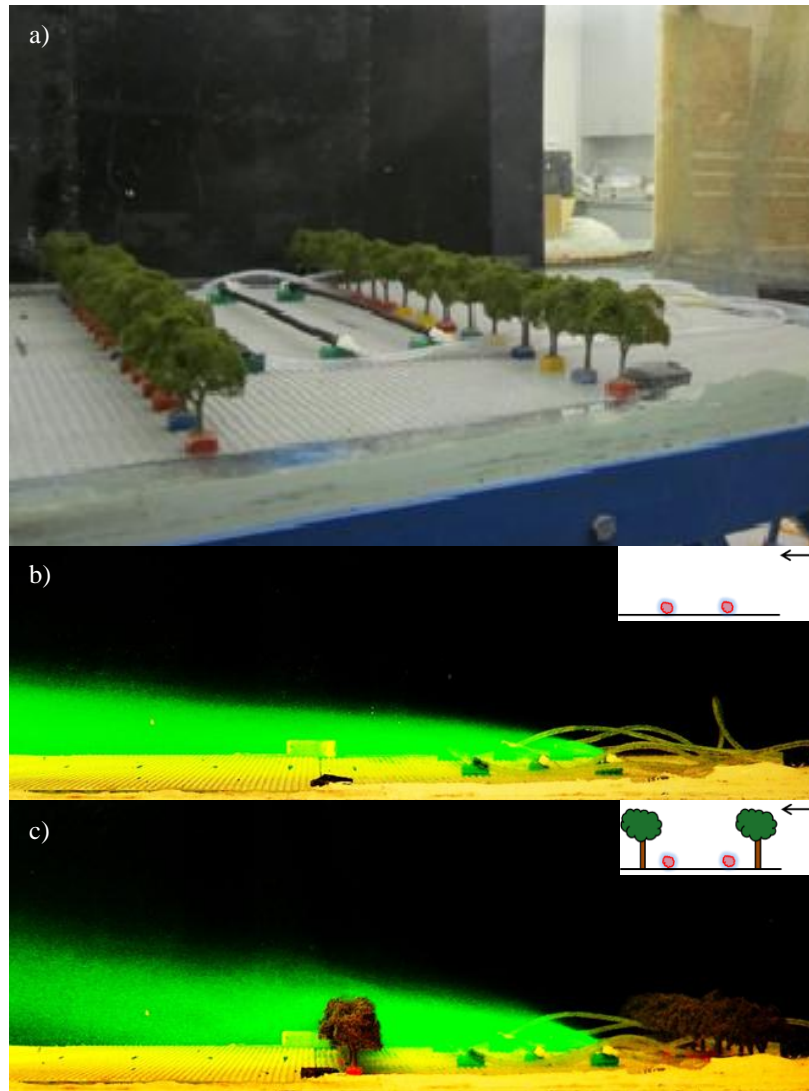
Figure 5-12. Vegetation Visualizations: a) Setup; b) No Trees; c) Trees on Both Sides of the Road

5.7. Visualization Results with Traffic Induced Turbulence (TIT)

The effects of Traffic Induced Turbulence (TIT) were studied for the roadway configuration of No SB and $H_{up} = H_{down}$ for both low and high traffic frequencies (1.4 Hz and 2.8 Hz) as well as low (0.079 vehicle-cm^{-1}, Figures 5-13 and 5-15) and high traffic (0.16 vehicle-cm^{-1}, Figures 5-14 and 5-16) densities and this was done at high (Figures 5-13 and 5-14) and low (Figures 5-15 and 5-16) wind speeds (further description of the traffic frequencies and densities can be found in Section 4.6). For the roadway configuration of no SB with high wind, there is

increased vertical plume spread compared to the case without traffic, also it is seen that the low traffic density (Figure 5-13a, b) has higher vertical spread than the high traffic density (Figure 5-14a, b). For all cases, the higher traffic frequency results in an increased downwind vertical spread. For the roadway configuration of $H_{up} = H_{down}$ with high wind speed (Figure 5-14), there is little to no effect for the low traffic frequency, but there is increased vertical spread for the high traffic frequency. For the roadway configuration of no SB with low wind, there is noticeable increase in vertical plume spread. For the roadway configuration of $H_{up} = H_{down}$ with low wind speed it was observed during the experiments that a portion of the plume was advected laterally towards the water channel wall where the plume partially climbed up the wall before the mean flow push the plume downwind. This rise next to the channel wall due to the lateral advection caused by oscillating obstacles causes appearance of higher plume spread than it actually is. Figures 5-16c and d depict this best where close to the SB higher plume is present than further downwind.. This high plume rise close to SB is a consequence of the plume deflection by the water channel wall. The reason for this plume motion along the road is currently unknown and further research is needed. This oscillation driven lateral plume advection is likely responsible for lack of ground level concentration in Figure 5-15c.
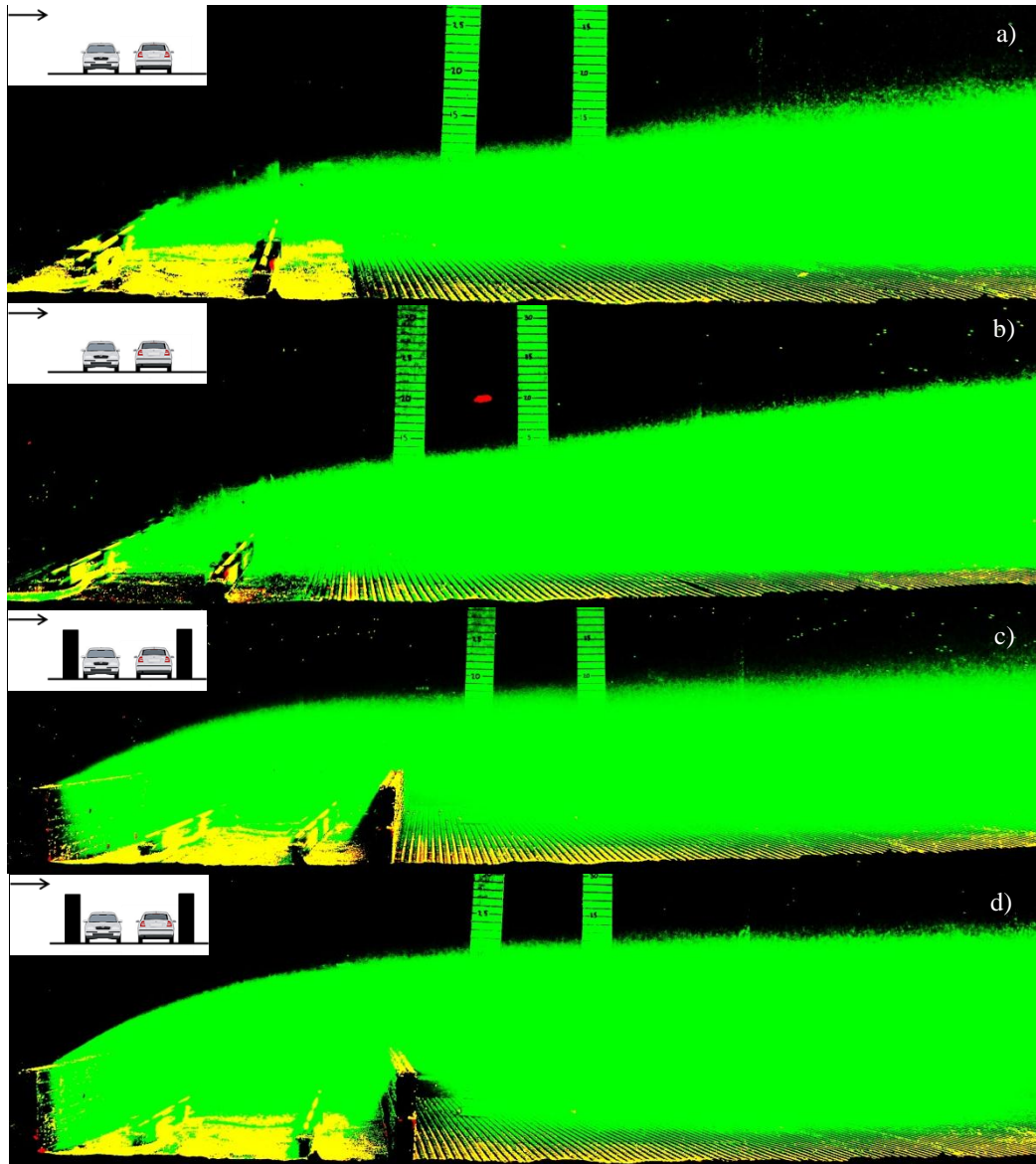
Figure 5-13. TIT Visualizations With High Wind and Low Density: a) No SB Low Frequency; b) No SB High Frequency; c) $H_{up} = H_{down}$ Low Frequency; d) $H_{up} = H_{down}$ High Frequency
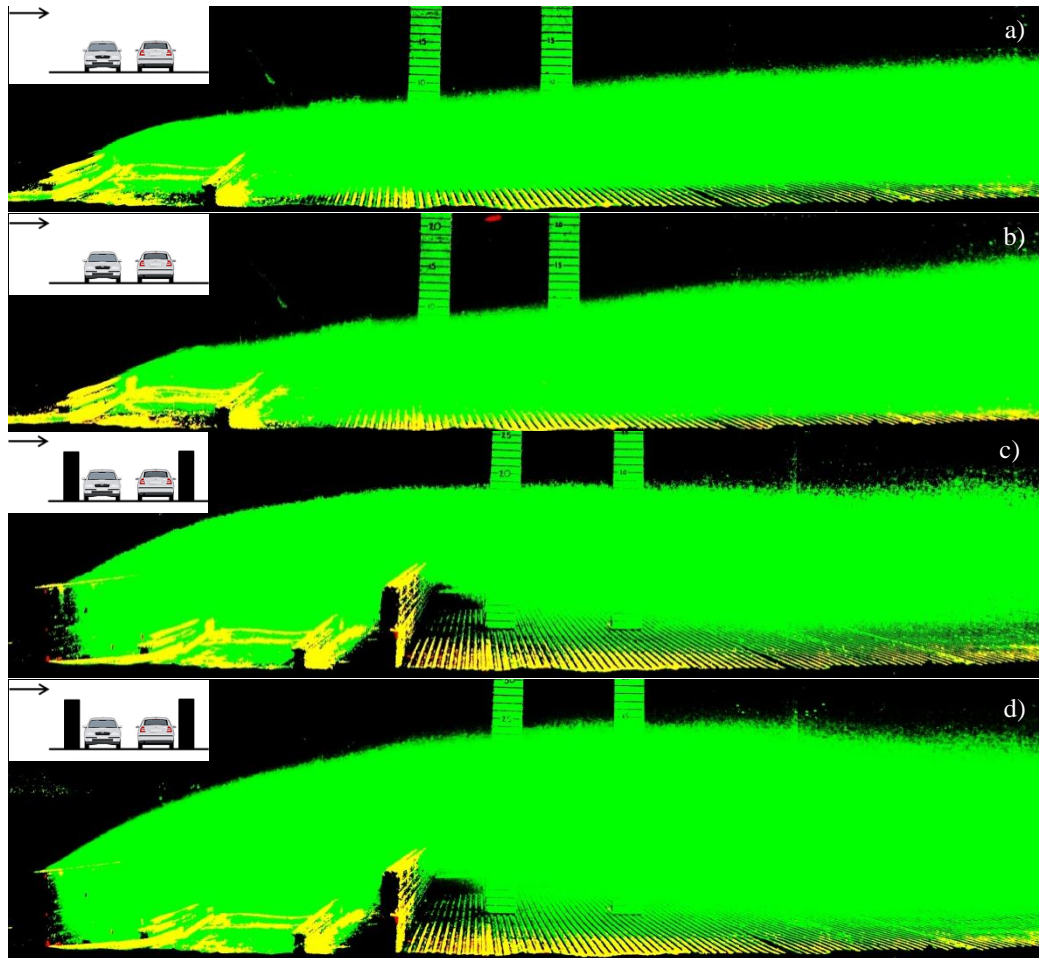
Figure 5-14. TIT Visualizations With High Wind and High Density: a) No SB Low Frequency; b) No SB High Frequency; c) $H_{up} = H_{down}$ Low Frequency; d) $H_{up} = H_{down}$ High Frequency
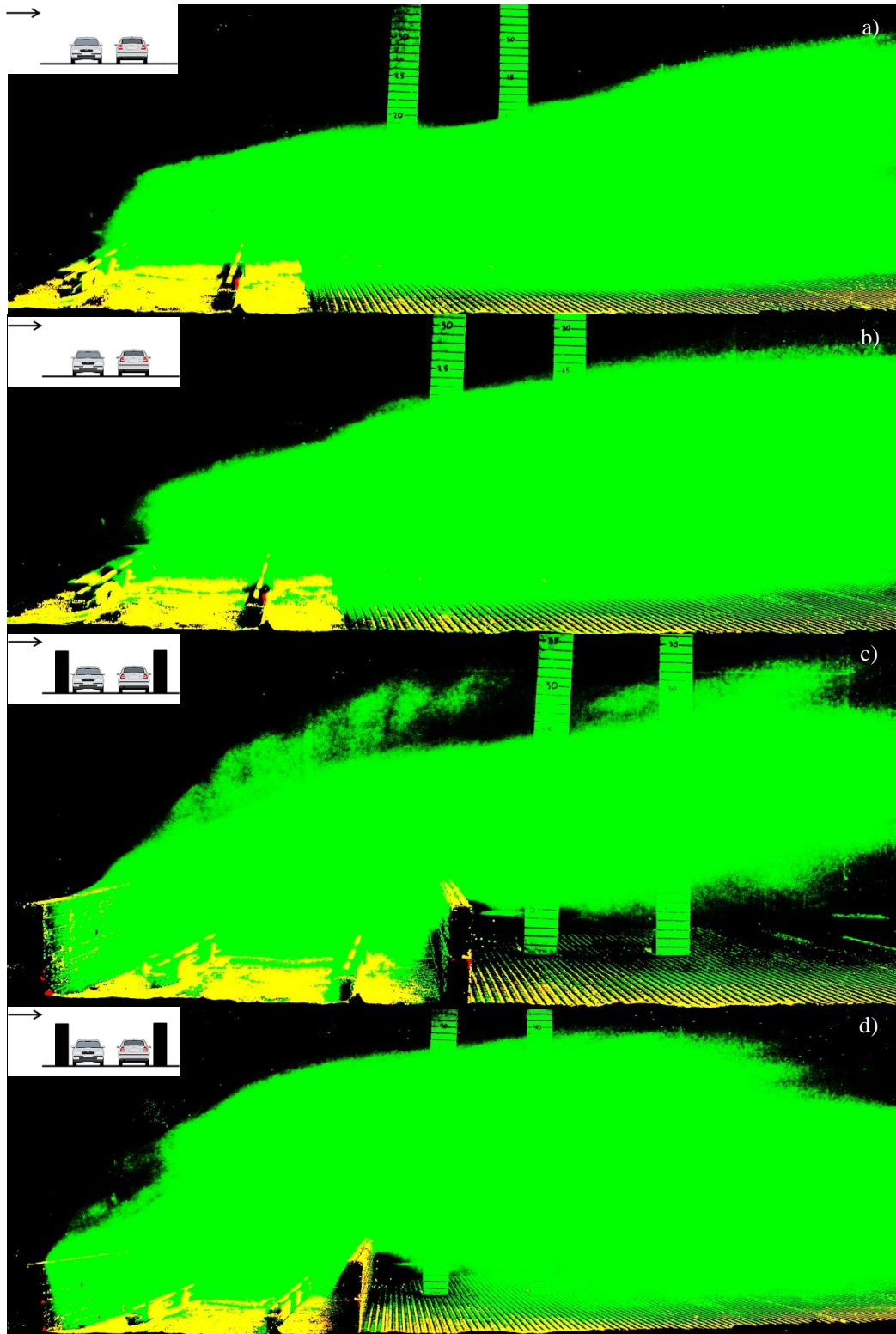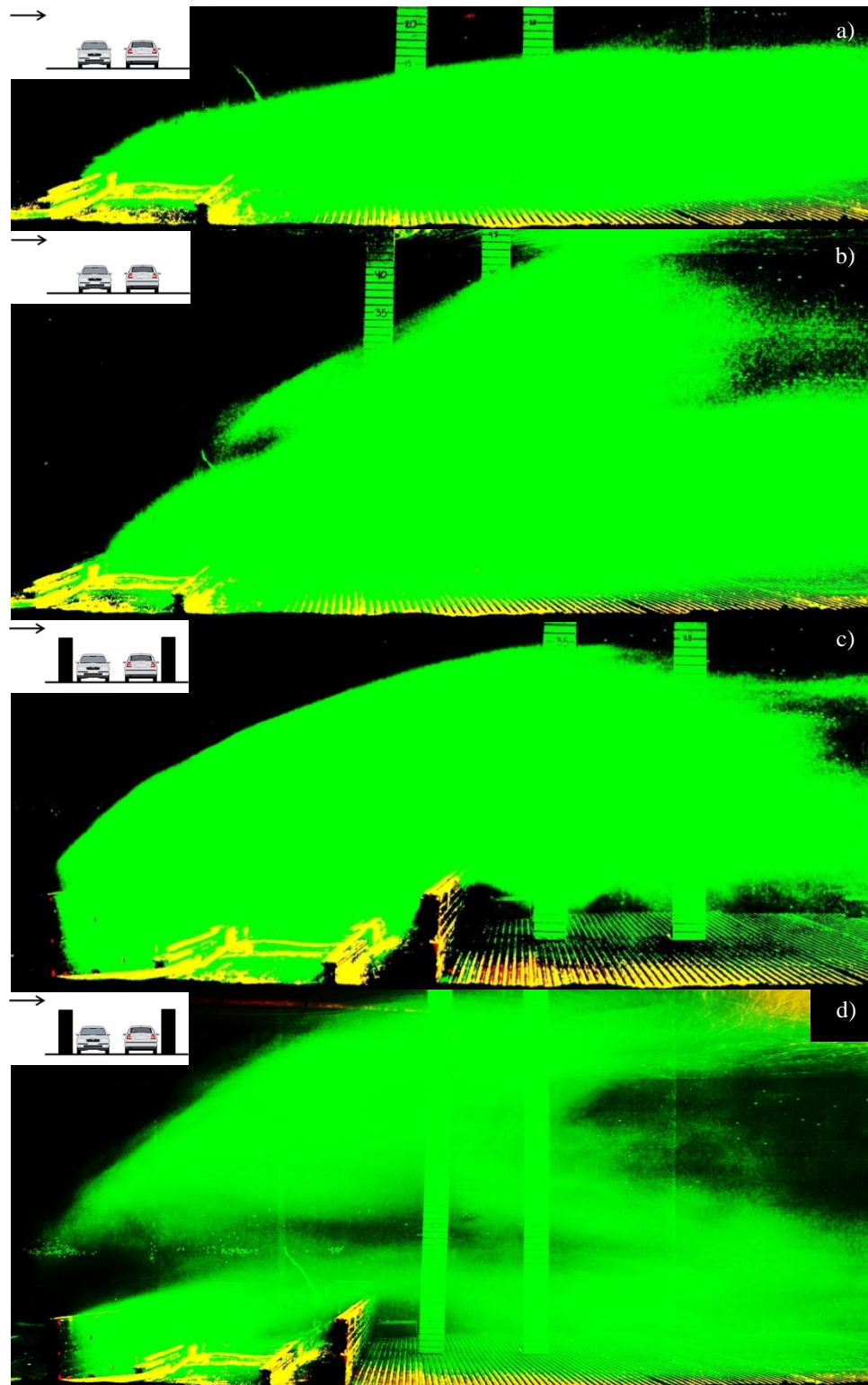
Figure 5-15. TIT Visualizations With Low Wind and Low Density: a) No SB Low Frequency; b) No SB High Frequency; c) $H_{up} = H_{down}$ Low Frequency; d) $H_{up} = H_{down}$ High Frequency

Figure 5-16. TIT Visualizations With Low Wind and High Density: a) No SB Low Frequency; b) No SB High Frequency; c) $H_{up} = H_{down}$ Low Frequency; d) $H_{up} = H_{down}$ High Frequency

5.8. Visualization Results in the Presence of Ground Heating

All of the previous experiments were done under neutral atmospheric conditions in order to isolate the results from exterior effects, such as convection. In reality, during the day solar radiation reaches the ground. The ground heating results in the sensible heat flux that causes the convective air motion. This leads to unstable atmospheric conditions in which the upward heat flux causes buoyancy forces, and these forces generate convective turbulence in the boundary layer. To model an unstable boundary layer in the water channel, submerged heaters covering the whole test section are used. The scaled parameter that is matched from the field to the lab is the convective velocity scale [w_* (m s^{-1})]. The convective velocity scale is defined as (Stull 1988):

$$w_* = \left(\frac{g}{T_a} Q_o z\right)^{\frac{1}{3}} \tag{5-1}$$

where Q_o (m K s^{-1}) is the kinematic hear flux, g (m s^{-2}) is gravitational acceleration, T (K) is temperature and z (m) is the height. Equation (5-1) is valid for air and this can be easily derived and will not be shown here, however, the derivation of the convective velocity scale for water is shown as below. In the derivation of (5-1), the thermal expansion coefficient (β) is taken to be $1/T_a$, which is only valid for the air. In order to relate this to the water channel a new convective velocity scale for water will be derived. Looking at a buoyant parcel of air (or water) which is heated due to convection, the net force is

$$F_{net} = \rho_a g V - mg \tag{5-2}$$

where ρ_a is air density, g gravitational acceleration, V parcel volume, and m is parcel mass. Taking the net force per unit mass, using ρ_p for parcel density, and rearranging gives

$$F_{net} = g\left(\frac{\rho_a}{\rho_p} - 1\right) = g\left(\frac{\rho_a - \rho_p}{\rho_p}\right) \tag{5-3}$$

Using thermal expansion, $\beta = -\frac{1}{\rho}\frac{\partial \rho}{\partial T}$, and substituting into (5-3) after rearranging gives

72

$$F_{net} = g\beta(T_a - T_p) \tag{5-4}$$

where T_a and T_p are ambient and heated parcel temperatures, respectively. This force acting over a vertical distance (z) generates a kinetic energy proportional to the square of vertical velocity (w), i.e.

$$g\beta(T_a - T_p)z = g\beta\Delta Tz = w^2 \tag{5-5}$$

Multiplying both sides by w gives

$$w^3 = g\beta\Delta Twz \tag{5-6}$$

where ΔT is the temperature excesses of the fluid parcel relative to its surroundings. This temperature excess when multiplied by the vertical velocity (w) is proportional to the sensible heat flux (*SHF*). Since the sensible heat flux is given as $SHF = \rho C_p\overline{w'T'}$ (C_p is specific heat and primes denote fluctuating components), the following relation can be made, $\Delta Tw \approx \overline{w'T'}$, where the kinematic heat flux is defined as $Q_o = \overline{w'T'}$. Combining equation (5-6) and the kinematic heat flux gives an equation for the convective velocity scale in water:

$$w_* = (g\beta Q_o z)^{\frac{1}{3}} \tag{5-7}$$

These convective velocities in the field and the water channel must be matched for the heater experiments. *SHF* for the field can be approximated as 200 W m^{-2} and z for the field can be approximated as 1.5 km. z for the water channel is 50 cm and *SHF* is to be determined by solving both equations. The resultant value was set as power output of the heaters. Relatively small z in the water channel would affect the quantitative measurements by limiting the vertical convective motion but the qualitative visualized pattern would be similar.

Flexible heaters were purchased from Watlow (Figure 5-17). As these heaters are not water proof, a custom made enclosure (Figure 5-17b) was made for each heater out of 22 gauge galvanized sheet metal. The heaters were all individually wired and controlled using variable controllers (Figure 5-17c), to obtain a desired heat flux.

Under high wind speed conditions (Figure 5-18) the heaters have no impact on the dispersion pattern or vertical plume spread. Under low wind speed conditions (Figure 5-19) the heaters significantly increase the vertical spread of the plume relative to no heaters. The vertical plume spread for both No SB and $H_{up} = H_{down}$ increases monotonically with distance.
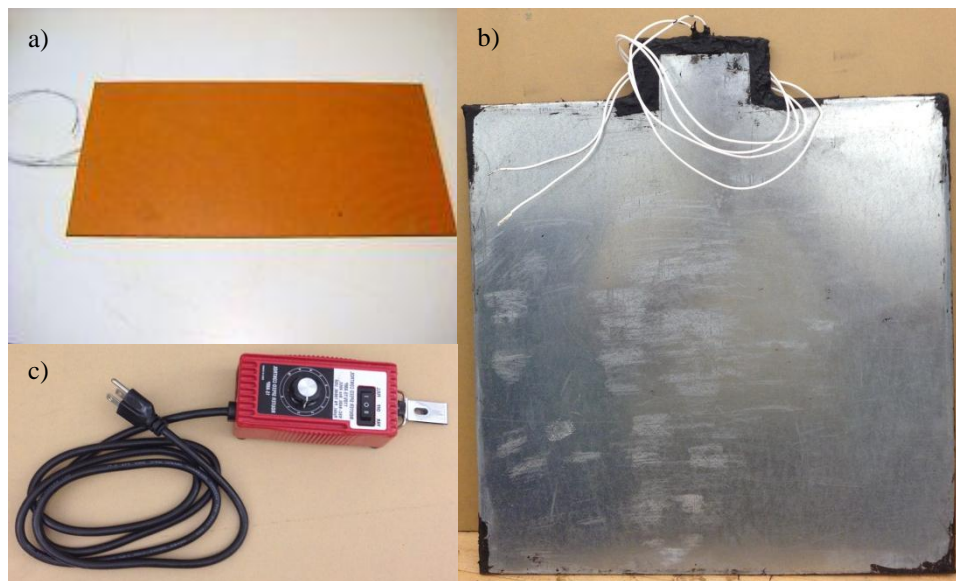
Figure 5-17. Heaters: a) Watlow Flexible Heater; b) Heater in Custom Enclosure; c) Controller
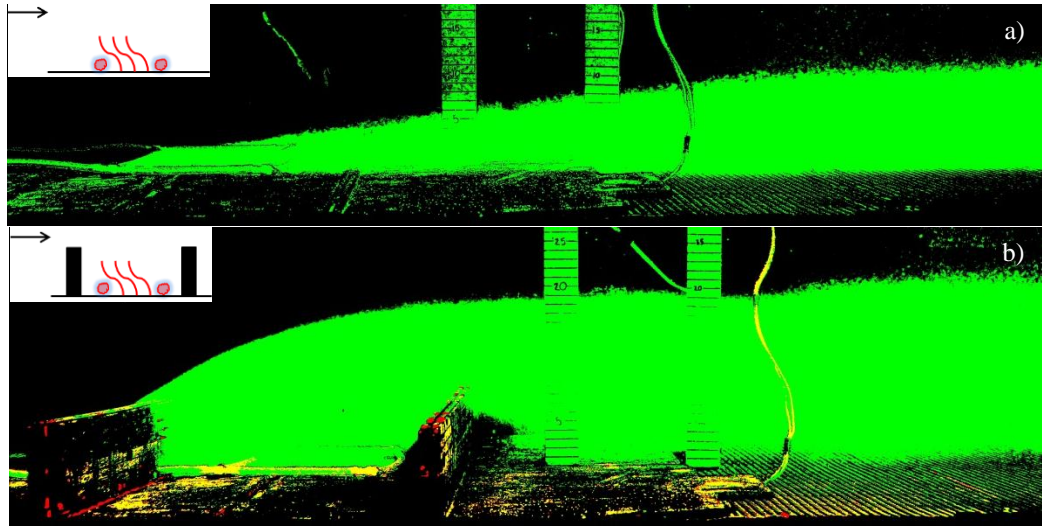
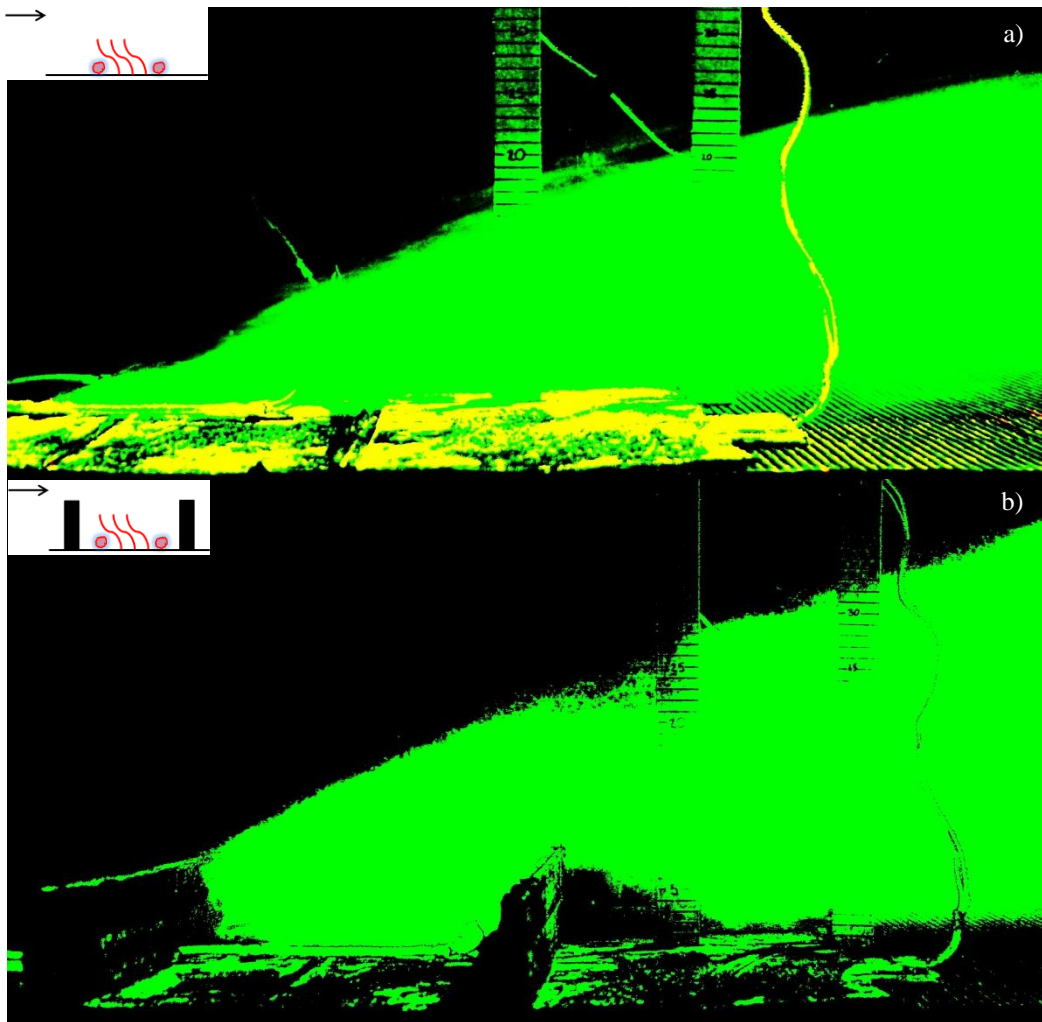**Figure 5-18.** Heater Visualizations with High Wind: a) No SB; b) $H_{up} = H_{down}$

Figure 5-19. Heater Visualizations with Low Wind: a) No SB; b) $H_{up} = H_{down}$

5.9. Fan Visualizations

As shown in the PIV results, the fans were tested at three different settings. However, the fan visualizations were only done for the medium setting because the low setting has very little impact on pollutant dispersion and the high setting would likely be infeasible in a field application due to power limitations. As shown in the following pictures, the plume rise under low wind speed conditions is highly enhanced by fans and there is insignificant impact under high wind speed conditions. For the roadway configurations with downwind fans, the highest plume rise is for the configuration of downwind only SB. For this configuration the plume is dispersed above the downdraft caused by the barrier, whereas the roadway configuration has larger vertical spread due to the plume getting caught in the down draft of the downwind SB. Even with the downdraft caused by the recirculation on the lee side of the downwind barrier, the fans disperse the plume high enough to where there is very low concentrations observed near the ground over five SB heights downwind of the source. For the roadway configurations with the upwind fans the plume rise is similar for the roadway configurations of upwind only SB and $H_{up} = H_{down}$. However, for the configuration of $H_{up} = H_{down}$, the plume begins to descend further downwind due to the downdraft induced by the downwind SB.
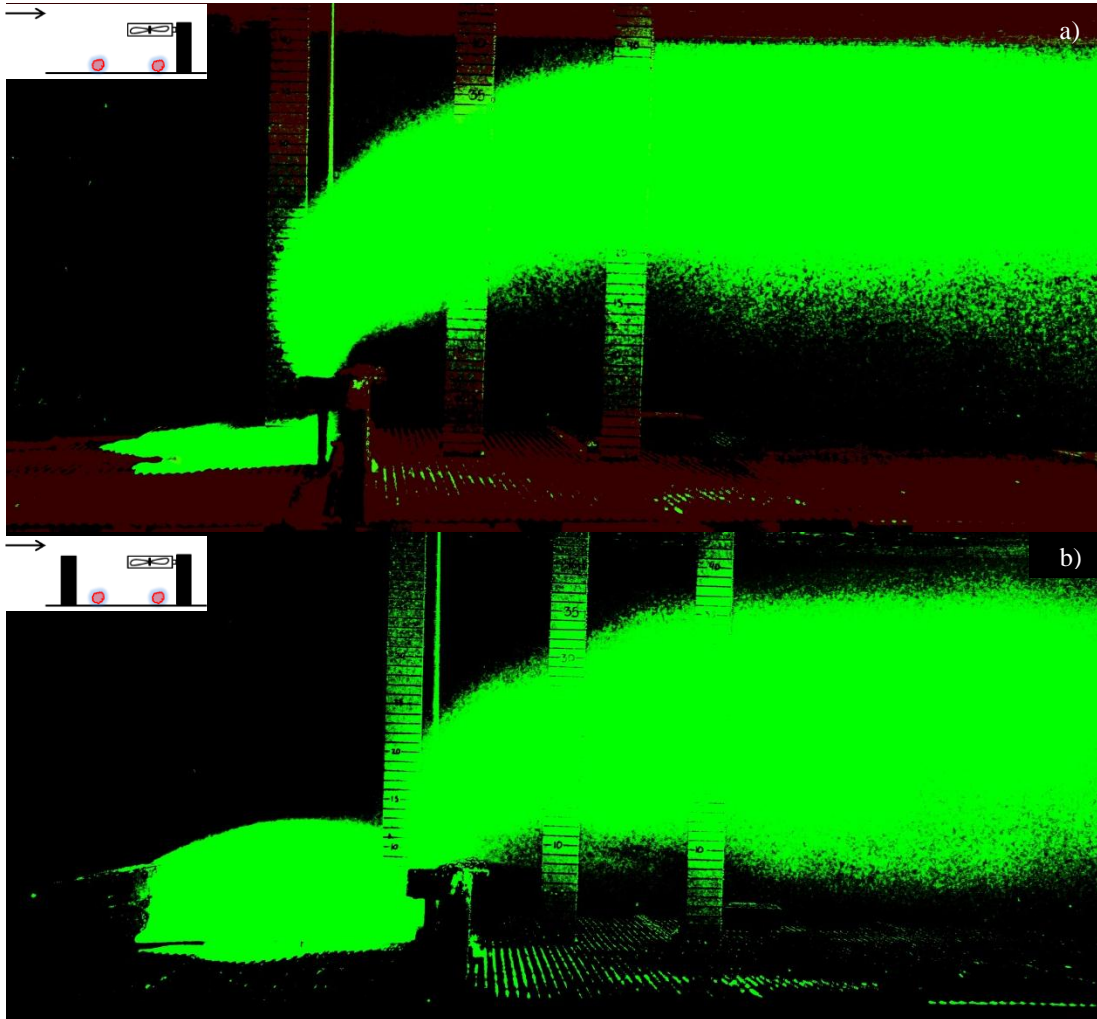
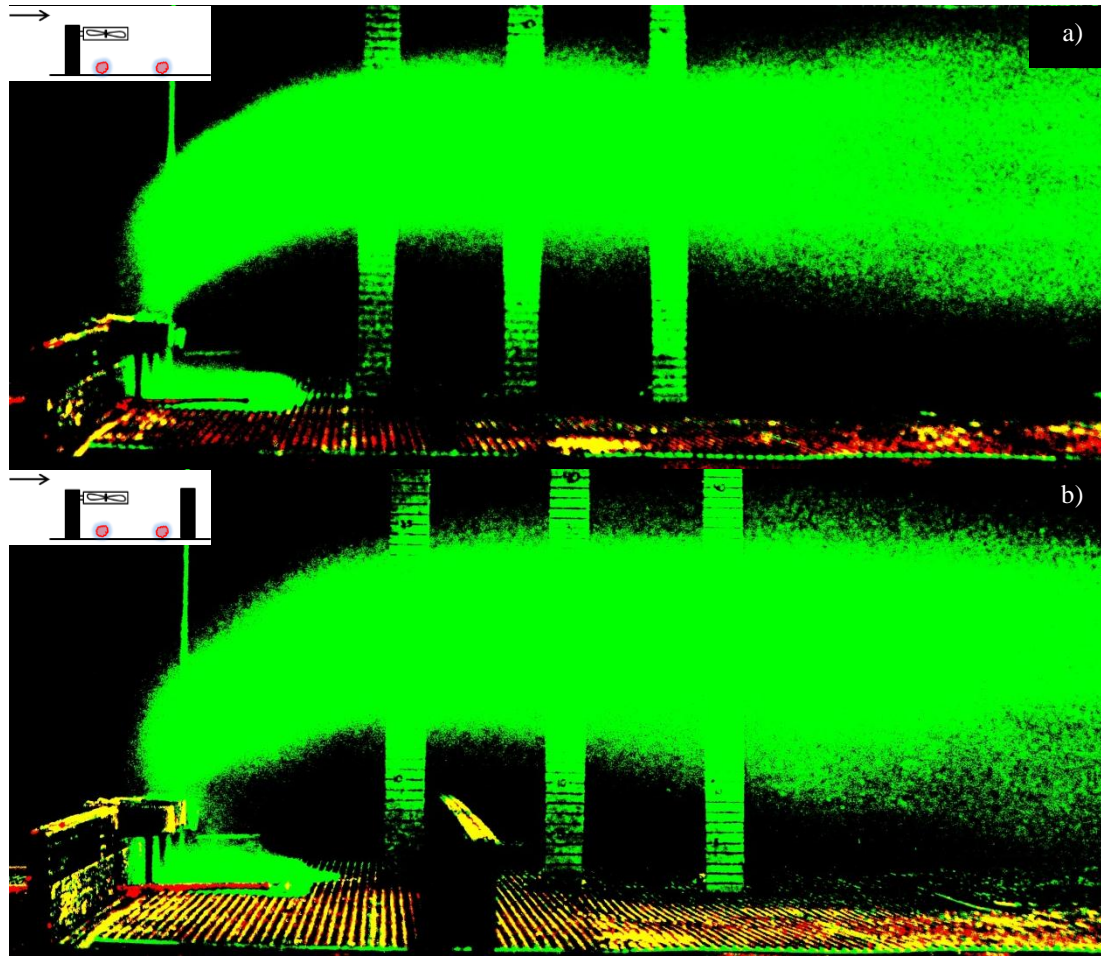**Figure 5-20.** Downwind Fan Visualizations with Low Wind: a) Downwind Only SB; b) $H_{up} = H_{down}$

Figure 5-21. Upwind Fan Visualizations with Low Wind: a) Upwind Only SB; b) $H_{up} = H_{down}$
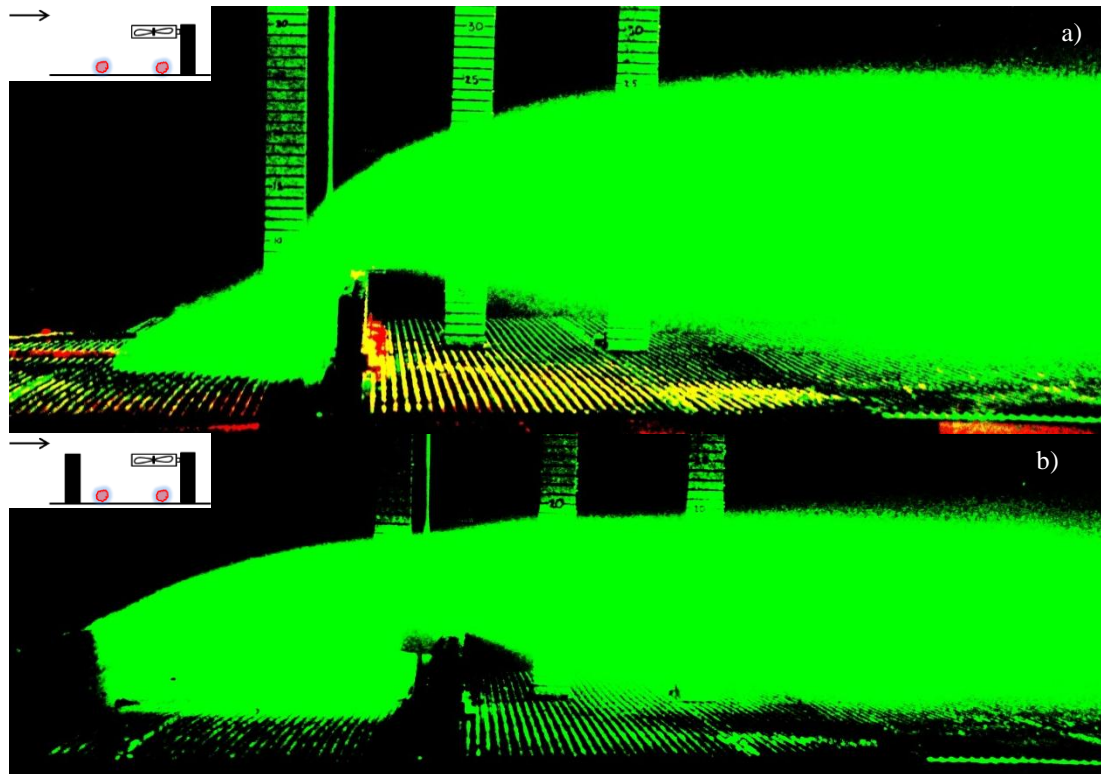
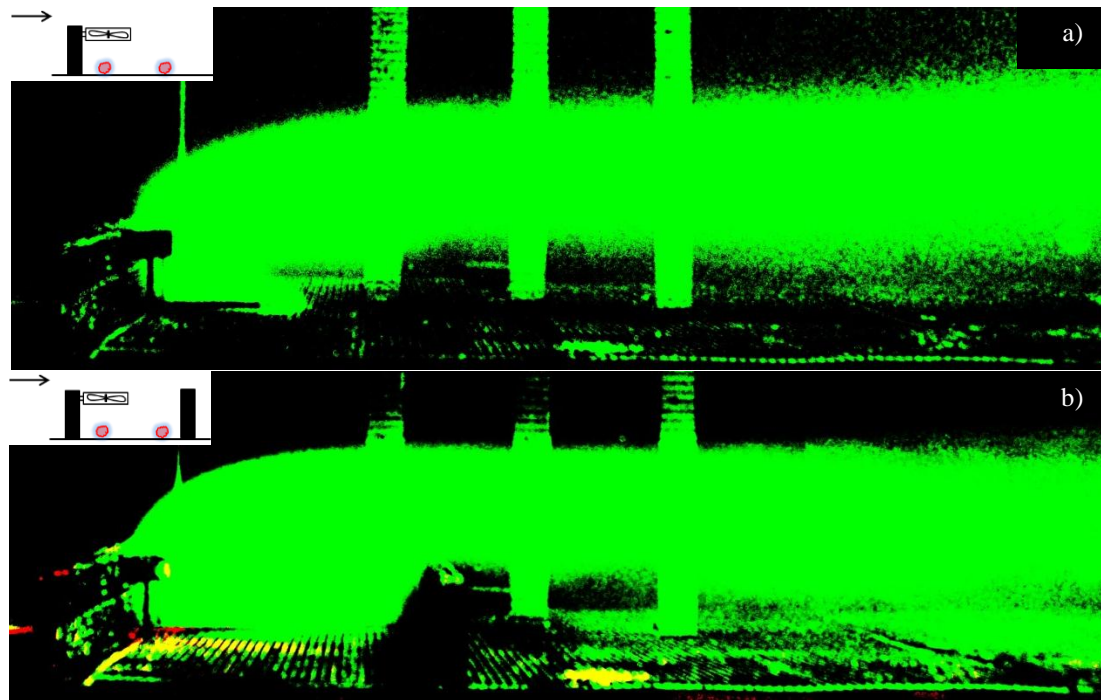**Figure 5-22**. Downwind Fan Visualizations with High Wind: a) Downwind Only SB; b) $H_{up} = H_{down}$

Figure 5-23. Upwind Fan Visualizations with High Wind: a) Upwind Only SB; b) $H_{up} = H_{down}$

The preceding fan visualizations were done using larger diameter fans. The large fan blade size would be impractical for a field application so custom made fan blades were fabricated. The new, smaller fan blades measure 17 mm in diameter. These smaller fans still have a significant impact on the dispersion; however, due to the smaller fan size the flow rate is decreased whereas the outlet velocity is maintained (Figures 5-24, 25). Due to the decrease in flow rate the fans do not capture all of the pollutants and there is spillage over the SBs. This results in pollutants being trapped in the downdraft of the downwind SB. It is very likely that less of the plume is trapped compared to SB without fans (no actual concentration measurements were done).
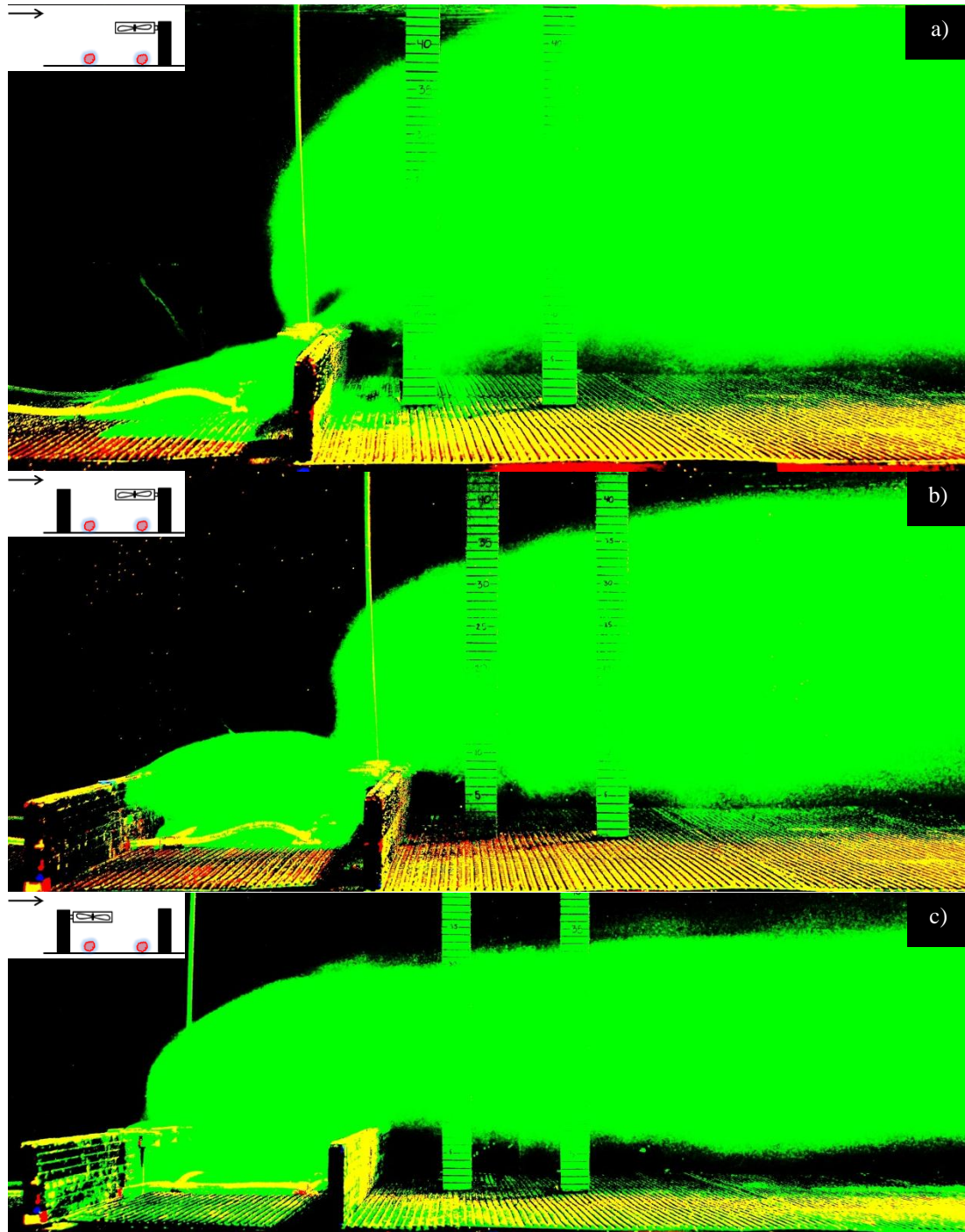
Figure 5-24. Small Fan Visualizations with Low Wind: a) Downwind Only SB with Downwind Fans; b) $H_{up} = H_{down}$ with Downwind Fans; c) $H_{up} = H_{down}$ with Upwind Fans
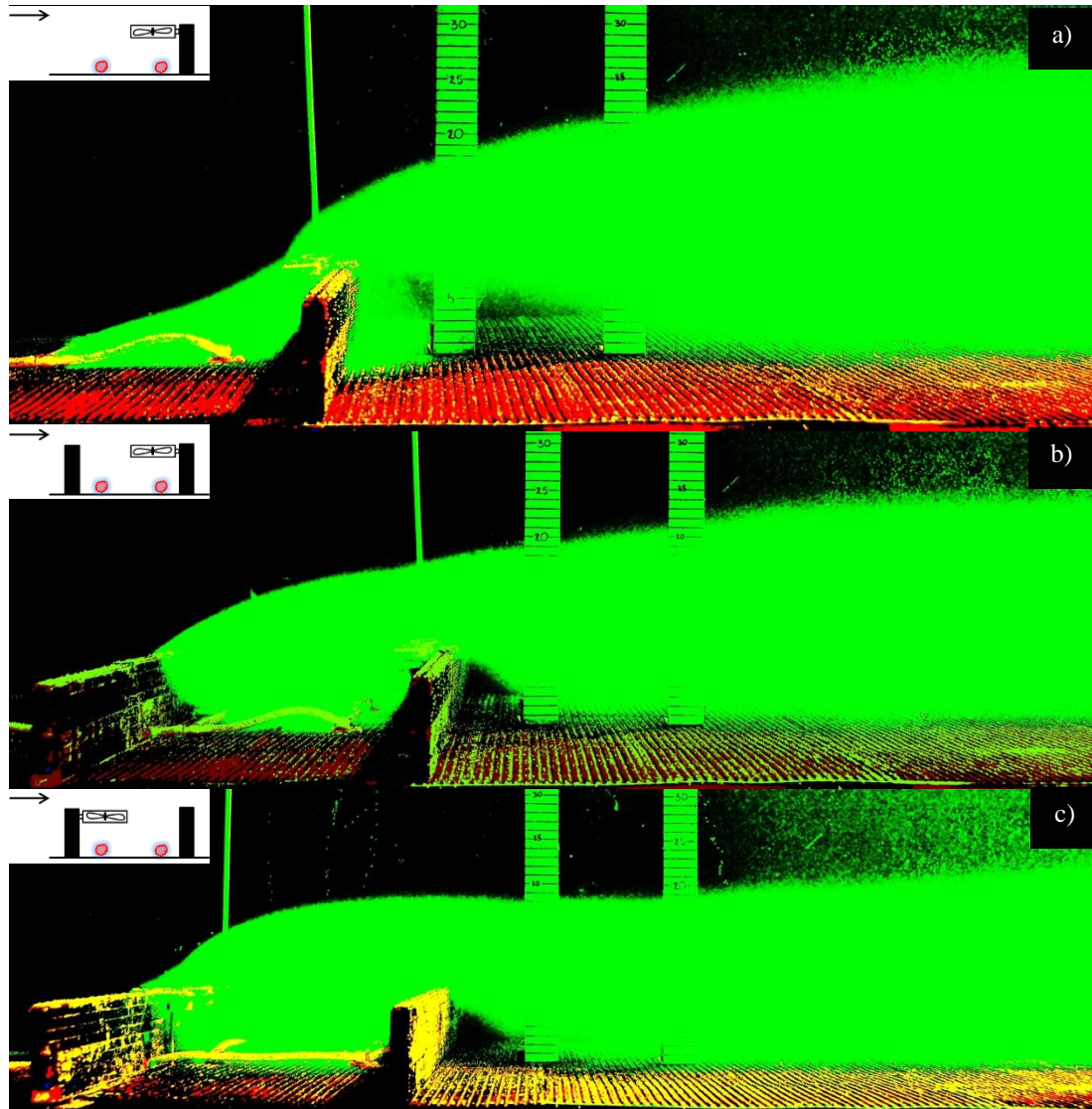
Figure 5-25. Small Fan Visualizations with High Wind: a) Downwind Only SB with Downwind Fans; b) $H_{up} = H_{down}$ with Downwind Fans; c) $H_{up} = H_{down}$ with Upwind Fans

5.10. Visualization Results with Low Wind Speed

Under low wind speed conditions for the roadway configurations of no SB and $H_{up} = H_{down}$ (Figure 5-26), the dispersion pattern is similar to that of high wind speed conditions, however, for the case of $H_{up} = H_{down}$ the vertical plume spread is lower. A high wind speed, such as that used for most of the experiments (4.2 m s^{-1}) is usually associated with slightly unstable

conditions during the day and neutral conditions at night. A low wind speed of 1.5 m s^{-1} is typically associated with extremely to moderately unstable conditions during the day and stable conditions during the night. Since this low wind speed would not be typical of neutral stability the experiments should be conducted with the heaters on. It is noted that at a lower wind speed the experiments with SBs were ran longer in order for the dye (pollutant) to make it far enough downwind to capture a long exposure image of acceptable quality. The time scale for pollutant traveling downwind for roadway configurations with SBs is much higher. Under these low wind speeds it takes a much longer time for the pollutants to make it over the SBs and for short testing durations this leaves the roadway with very high concentrations and lower downwind concentrations. For a comparison of the effects of time scales at low wind speeds one experiment was ran for the same duration as that of the high wind speed experiments (approximately one minute) and a second experiment was ran for double the time. As shown in Figure 5-26c there appears to be almost no pollutants downwind of the roadway below the height of the SB and this shows that under low wind speeds the pollutants can get trapped in a roadway with SBs.
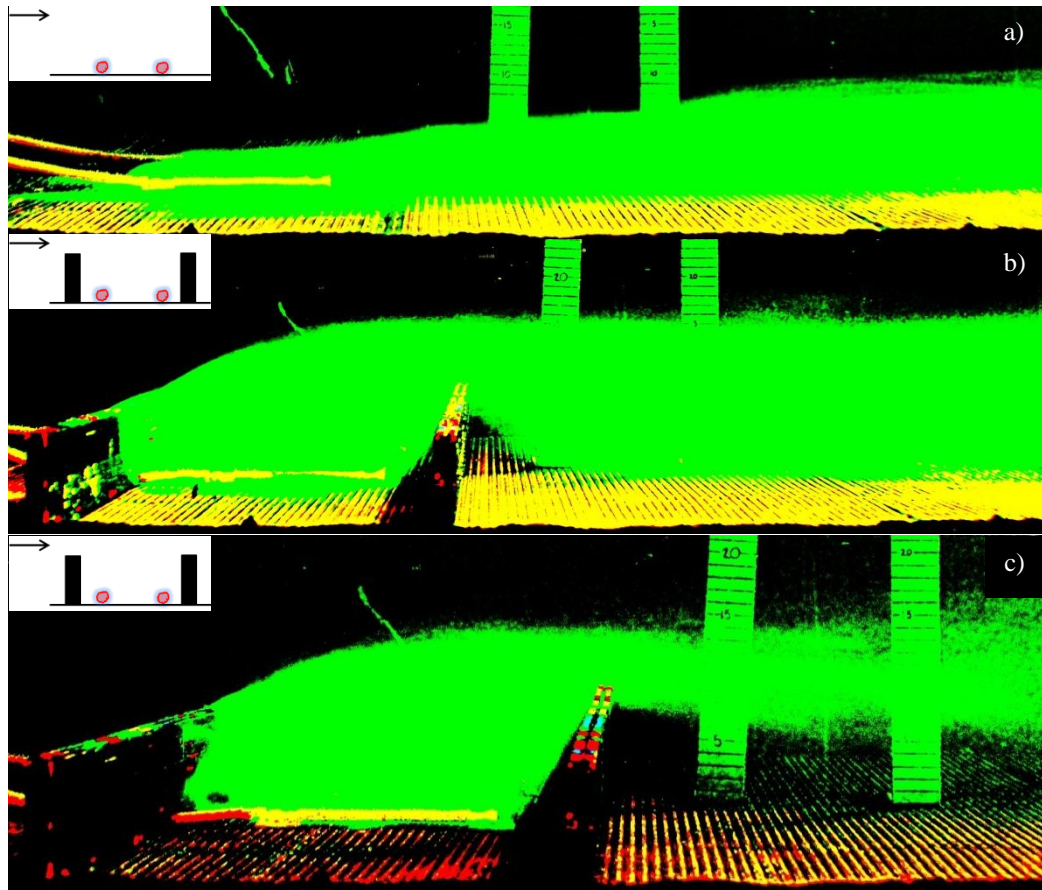
Figure 5-26. Low Wind Visualizations: a) No SB; b) $H_{up} = H_{down}$; c) $H_{up} = H_{down}$ Short Run Time

5.11. Visualization Results for Inclined Sound Barriers

A special case of SBs inclined at 30° and 60° was studied (Figure 5-27). For the case of 30° the plume follows the terrain which helps lift the plume slightly but the plume rises no further past the downwind SB where it gets caught in the downdraft of the SB. For the case of 60° the plume rise is virtually the same as that for the configuration of $H_{up} = H_{down}$.
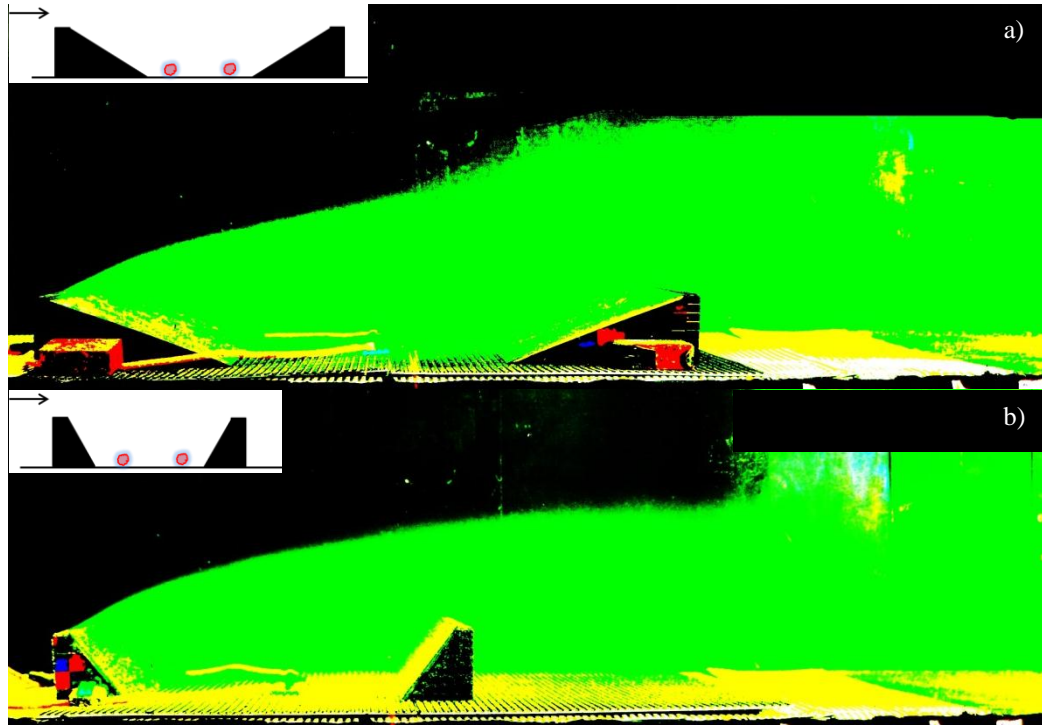
Figure 5-27. Angled SB Visualizations: a) 30°; b) 60°

6. Quantitative Results

Based on the visualization results the most relevant roadway configurations were chosen to perform concentrations measurements. The configurations chosen were the base case of no SB, upwind only SB, downwind only SB, equal height SBs ($H_{up} = H_{down}$), upwind SB double the height of the downwind SB ($H_{up} = 2H_{down}$), and downwind SB double the height of the upwind SB ($H_{down} = 2H_{up}$). These concentration measurements are presented next.

6.1. Fiber Optic Assisted Laser Induced Fluorescence

The FOALIF (see Section 2.3 for FOALIF technique description) experiments were performed for the roadway configurations of no SB, upwind only SB, downwind only SB, $H_{up} = H_{down}$, $H_{up} = 2H_{down}$, and $H_{down} = 2H_{up}$. The sensors were paced 1 cm from the ground which

corresponds to 1 m above the ground in the field. The results for the FOALIF measurements for each case are shown in Figure 6-1. The error bars for each experiment are calculated as follows:

$$\sigma_C = \sqrt{\frac{\Sigma(C - \overline{C})^2}{N}} \qquad (6\text{-}1)$$

$$E_C = \frac{\sigma_C}{\overline{C}} \qquad (6\text{-}2)$$

where σ_C is the standard deviation of the concentration measurements, C is the instantaneous concentration measurements, $\overline{C}$ is the averaged concentration, N is the number of measurements, and E_C is the standard deviation normalized by the average concentration.

As predicted, the case of no SB results in the highest ground level concentrations. It can be seen that given any SB configuration further downwind of the source the results converge. It is noted that the far field concentrations do not drop off as rapidly as that for the case of no SB and this is in part due to the higher on road concentrations. For each roadway configuration there is at least 50% decrease in ground level concentration relative to the case of no SB (due to increased vertical spread caused by SB), and this is observed downwind of the roadway. The concentration results for each of the different roadway configurations will be discussed in more detail in the next section together with the numerical modeling results.
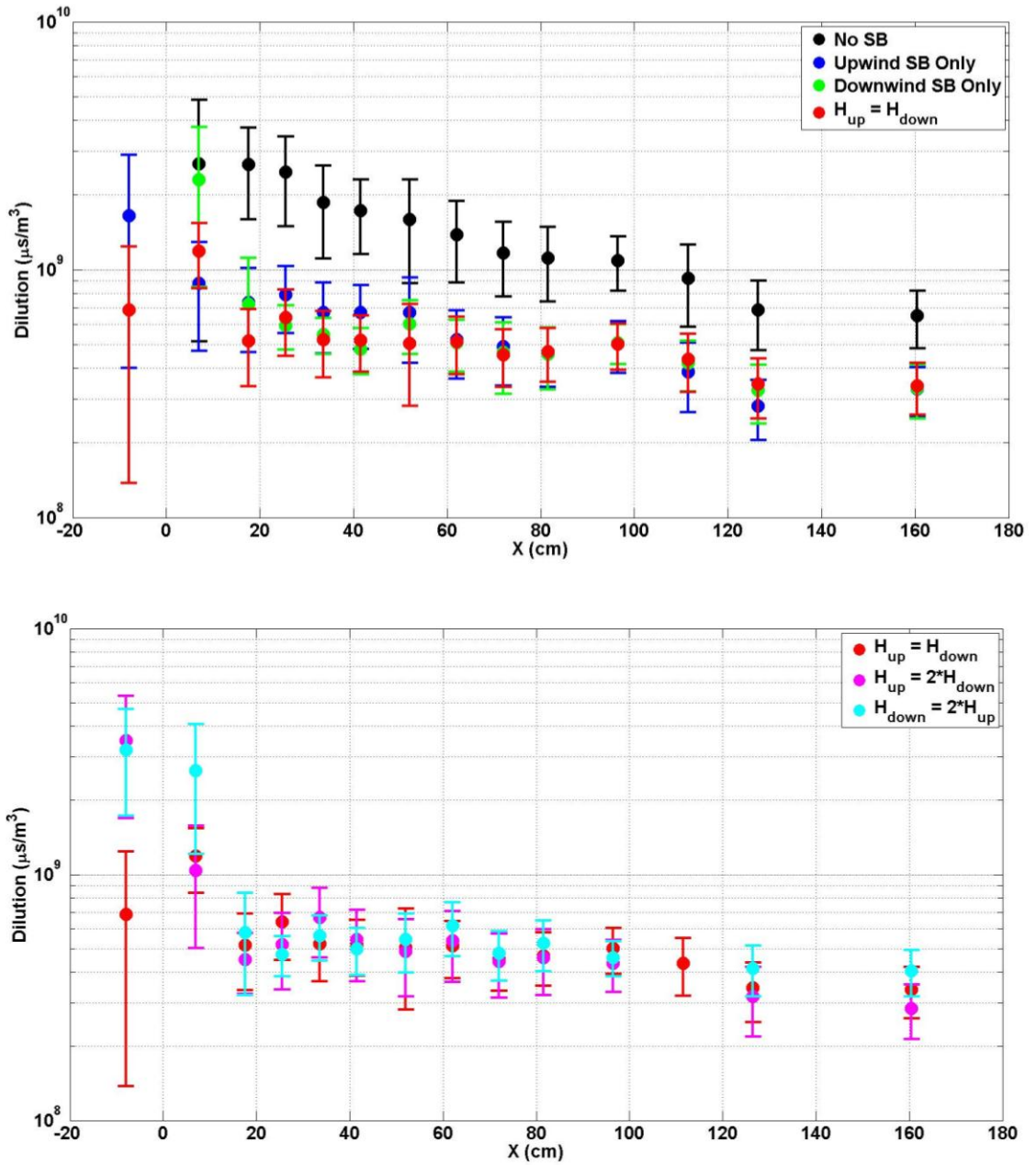
Figure 6-1. FOALIF Concentration Measurements

6.2. QUIC Concentration Results

In this study a limited number of QUIC simulations were performed with no model modifications.

QUIC was set to simulate the tested water channel configurations in the full (field) scale. The road width was chosen as 30 m and a finite line source of 20 m was placed in the center of the roadway. The domain in QUIC was set as 300m×100m×50m ($X \times Y \times Z$) to be the same as the water channel experiments, but extended in the x-direction to capture measurements further downwind of the source. An incoming logarithmic velocity profile with mean stream velocity of 4.2 m s^{-1} and a surface roughness (z_o) of 0.03 m was used. It is noted that QUIC does not accept the friction velocity (u_*) as an input, but the velocity profile can be manipulated by adjusting z_o, the reference velocity and the reference height to obtain a velocity profile that matches that of the water channel. For the case of QUIC-URB discrete data points can be input (i.e. the same values found from PIV). Velocity profiles in the water channel at certain pump frequencies are known from previous experiments. Both QUIC-URB as well as QUIC-CFD wind models were used with QUIC-PLUME and the results are discussed below.

A neutral release with constant mass flow rate of 10 g s^{-1} was released through the line source. It is noted that QUIC does not have the capability to simulate buoyant releases, however for the purposes of simulating vehicle exhaust a neutral release is a valid assumption. It is true that vehicle exhaust is hot relative to ambient conditions however, once the exhaust gases exit the tail pipe the plume becomes immediately well mixed due to the rapid entrainment of ambient air and surrounding traffic. The options in QUIC-PLUME were selected based on recommended optimizations provided by QUIC developer, Dr. Michael Brown at LANL. For example, the simulation duration can be roughly estimated based on the amount of time it would take a particle to travel across the domain and the time step can also be estimated based on the amount of time it would take a particle to cross a grid cell. These parameters along with the number of particles released were adjusted until the particles released made it across the domain, the simulation time

was minimized, and the concentration results became invariant to the number of particles and time step.

The same simulations were done as that of the FOALIF experiments. Figures 6-2 through 6-8 show the ground level center line concentration results produced by QUIC for each of these configurations. The results shown are normalized concentration versus normalized downwind distance. Normalized concentration is calculated as

$$\chi = \frac{CUL_xL_y}{Q} \tag{6-1}$$

where C (kg m^{-3}) is the concentration, U (m s^{-1}) is the mean velocity, Q (kg s^{-1}) is the emission rate, L_x (m) and L_y (m) are horizontal and lateral length scales. U and Q are known for both the FOALIF experiments and QUIC as they are model and experimental inputs. L_x and L_y were chosen as the road width and source length respectively. It does seem to make more sense to normalize the concentration results for the case of no SB based on the friction velocity and roughness length, however, in order to have equal comparison for each roadway configuration the case of no SB was normalized in the same way. As can be seen, for each of the different roadway configurations QUIC overestimates the on road concentrations. Within $2H_{SB}$ to $10H_{SB}$ downwind of the road the QUIC results are very comparable to the FOALIF results, however, the far field concentrations from QUIC decrease faster than that of the FOALIF. As was described in Section 3, QUIC-CFD uses a zeroth order turbulent closure based on Prandtl's mixing length. Figure 6-5 shows the concentration results produced when using the default mixing length (equation 3-4) calculated in the QUIC-CFD wind model and as shown, the concentration results up to $15H_{SB}$ are highly under predicted. Based on these results the mixing length was increased to 30 m and this produced much better results (Figure 6-6, 6-7, 6-8). The QUIC results do not match well that of the FOALIF, nor should they perfectly match that of field experiments, but due to the ease of use,

speed and the model availability, QUIC yields reasonable results. Note that in this study no QUIC model corrections/tweaks were used so it is not surprising that it some cases and locations the predictions are factor of 5 off but in 75% of cases predictions are within a factor of 2.

For the case of upwind only SB (Figure 6-3) there is high concentrations near the lee side of the SB due to the recirculation on the roadway (Figure 6-9a), which brings pollutants back towards the barrier where they get advected up. The on road concentration results near the SB produce by QUIC are nearly five times higher than that of the FOALIF results. Downwind of the source up to $10H_{SB}$ the QUIC-URB results compare well to the FOALIF results. Overall the FOALIF and QUIC results correlate with the visualizations and PIV results as the highest ground level concentrations should be observed near the lee side of the SB and the concentration should fall off downwind of the roadway.

For the case of downwind only SB (Figure 6-4) there are high concentrations near the upwind side of the SB, which correlates with the visualizations. The QUIC results upwind of the SB are much higher than that of the FOALIF results and downwind of the SB up to $15H_{SB}$ the QUIC-URB results compare well to the FOALIF results. Per the visualizations (Figure 5-3a) there is a region of low concentrations extending roughly $1H_{SB}$ downwind of the SB; this can also be seen in the PIV results (Figure 4-2c and 4-27a), which shows low velocities and turbulence in this region. The QUIC-URB results show this decrease in concentration and the FOALIF show a decreasing trend up to $5H_{SB}$, however this decrease is not as pronounced as in QUIC simulations. It is hypothesized that this region, as shown in the visualizations, should have low concentrations and the error bars in the FOALIF show that the concentration could be lower in this region. Though there is a recirculation on the lee side of the SB (Figure 6-9b), which would account for some concentrations and not zero concentration, there would be very low entrainment due to the higher velocities above the SB and the low region of turbulence in the lee of the SB. As seen in

the visualizations (Figure 5-3b), decreasing the SB height reduces the lee side cavity resulting in increased ground level concentrations.

For the case of $H_{up} = H_{down}$ (Figure 6-6) the QUIC results show high on road concentration near the lee side of the upwind SB due to the recirculation on the roadway (Figure 6-9c), which brings pollutants back towards the barrier where they get advected up. The FOALIF results do not show high concentrations in this region and this does not correlate with the visualizations (Figure 5-4a); the uncertainty in the FOALIF may account for this. Just downwind of the SB the visualizations show a low concentration region and the PIV results (Figure 4-3a and 4-28a) show very low velocities and turbulence in this region. It would be expected to see a dip in concentration near the lee side of the downwind SB, which the FOALIF results do somewhat show, but not as large of a drop as seen in QUIC. There is a lee side cavity produced (Figure 6-9c), however due to the presence of the upwind SB it is smaller than that of the case of downwind only SB. Downwind of the source up to $10H_{SB}$ the QUIC-URB results compare well to the FOALIF results. As seen in the visualizations (Figure 5-4b), decreasing the SB height reduces the lee side cavity resulting in increased concentrations.

For the case of $H_{up} = 2H_{down}$ (Figure 6-7) there is high concentrations near the lee side of the upwind SB due to the recirculation on the roadway (Figure 6-9d), which brings pollutants back towards the barrier where they get advected up. The on road concentration results produced by QUIC can be misleading since the QUIC-URB results show lower concentrations near the upwind SB and the QUIC-CFD results show higher concentrations near the upwind SB. The FOALIF and QUIC-CFD results show higher on road concentrations near the upwind SB than that near the downwind SB, which makes sense. Due to the lower downwind SB less pollutants are caught in the downdraft of the downwind SB as in the case of $H_{up} = H_{down}$, resulting in concentrations near the downwind SB that are lower than that of $H_{up} = H_{down}$. The concentration

results on the lee side of the downwind SB are the lowest for this case compared to all other cases, but based on the visualizations (Figure 5-5) and PIV (Figure 4-3b) results it would be expected that the concentration results in this region should be higher than that of $H_{down} = 2H_{up}$ and also $H_{up} = H_{down}$, and the uncertainty in the FOALIF may explain this. The QUIC results do not show a dip in concentration on the lee side of the downwind SB. Downwind of the roadway from $5H_{SB}$ to $15H_{SB}$ the QUIC-URB results compare well to the FOALIF results.

For the case of $H_{down} = 2H_{up}$ (Figure 6-8) there are high concentrations near the lee side of the upwind SB due to the recirculation on the roadway (Figure 6-9e), which brings pollutants back towards the barrier where they get advected up. Due to the shorter upwind SB the on road eddy is shorter (Figure 6-9e), thus decreasing the advection height and this results in more pollutants being brought back down into the roadway by the downdraft of the downwind SB. As seen in the visualizations (Figure 5-6) there is a region of low concentrations on the lee side of the downwind SB similar to roadway configuration of downwind only SB. The QUIC-URB results show a region of low concentration on the lee side of the downwind SB which correlates with that of the visualizations. The FOALIF results show a decrease in concentrations in this region, however these concentrations results are higher than that of $H_{up} = H_{down}$ and $H_{up} = 2H_{down}$, whereas based on the visualizations it would be expected to be lower; the uncertainty in the FOALIF show that the concentrations could be lower in this region.
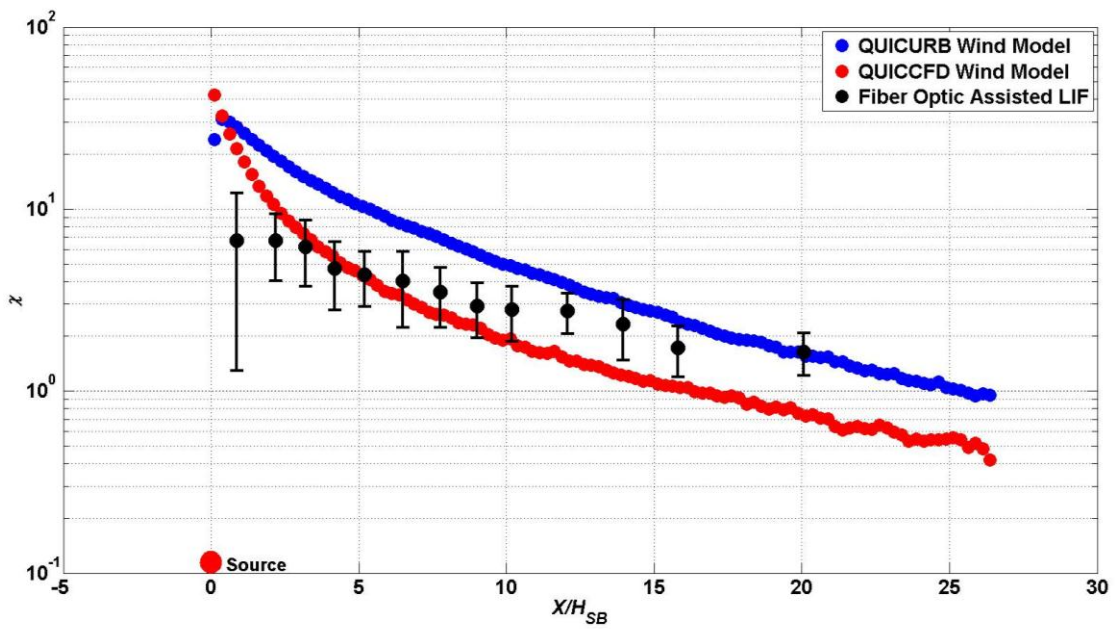
Figure 6-2. QUIC versus FOALIF Concentration Results: No SB. Normalized concentration is presented versus distance given in heights of SB (i.e. SB is at X/H_{SB}=1)
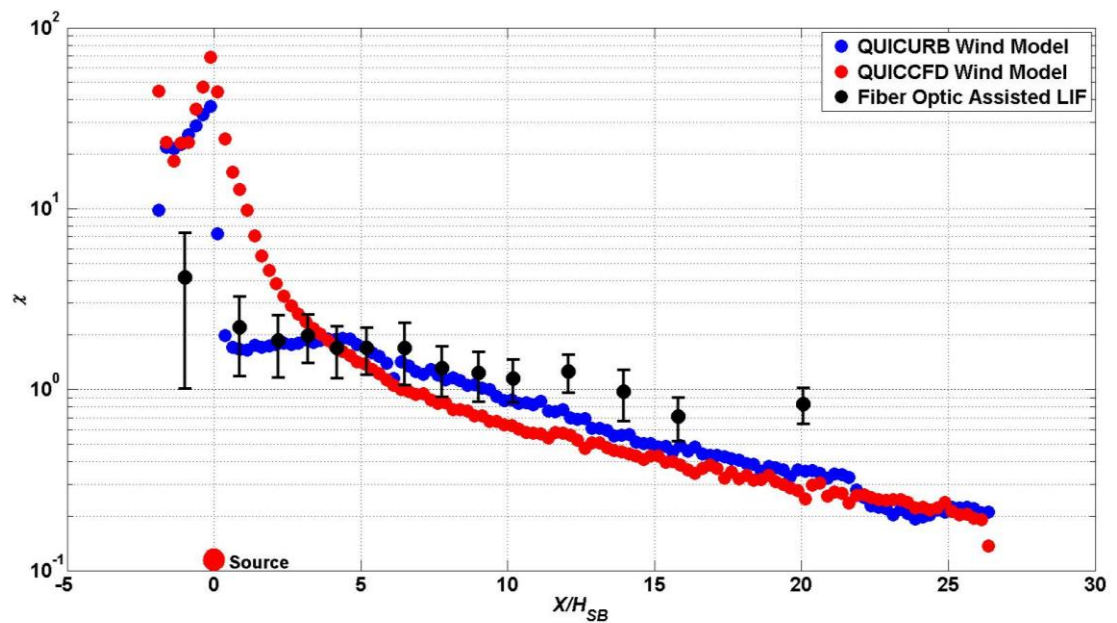
Figure 6-3. QUIC versus FOALIF Concentration Results: Upwind Only SB
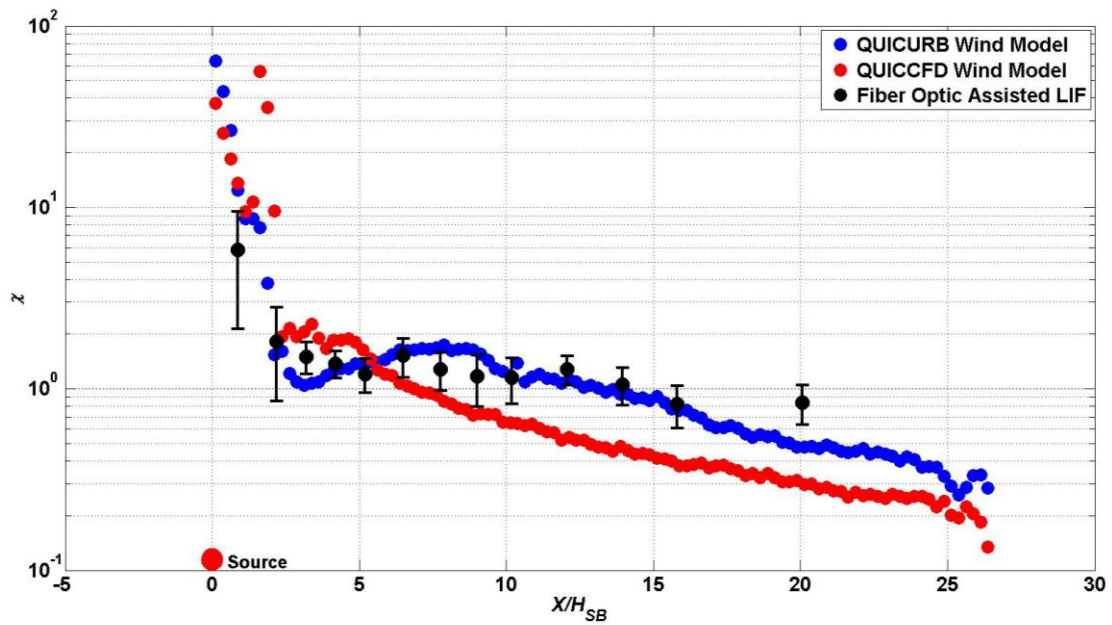
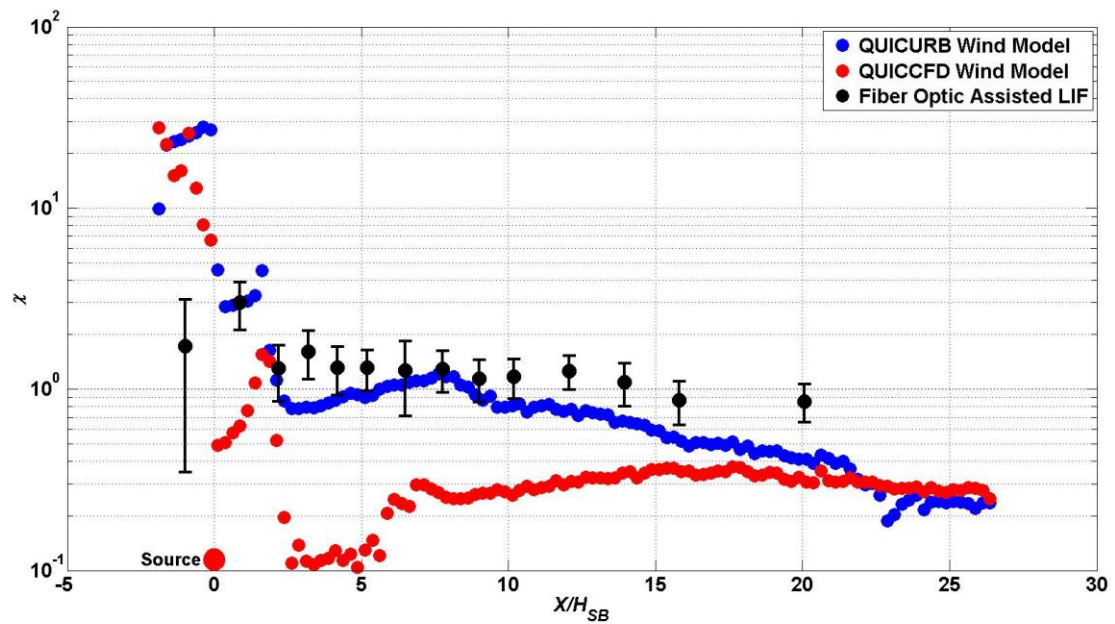**Figure 6-4.** QUIC versus FOALIF Concentration Results: Downwind Only SB

Figure 6-5. QUIC versus FOALIF Concentration Results: $H_{up} = H_{down}$, QUIC CFD with default l_{mix} (equation 3-4)
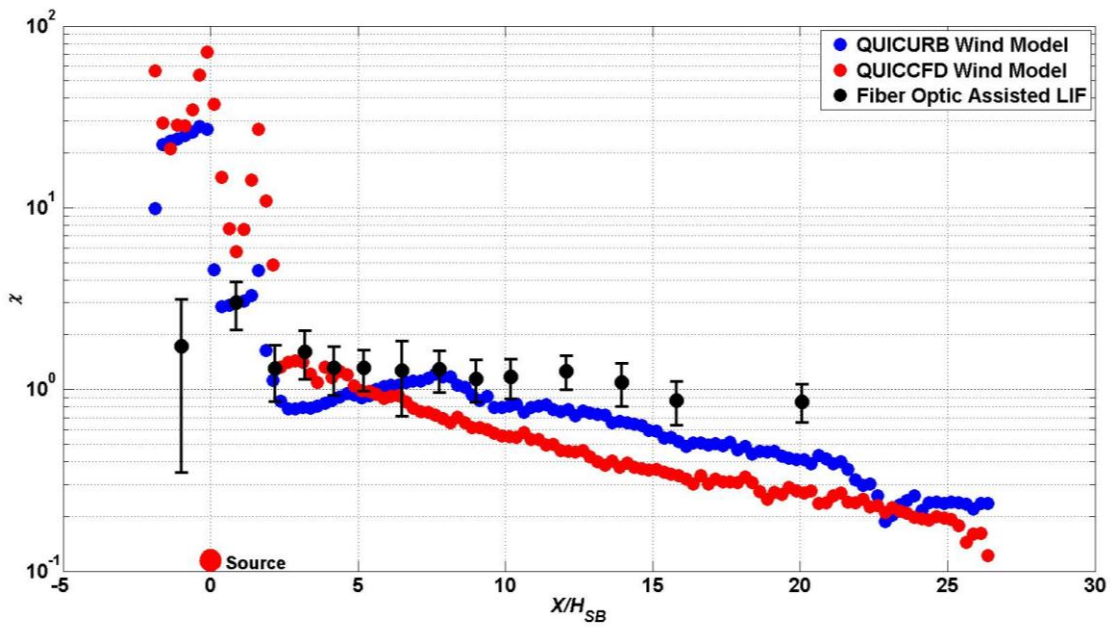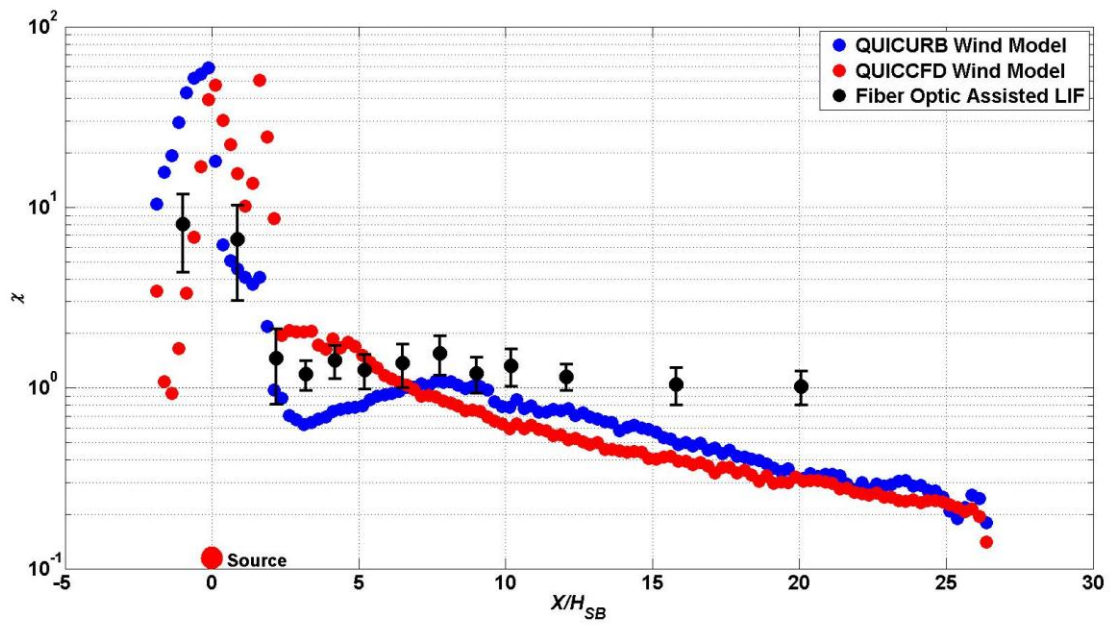
Figure 6-6. QUIC versus FOALIF Concentration Results: $H_{up} = H_{down}$
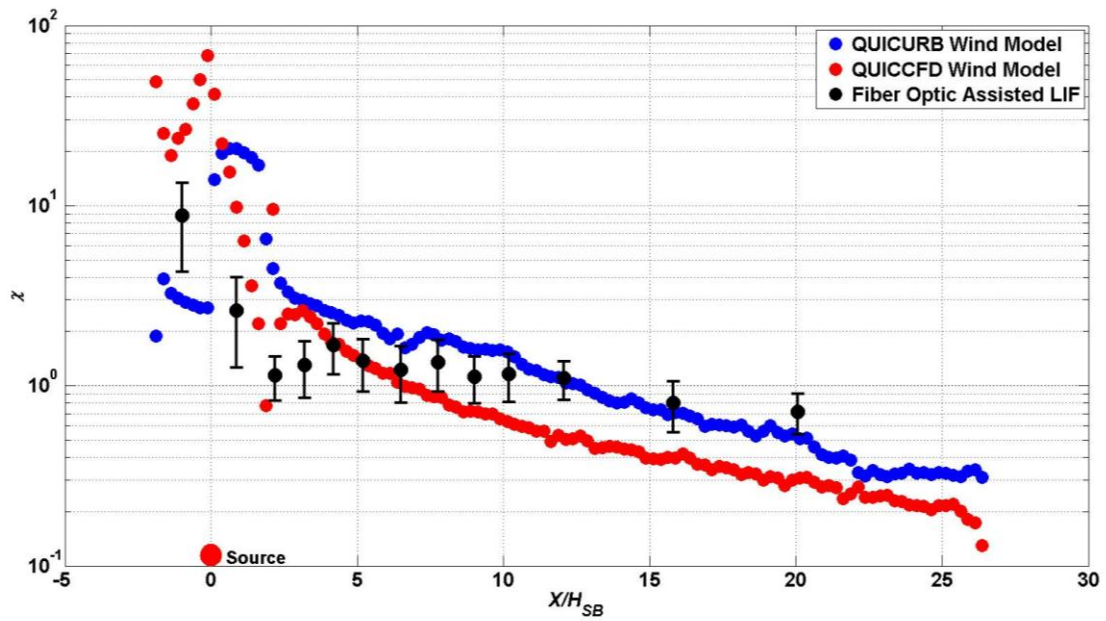
Figure 6-7. QUIC versus FOALIF Concentration Results: $H_{up} = 2H_{down}$

95

Figure 6-8. QUIC versus FOALIF Concentration Results: $H_{down} = 2H_{up}$
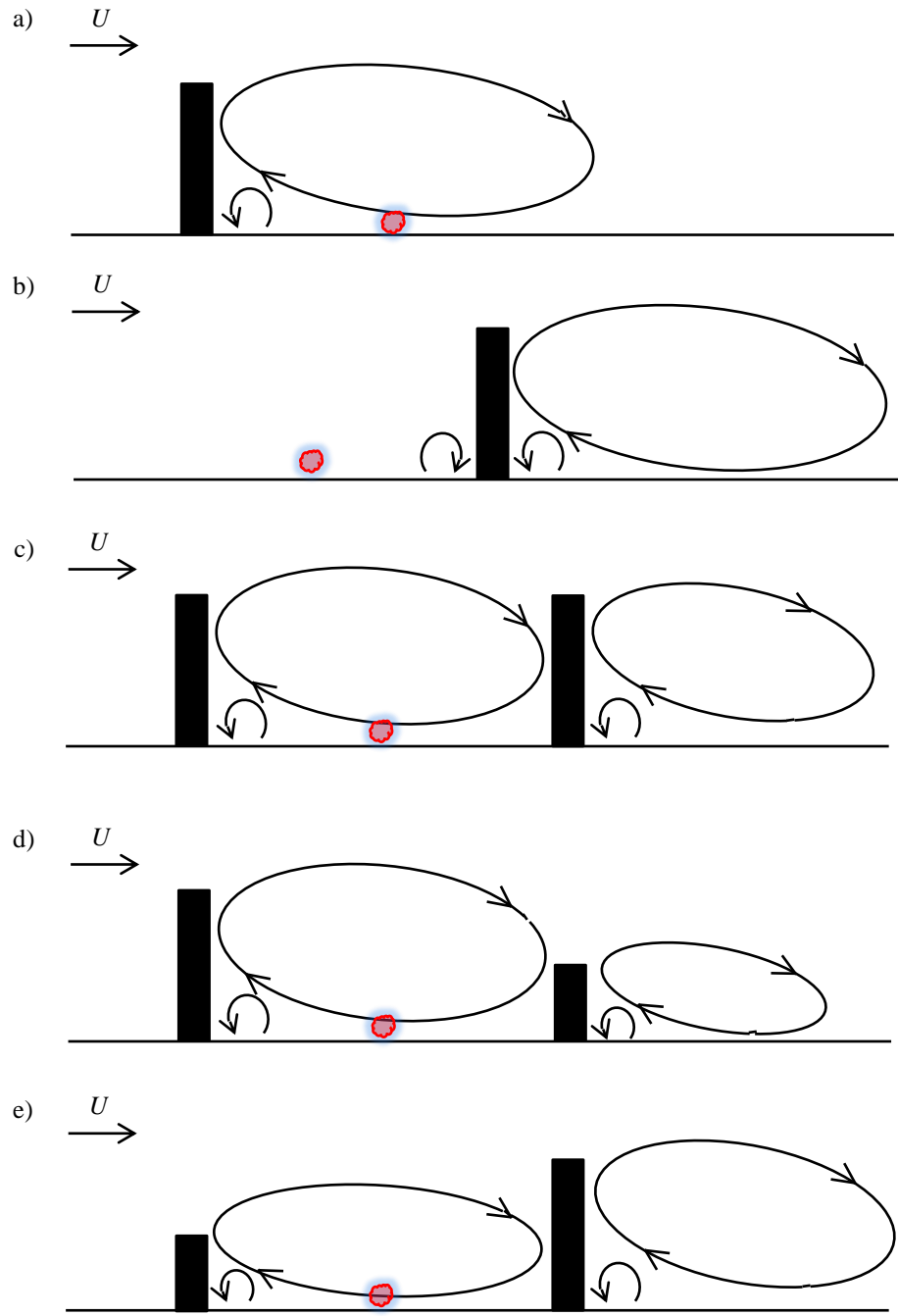
Figure 6-9. SB Produced Eddies: a) Upwind Only SB, b) downwind only SB, c) $H_{up} = H_{down}$, d) $H_{up} = 2H_{down}$, e) $H_{down} = 2H_{up}$

The QUIC-CFD results with the default mixing length (equation 3-4) are shown in Figure 6-10. For each of the SB configurations it is seen that there is a large drop in concentration approximately $5H_{SB}$ downwind of the source. This distance however is overestimated. As it is hypothesized that there is a drop in concentration behind a downwind SB, this concentration drop would not extended that far downwind, as per the visualizations and PIV results, this region extends at most a little over $1H_{SB}$ (depending on SB configuration) downwind of the downwind SB. In this region there are very low velocities and very low dye intensities, and this would signify low concentrations. As was described early and shown in Figure 6-5 the QUIC-CFD results using the default mixing length within the region of $2H_{SB}$ and $15H_{SB}$ are much lower than the FOALIF and QUIC-URB results. As shown in Figure 6-9 next to each SB is a large eddy and a small counter rotating eddy. As the mixing length is increased the larger eddy decreases and the smaller eddy disappears, this allows more pollutants to get mixed in the wake of a SB, thus increasing the concentrations from what is seen in Figure 6-10 to what is seen in Figures 6-3 through 6-8.
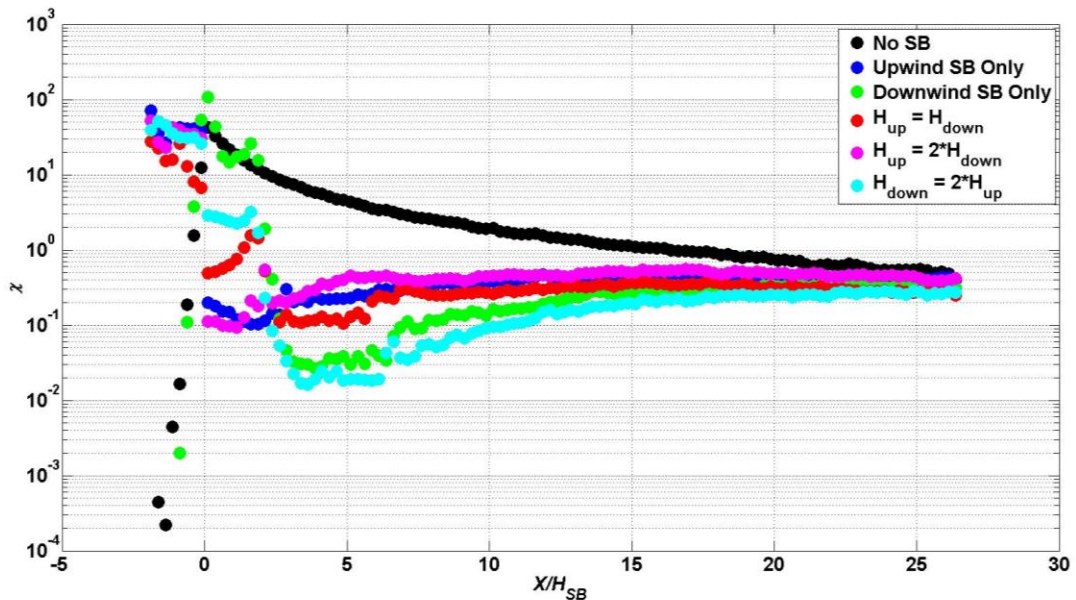
Figure 6-10. QUIC-CFD Concentration Results, Default l_{mix} (equation 3-4).

The observed (FOALIF) versus the estimated (QUIC) concentration results at each measurement location in the water channel are shown in Figures 6-11 through 6-16. As shown, 75% of the results fall within the factor of 2. QUIC underestimates the concentration for each roadway configuration except that of no SB with the QUIC-URB wind model. The concentration underestimation is due to the far field concentration results in QUIC falling off faster than that of the FOALIF. It is hypothesized that this is due to the on road concentrations in QUIC being approximately five times higher than that of the FOALIF results. The higher on road concentrations lead to lower downwind concentrations resulting in the discrepancy between the laboratory and numerical results. For future research it may be best to look at the cross wind integrated concentration, and for that it is recommended to place sensors at the edge of the water channel, in line with center line sensors. The cross wind integrated concentration will better describe the overall mass flux and this can help in finding the actual discrepancies seen between the laboratory and numerical results.
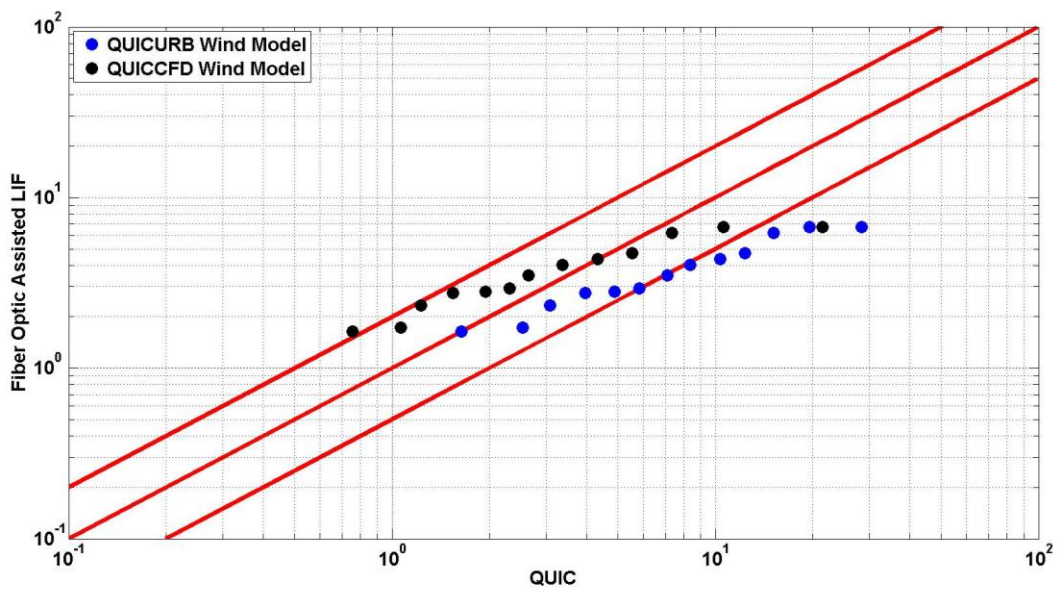
Figure 6-11. QUIC versus FOALIF Dimensionless Concentration Results: No SB
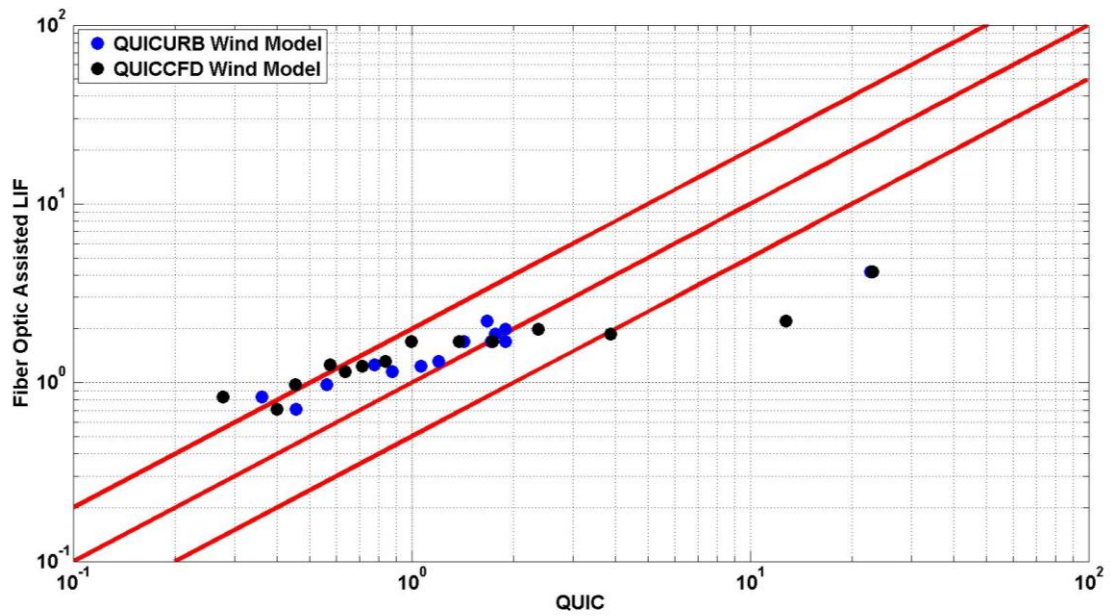
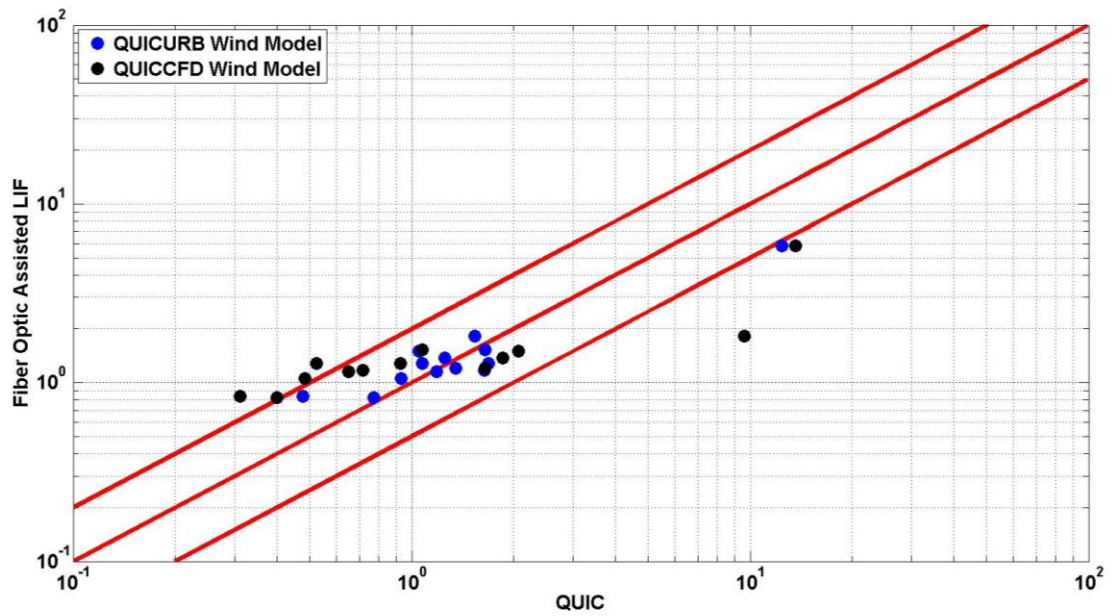**Figure 6-12.** QUIC versus FOALIF Results: Upwind Only SB

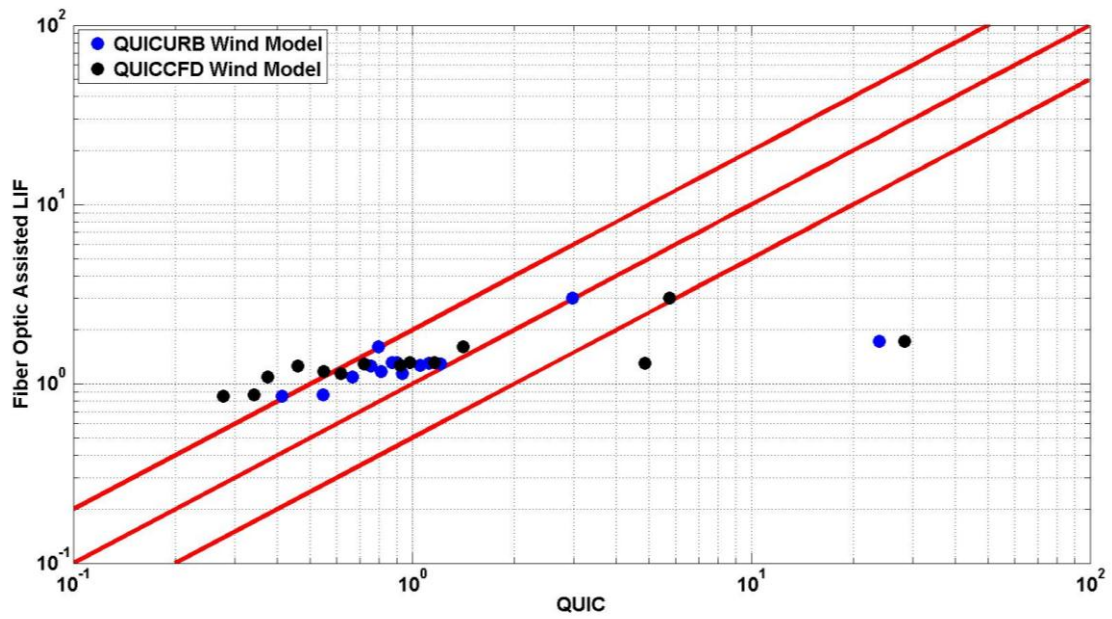**Figure 6-13.** QUIC versus FOALIF Results: Downwind Only SB

100

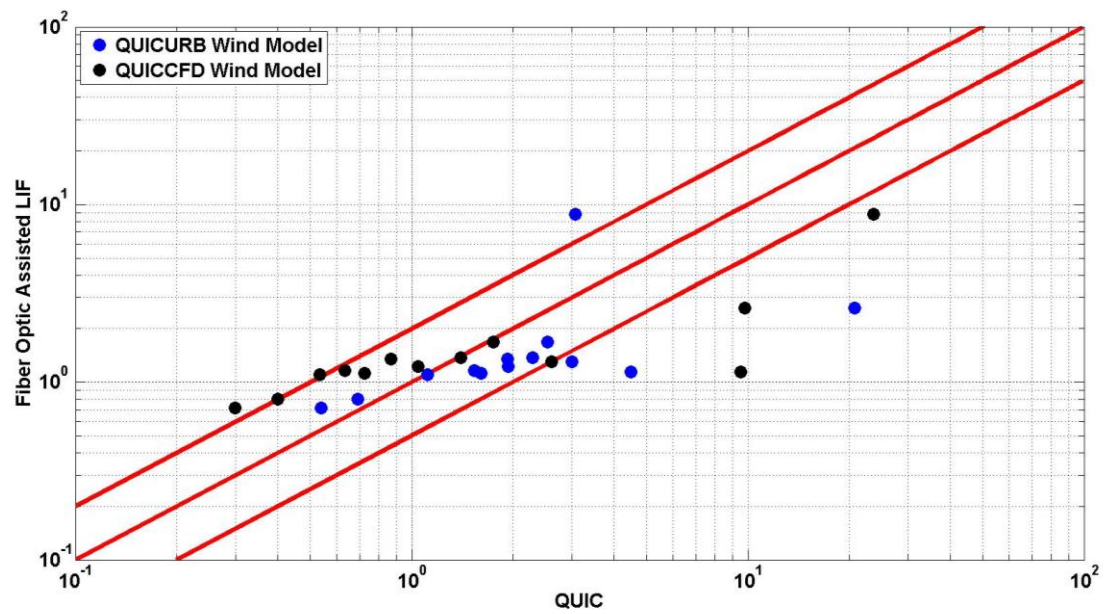**Figure 6-14.** QUIC versus FOALIF Results: $H_{up} = H_{down}$

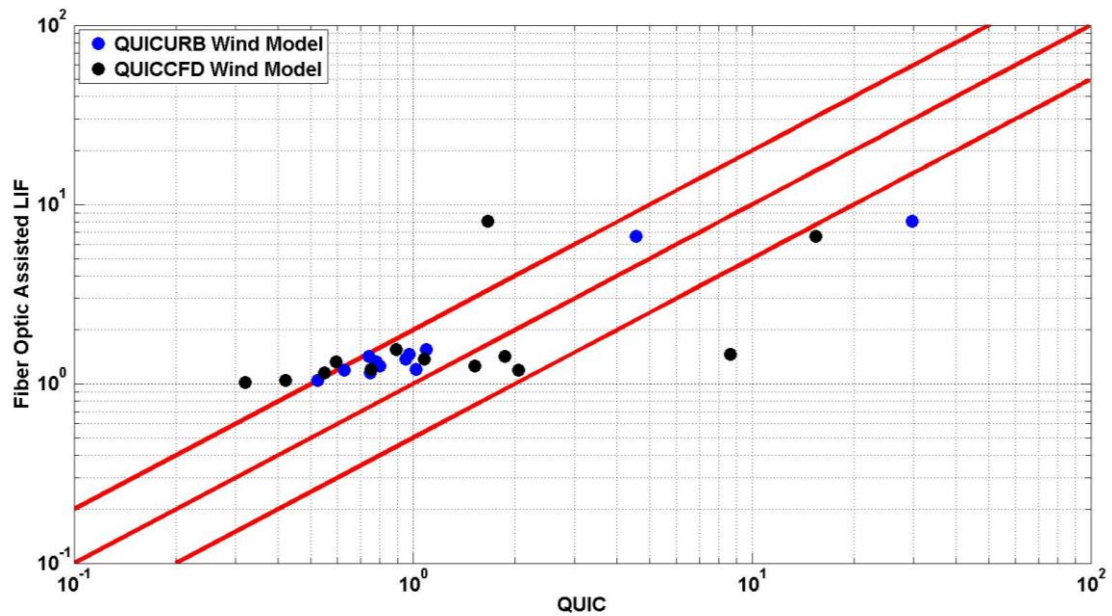**Figure 6-15.** QUIC versus FOALIF Results: $H_{up} = 2H_{down}$

Figure 6-16. QUIC versus FOALIF Results: $H_{down} = 2H_{up}$

It has been shown that QUIC yields acceptable results (75% within a factor of 2) and for that reason, concentration results under low wind speeds conditions for the main roadway configurations are presented. Shown in Figures 6-17 through 6-20 are comparisons of dilution for low wind speeds (1.5 m s^{-1}) and high wind speed (4.2 m s^{-1}). Just downwind of the roadway (approximately three SB heights), with the exception of the case of no SB, the ground level concentration results are higher for the case of high wind. This result is unexpected, however, there are several reasons why this is correct. During low wind speed conditions the on road concentrations are much higher and the downdraft velocities in the wake of a SB are much higher during high wind speed conditions which results in more pollutants being brought towards the ground.
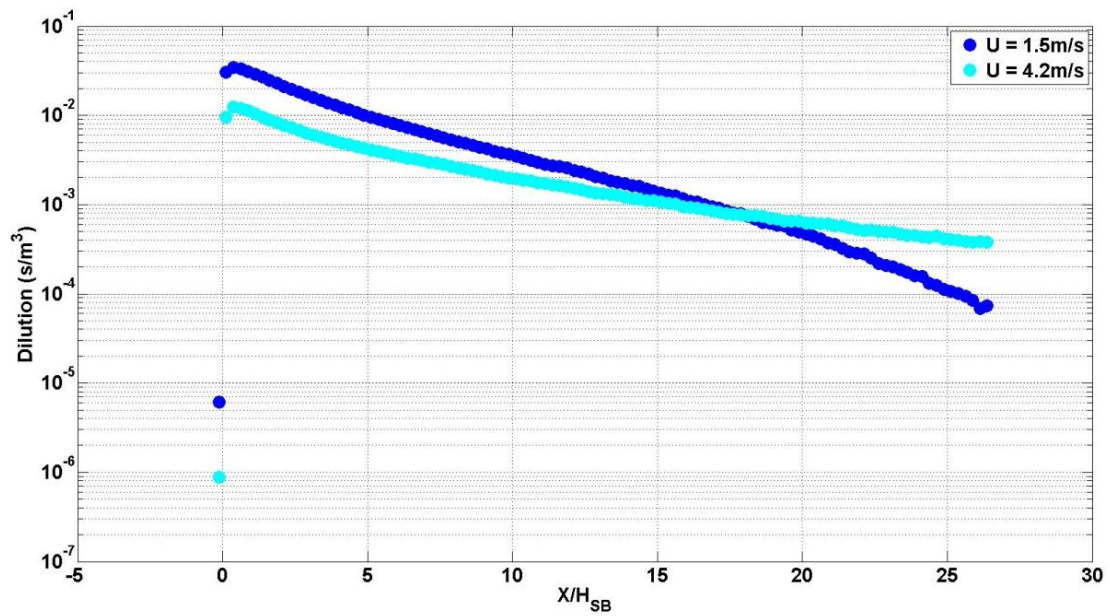
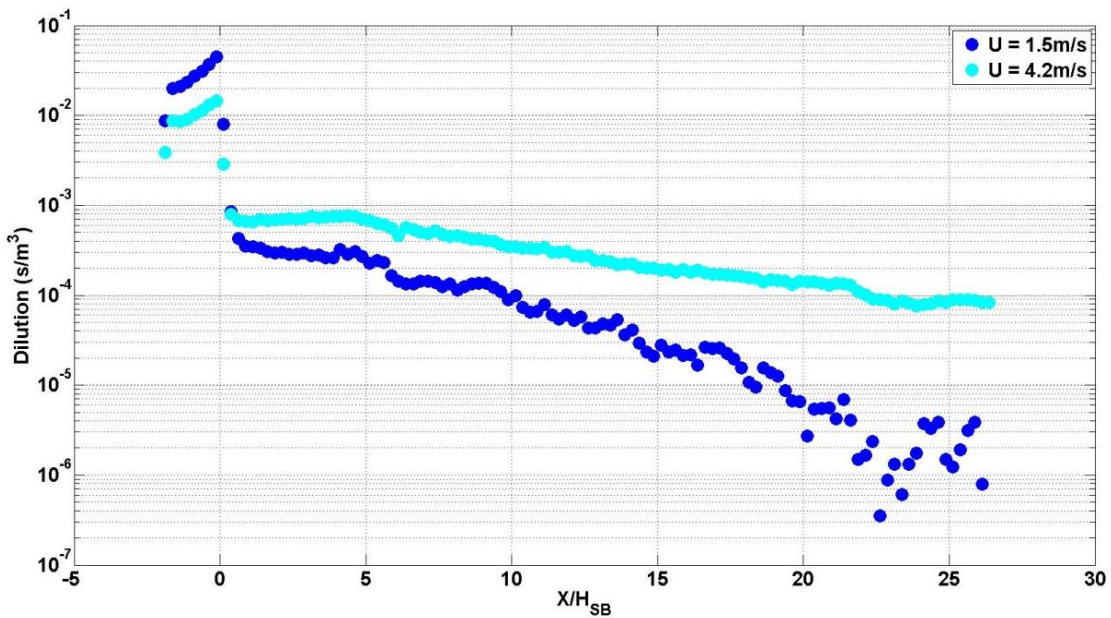**Figure 6-17.** QUIC Wind Speed Results: No SB

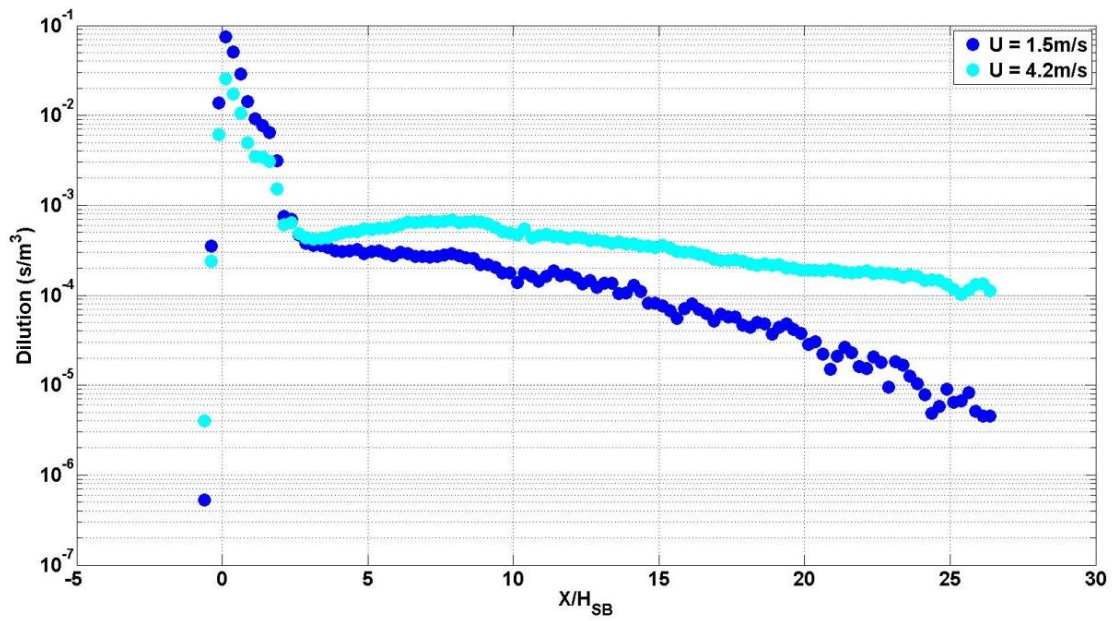**Figure 6-18.** QUIC Wind Speed Results: Upwind Only SB

103

Figure 6-19. QUIC Wind Speed Results: Downwind Only SB
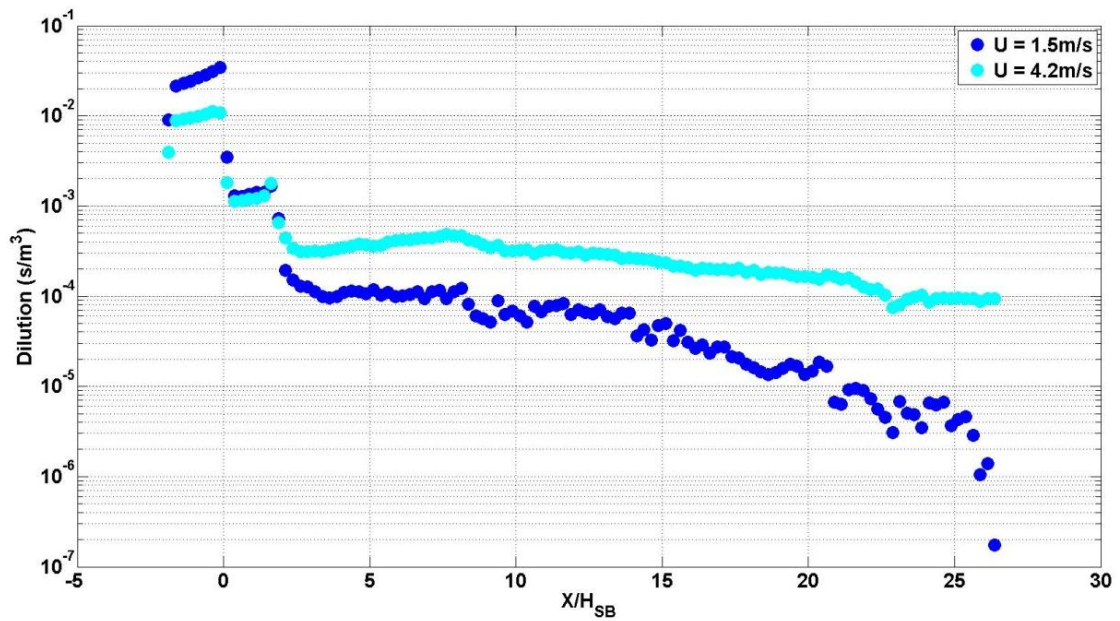

Figure 6-20. QUIC Wind Speed Results: $H_{up} = H_{down}$

6.3. Gaussian Model and Venkatram 2004 Model Results

The setup for the Gaussian Model and the Venkatram 2004 Model matches that of the water channel. Since due to their very nature (i.e. they cannot predict any kind of flow patterns caused by obstacles) these models have to be tweaked for all configurations that differ from simple flat terrain (i.e. "the new model has to be built"). Here the tweaks consisted of moving the source location and prescribing the initial spread. For each SB configuration the source was placed on top of a SB, as shown in Figure 6-21. The Venkatram 2004 model slightly overestimates the concentrations; however the concentration trend (decreasing pattern) is very similar to that of the FOALIF. The results for the Upwind Only SB show good agreement with the model slightly underestimating the concentrations. The model results for the cases of Downwind Only SB and $H_{up} = H_{down}$ underestimate the concentrations by an average of 50%, with the highest being two times underestimated and a minimum of 20% underestimated.
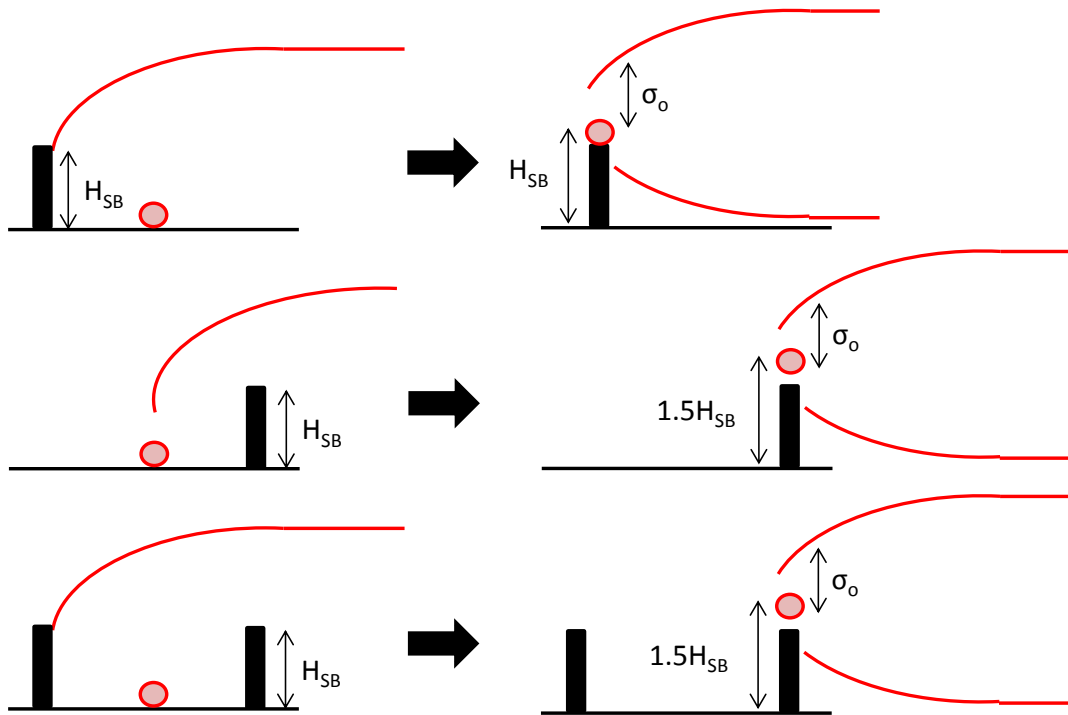

Figure 6-21. Needed adjustments to Gaussian Models to account for sound barrier. In general source should be moved above the sound barrier and the initial spread has to be prescribed.
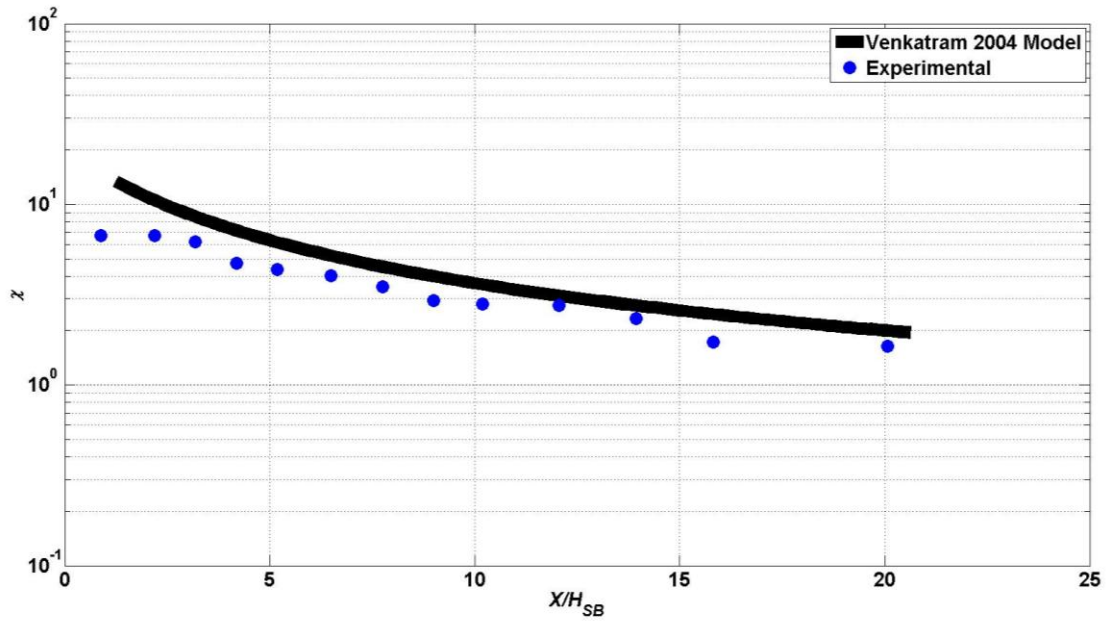
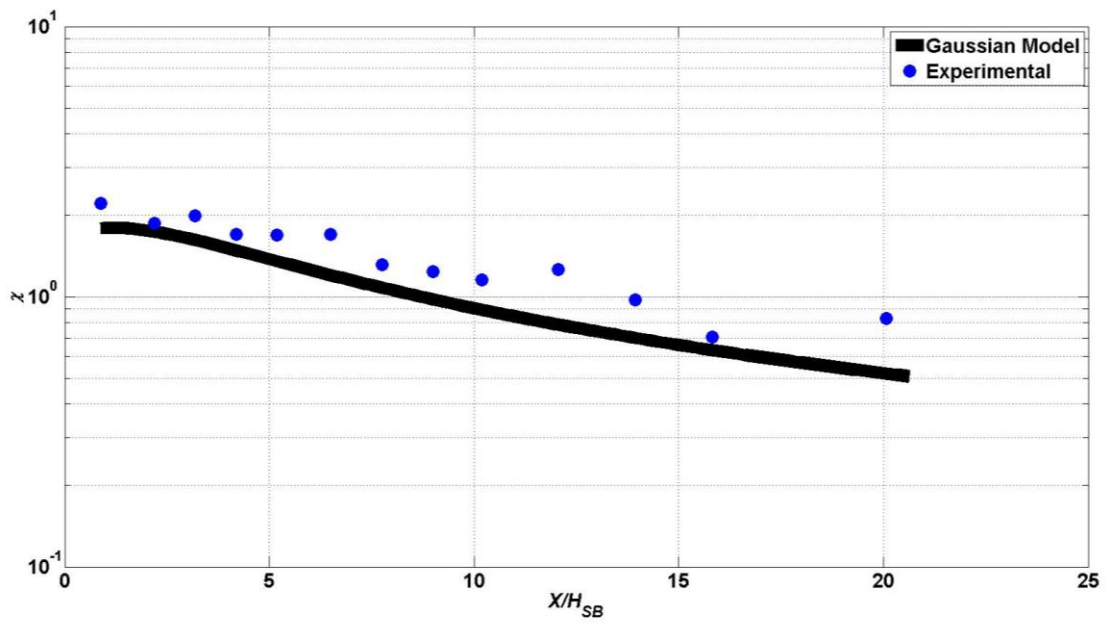**Figure 6-22.** Venkatram 2004 Model vs. FOALIF: No SB

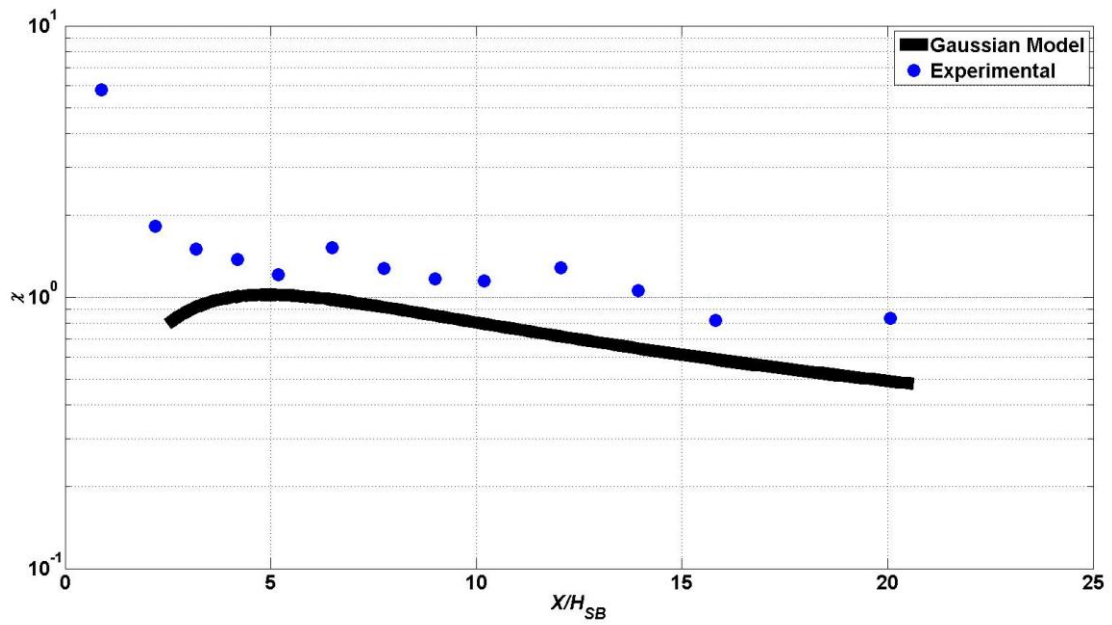**Figure 6-23.** Gaussian Model vs. FOALIF: Upwind Only SB

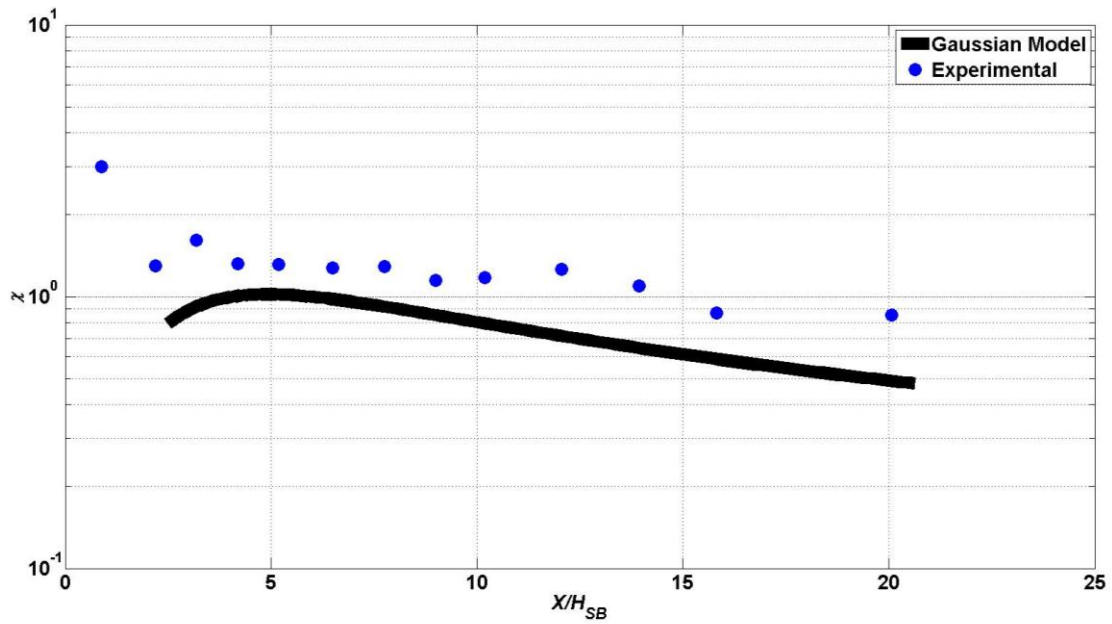**Figure 6-24.** Gaussian Model vs. FOALIF: Downwind Only SB

Figure 6-25. Gaussian Model vs. FOALIF: $H_{up} = H_{down}$

Referring to Equations (3-11) and (3-12) that lateral and vertical plume spreads were calculated based on the water channel dimensions. The variables x_{oy} and x_{oz} can be changed

depending on the domain of the problem, so for comparisons of the Gaussian model and QUIC, x_{oy} and x_{oz} are then changed to 100 m and 50 m respectively. Starting past five SB heights downwind there is great agreement between the Gaussian model and QUIC. The discrepancies upwind of this point are because the source was placed on top of a SB (Figure 6-21), so the results give no information of concentrations on the road. Even through for the case of upwind only SB the source is placed upwind of the road, it is seen that this model cannot account for the high on road concentrations (Figure 6-26). Referring to Figures 4-26, 27 and 28 there is high shear and turbulence around the SBs and low velocities on the road. As the Gaussian model cannot account for the significant changes in the mean velocity it is expected to see such discrepancies in the concentration results whenever dispersion in the presence of obstacles is investigated by Gaussian-like models. It is hypothesized that past $5H_{SB}$ downwind the velocities are stable and constant and thus the concentration results are in good agreement; this however is not confirmed from the PIV results since this distance is outside of the measured field of view.
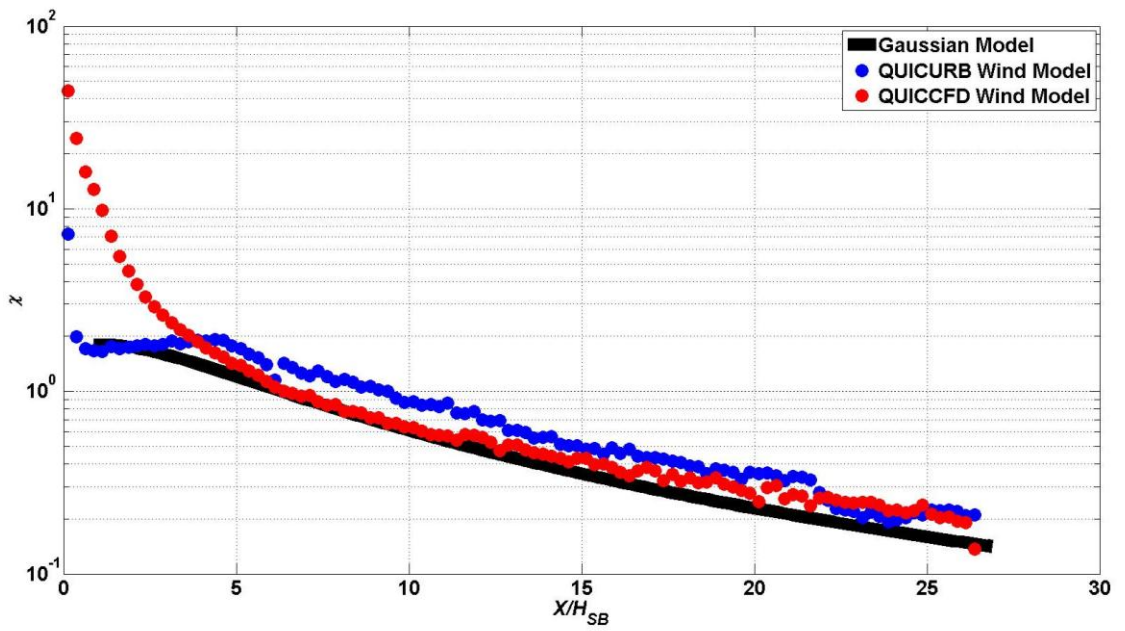
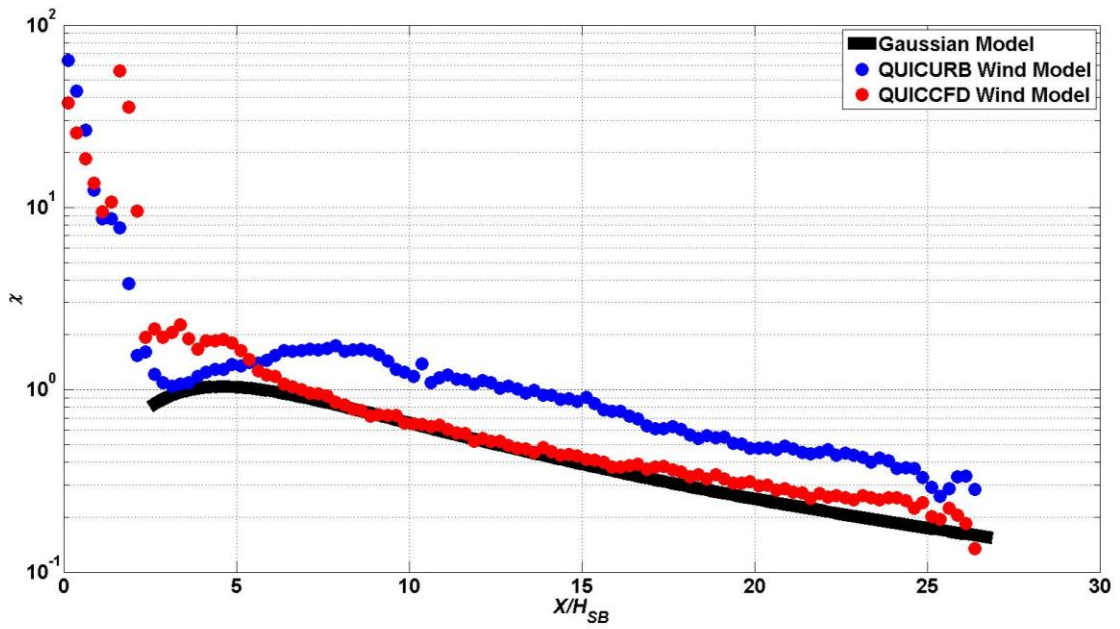**Figure 6-26.** Gaussian Model vs. QUIC: Upwind Only SB

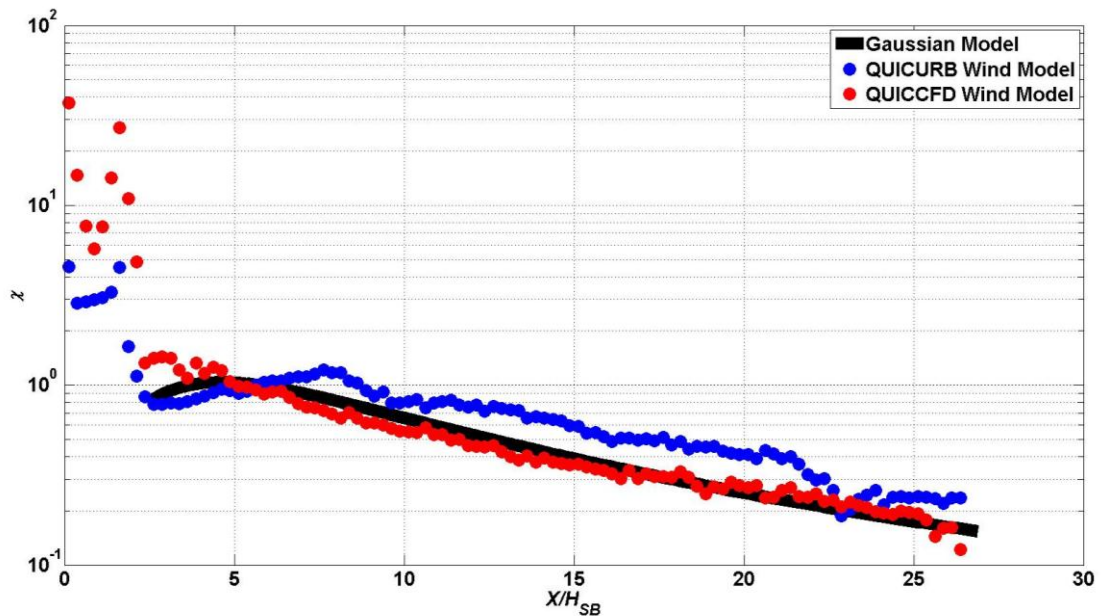**Figure 6-27.** Gaussian Model vs. QUIC: Downwind Only SB

Figure 6-28. Gaussian Model vs. QUIC: $H_{up} = H_{down}$

7. Conclusion

The water channel at the LEFM was used to study the near field effects SBs have on flow and dispersion through PIV, visualizations and FOALIF. The results show that the addition of SBs increases mixing and vertical spread of the plume relative to the case with no SBs, and this results in decreased downwind concentrations. For the case of upwind only SB there is an on road eddy which brings pollutants back towards the barrier where they are advected up. For the case of downwind only SB, the flow is decelerated by the SB which forces the flow up and down along the vertical of the SB. There is an eddy that develops on the road below about $0.5H_{SB}$ and this results in high concentrations near the upwind side of the SB, a concentration decrease is also found on the lee side of the barrier. For the case of equal height SBs there is a combination of flow patterns from the previous two cases.

Through visualizations the time averaged plume was investigated. A raised roadway resulted in the same plume pattern as flat roadway but the plume was displaced vertically by an amount equal to the roadway height. The downdraft from the downwind SB is not strong enough

110

to quickly bring the concentrations to the ground as seen for flat roadways and this would lead to lower ground level concentrations since the plume has increased vertical spread. For the case of a sunken roadway with no SB the plume follows the terrain and the vertical spread is comparable to that of a flat roadway. For the case of a sunken roadway with SBs there is a large recirculation that develops in the roadway resulting in much higher vertical spread than that of the flat roadway, presumably leading to lower downwind concentrations. The addition of trees instead of SBs increased the vertical spread compared to the case of no trees, but there was not as significant vertical spread as with the presence of SBs. It cannot be seen from the visualizations if the trees added any filtration or helped with deposition. The addition of traffic had little impact on the plume under high wind speeds but had a significant impact on low wind speeds for the cases of no SB only. As described in Section 5.7 there is an experimental uncertainty with the traffic setup. Since the water channel is neutral and a high wind speed of 4.2 cm s^{-1} would be associated with neutral conditions an attempt to look at the effects of unstable conditions was made. This was done by using heater plates as described in Section 5.8. Sensible heat flux had very little impact on dispersion under high wind speeds but had a significant impact on low wind speeds and due to the increased vertical spread lower downwind concentrations should be observed. A field study by Finn et al. (2009) showed lower concentrations downwind of a roadway under unstable conditions compared to neutral and stable conditions. The concentration measurements from FOALIF show that all SB configurations lead to lower concentrations compared to the case of no SB. Further downwind of the roadway the concentration results converge for cases with SBs with the largest difference in concentrations seen on the roadway. The QUIC results using the QUIC-URB wind model and the QUIC-CFD wind model with the modified mixing length show reasonable agreement (75% of data is within factor of 2 with no model adjustments) to the measured concentration results. For the cases in which there is a downwind SB the QUIC-URB

results show a slight concentration drop in the lee of the barrier, the QUIC-CFD with the modified mixing length does not show this. This drop in concentrations is somewhat noted in the FOALIF concentration results when compared to the on road concentrations, however this concentration drop is not significant compared to the downwind concentrations. The QUIC-CFD results with the default mixing length show an extreme drop in concentrations on the lee side of the downwind SB. The visualizations also show a decreased concentration area in the lee of the SB, but this area does not extend as far as shown in the QUIC-CFD results with default mixing length. The magnitude of the concentrations behind the downwind SB is not exactly known, and it is hypothesized that the QUIC-URB results are the most accurate due to it being empirically derived from wind tunnel experiments. It is also speculated that the FOALIF results may be slightly overestimated downwind due to the plume not being able to extend further than the water channel walls, thus leading to higher concentrations.
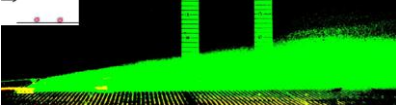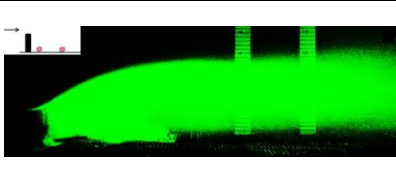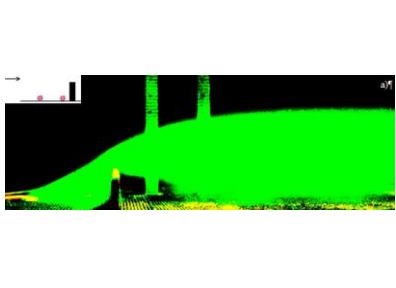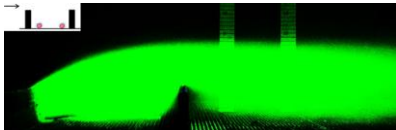
The simple Gaussian type models were also tested. After proper adjustments for given configuration these models can give reasonable results. The fact that these models do not and cannot solve the flow field seems to be not well recognized within regulatory agencies and the push is to apply them where the flow field is highly modified by urban obstacles. If some object placed in the flow is sufficiently large to modify the mean flow (e.g. sound barrier or buildings) these models will not recognize that and have to be tweaked. The most common tricks used in these models to compensate for updrafts/downdrafts/lateral channeling or any other mean flow features that deviates from straight, horizontal, unidirectional wind, are to move the source location to some other "logical" place (e.g. top of up or downwind sound barrier), to introduce "initial spread" just appropriately to best match the available measurements, to introduce "meandering" effect by increasing lateral spread proportionally to wind direction variability to match concentration where measurements are available. Once adjusted to given configuration
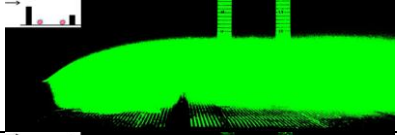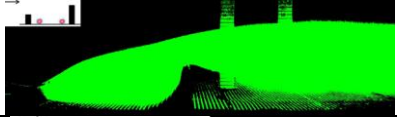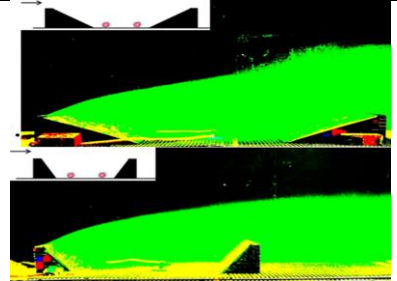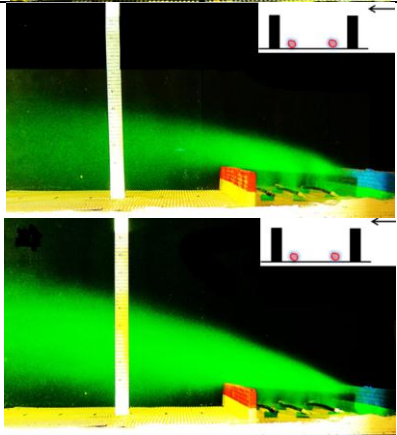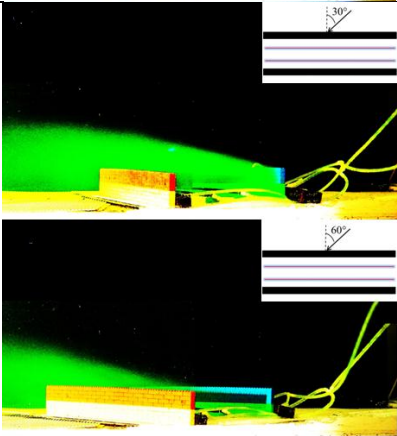
these models can be used. These adjustments to source location and spread parameter are then commonly referred as "a new model". In this way "a new model" has to be built for any obstacle configurations, terrain and atmospheric conditions – the practice commonly sponsored by CARB, CEC and AQMD.

Based on the presented experimental and numerical work, it is better to have some kind of SB setup rather than no SB as the concentrations are significantly decreased. The SB configuration recommended would depend on the surrounding areas and climate. In sensitive areas the additions of mechanical ventilation (fans) to move the pollutants above the wake of the SB should be further evaluated to determine potential real-world effectiveness.
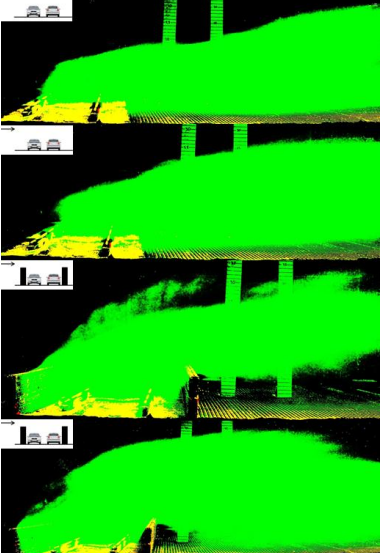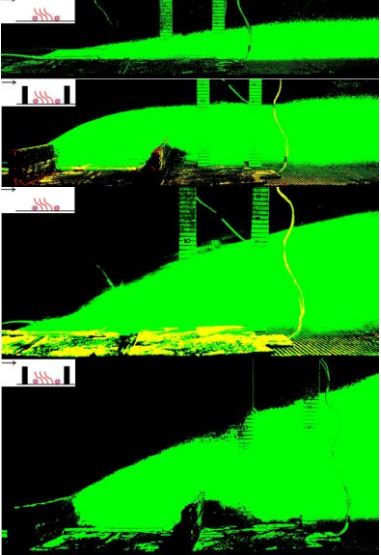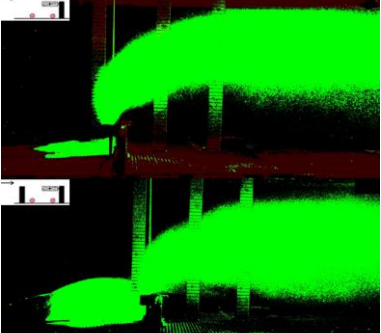
A summary of tested configurations with comments is given in Table 7.1

Table 7.1 – Tested configurations and main characteristics

Configuration	Comment	Relevant Visualization
No sound barriers	Plume is advected above the ground. Vertical mixing is only due to turbulence.	
Upwind barrier	Flow recirculation will redirect emissions upwind towards the barrier. Recirculation assists plume rise and results in significant decrease of ground level concentration (GLC).	
Downwind barrier	All emissions are advected towards the barrier. Resulting flow is partially assisting the plume rise since there is a small downdraft region in the lower part of the barrier. Visualizations indicate that most of the plume released at the middle of the road follow the updraft.	
Both barriers of equal height	Combines benefits of upwind and downwind barriers. Presence of both barriers intensifies on road recirculation.	

Upwind barrier taller than downwind	Similar to upwind only	
Downwind barrier taller than upwind	Similar to downwind only	
Inclined sound barriers	No significant difference from vertical barriers of the same heights. More cumbersome construction and space waste.	
Buoyant exhaust	Not very likely and relevant case due to high on road mixing. Without mixing the warm plume would rise higher and can escape being trapped in the barrier wake.	
Wind under angle	Plume can be channeled along the road.	

Tall vegetation on both sides of the road	Trees locally enhance mixing.	
Raised road with no sound barriers	Plume can be taken down due to the recirculation in the wake of the road.	
Raised road with sound barriers	Sound barriers will lift the plume, but it can be taken down due to the wake recirculation.	
Sunken road	Plume follows the terrain.	
Sunken road with sound barriers	Barriers cause large recirculation above the road that advects the plume upwind where it gets lifted next to the upwind barrier.	

Traffic induced turbulence	Traffic induces additional turbulence that enhances vertical mixing. Several traffic and wind conditions were investigated. Similar as groung heating, traffic induced turbulence has major effect onder low wind conditions.	
Ground heating effects	Hot surface can have major effect on vertical mixing under low wind conditions. High wind speed cases are comparable to no heating conditions.	
Mechanical ventilation	Depending on the fan size and input energy, a major reduction in GLC is possible. Needs feasibility analysis.	

References

Adrian, R.J., 1988. Review of particle image velocimetry research. In: The symposium on optical methods in flow and particle diagnostics, 6th International Congress on Applications of Lasers and Electro-Optics. Vol. 9, 317-319, San Diego, CA: Optics and Lasers in Engineering.

Adrian, R.J., 1991. Particle-imaging techniques for experimental fluid-mechanics, Ann. Rev. Fluid Mech. 23, 261-304.

Adrian, R.J., 1997. Dynamic ranges of velocity and spatial resolution of Particle Image Velocimetry,   Meas. Sci. & Tech. 8(12), 1393-1398.

Baldauf, R., E. Thoma, A. Khlystov, V. Isakov, G. Bowker, T. Long, R. Snow, 2008. Impacts of noise barriers on near-road air quality. Atmospheric Environment 42, 7502–7507.

Bowker, G.E., R. Baldauf, V. Isakov, A. Khlystov, A. Petersen, 2007. The effects of roadside structures on the transport and dispersion of ultrafine particles from highways. Atmospheric Environment 41, 8128e8139.

Division of Traffic Operations, 2010. 2010 Traffic Volumes on the California State Highway System.

Finn, D., K.L. Clawson, R.G. Carter, J.D. Rich, R.M. Eckman, S.G. Perry, V. Isakov, D.K. Heist, 2009. Tracer studies to characterize the effects of roadside noise barriers on near-road pollutant dispersion under varying atmospheric stability conditions, Atmospheric Environment, doi:10.1016/j.atmosenv.2009.10.012

Gowardhan, A., E. Pardyjak, I. Senocak, M. Brown, 2010. A CFD-based Wind Solver for a Fast Response Transport and Dispersion Model. The Fifth International Symposium on Computational Wind Engineering.

Guilbault G.G., 1973. Practical Fluorescence: Theory, Methods and Techniques, Dekker, New York.

Harrison, R.M., P.L. Leung, L. Somerville, 1999. Analysis of incidence of childhood cancer in the West Midlands of the United Kingdom in relation to the proximity of main roads and petrol stations. Journal of Occupational and Environmental Medicine 56, 774e780.

Heist, D.K., S.G. Perry, L.A. Brixey, 2009. A wind tunnel study of the effect of roadway configurations   on the dispersion of traffic-related pollution. Atmospheric Environment 43, 5101e5111.

Houston D, P.M. Ong, J. Wu, A. Winer, 2006. Proximity of licensed childcare to near-roadway vehicle pollution. American Journal of Public Health 96(9), 1611–1617.

Jerrett, M., R. Burnett, C.A. Pope 3rd, D. Krewski, K.B. Newbold, G. Thurston, Y. Shi, N. Finkelstein, E.E. Calle, M.J. Thun, 2005. Spatial analysis of air pollution and mortality in Los Angeles. Epidemiology 16, 727e736.

Kodama, Y., K. Arashidani, N. Tokui, T. Kawamoto, K. Matsuno, N. Kunugita, N. Minakawa, 2002. Environmental NO2 concentration and exposure in daily life along main roads in Tokyo. Environmental Research 89, 236–244.

Kulchin Y.N, S.S. Voznesenskiy, E.L. Gamayunov, A.S. Gurin, A.A. Korotenko, A.Y. Maior, 2007. An Immersible Fiber-Optic Fluorometer, Instruments and Experimental Techniques 6. 117–122

McConnell, R., K. Berhane, L. Yao, M. Jerrett, F. Lurmann, F. Gilliland, N. Kuenzli, J. Gauderman, E. Avol, D. Thomas, J. Peters, 2006. Traffic, susceptibility, and childhood asthma. Environmental Health Perspectives 114 (5), 766–772.

Nelson, M., and M. Brown, 2009. The QUIC Start Guide (v5.6). Los Alamos National Laboratory report LA-UR-10-01062.

Pardyjak, E.R., and M.J. Brown, 2001. Evaluation of a Fast-Response Urban Wind Model – Comparison to Single-Building Wind Tunnel Data. Los Alamos National Laboratory report LA-UR-01-4028.

Pardyjak, E.R., and M.J. Brown, 2003. QUIC-URB v. 1.1: Theory and Users Guide. Los Alamos National Laboratory report LA-UR-07-3181.

Peters, A., S. von Klot, M. Heier, I. Trentinaglia, A. Hormann, E. Wichmann, H. Lowel, 2004. Exposure to traffic and the onset of myocardial infarction. New England Journal of Medicine 351, 1721e1730.

Pournazeri, S., M. Princevac, and A. Venkatram, Scaling of Urban Plume Rise and Dispersion in Water Channels and Wind Tunnels - Revisit of an Old Problem, Journal of Wind Engineering and Industrial Aerodynamics, 103, 16-30, 2012.

Prasad, A.K.; R.J. Adrian, C.C. Landreth, P.W. Offutt, 1992. Effect of resolution on the speed and accuracy of Particle Image Velocimetry interrogation, Experiments in Fluids, 13(2-3), 105-116.

Princevac, M., J.J Baik, X. Li, H. Pan., and S.B. Park, 2010. Lateral channeling within rectangular arrays of cubical obstacles. Journal of Wind Engineering and Industrial Aerodynamics, doi:10.1016/j.jweia.2009.11.001.

Rao, K.S., R.L. Gunter, J.R. White, and R.P. Hosker, 2001. Turbulence and Dispersion Modeling Near Highways. Atmospheric Environment Vol. 36 4337-4346.

Stull RB, 1988, An Introduction to Boundary Layer Meteorology, Springer-Verlag, New York.

Wilhelm, M., Ritz, B., 2003. Residential proximity to traffic and adverse birth outcomes in Los Angeles County, California, 1994e1996. Environmental Health Perspectives 111, 207e216.

Williams, M.D., M.J. Brown, D. Boswell, B. Singh, and E. Pardyjak, 2004. Testing of the QUIC-PLUME Model with Wind-Tunnel Measurements for a High-Rise Building. 5th AMS Urb. Env. Symp., Vancouver, B.C., Canada. Paper J5.3.

van Ulden, A. P., 1978. Simple Estimates for Vertical Diffusion from Sources Near the Ground. Atmospheric Environment Vol. 12 2125-2129.

Venkatram, A., 2004. The Role of Meteorological Inputs in Estimating Dispersion from Surface Releases. Atmospheric Environment Vol. 38 2439-2446.